Thermodynamic Modeling of the (Mg, Al)-Ca-Zn Systems

Sk. Wasiur Rahman

A Thesis
in

The Department
of
Mechanical and Industrial Engineering

Presented in Partial Fulfillment of the Requirements
for the Degree of Master of Applied Science (Mechanical Engineering) at
Concordia University
Montreal, Quebec, Canada

December 2008

ABSTRACT

Thermodynamic Modeling of the (Mg, Al)-Ca-Zn Systems

Sk. Wasiur Rahman

Critical assessment of the experimental data and re-optimization of the binary Mg-Zn, Ca-Zn, Al-Zn, Al-Ca systems and the Laves phase in the Mg-Ca system have been performed. A Comprehensive thermodynamic database of the Mg-Ca-Zn and Al-Ca-Zn ternary systems is presented from the constituent binary systems using suitable extrapolation methods. All available as well as reliable experimental data both for the thermodynamic properties and phase boundaries are reproduced within experimental error limits.

In the present assessment, the Modified Quasichemical Model in the pair approximation is used for the liquid phase to account for the presence of the short-range ordering properly. The intermediate solid solutions are modeled using the compound energy formalism. Since the literature included contradicting information regarding the ternary compounds in both ternary systems, thermodynamic modeling of phase equilibria is used to determine the most likely description of the two ternary systems and to exclude the self-contradicting experimental observations.

The constructed database is used to calculate both the integral and partial thermodynamic properties of the constituent binary systems. Moreover, the liquidus projections, isothermal sections and vertical sections of the ternary systems are also calculated and the invariant reaction points are predicted using the constructed database.

ACKNOWLEDGEMENTS

Many individuals helped me throughout this work that I should take this opportunity to acknowledge them. First of all, I would like to express my sincere gratitude and appreciation to my thesis supervisor Dr. Mamoun Medraj for his constant advice, guidance and invaluable suggestions during my studies at Concordia University. Without his unyielding support it would not be possible to conduct this work.

I would like to thank all the members of my research group especially, Dr. Dmytro Keverkov, Md. Mezbahul Islam, Rafid Mendwi, Mohammad Asgar Khan and former member Dr. Mohammad Aljarrah for their support and assistance during my research work.

I thank all the staff members of the mechanical engineering department for their kind help in solving my academic and technical problems.

Finally, I want to extend my warm and sincere thanks to my parents. Without their unconditional love, support and encouragement I would never have been able to stand at this point of my life. I should not forget my younger sister who always loves and supports me. And last but not least, I am grateful to my aunt, Monowara and uncle, Harun-or-Rashid and know that my debt to them is beyond measure.

Table of Contents

List of Figures

List of Tables

CHAPTER 1

Introduction

1.1 Thermodynamics of Phase Diagrams

For doing basic materials research in such fields as solidification, crystal growth, joining, solid-state reaction, phase transformation and oxidation, phase diagrams act as a foundation. It is a one type of visual representation of the state of materials as a function of temperature, pressure and composition of the constituent components [1]. In addition, a phase diagram also serves as a blueprint for material design and processing variables to achieve the desired microstructure [2].

The properties of cast or wrought materials derived from a specific alloy system depend first and foremost on the phases and microstructural constituents (eutectics, precipitates, solid solutions etc.) that are present. The alloy systems containing several alloy elements have complex phase relations [3]. A Phase diagram is essential for better understanding and investigating these complex phase relationships. However, experimental determination of phase diagrams is a time-consuming and expensive task and becomes more pronounced as the number of components increases.

To overcome these difficulties, the calculation of phase diagrams can be very handy. A thermodynamic database containing model parameters, giving the thermodynamic properties of all the phases as functions of temperature and composition, will serve to construct the required phase diagrams. The CALPHAD method [4], is

regarded as the most scientific way of calculating the phase diagram. It is based on minimization of the Gibbs free energy of the system and is, thus, not only completely general and extensible, but also theoretically meaningful.

Thermodynamic descriptions of the constituent lower order systems, usually binaries and ternaries, are obtained based on the experimental phase equilibrium data. Once the descriptions for the lower order systems are known, then it is possible to obtain thermodynamic descriptions of the higher order systems using a suitable extrapolation method [2]. Calculation of phase equilibrium provides information not only about the phases present and their compositions, but also provides numerical values for different thermodynamic properties i.e. enthalpy, entropy, activity etc. This is very important for multi component systems especially for systems having more than three constituent elements, where the graphical representation of the phase diagram becomes complicated. The lack of sufficient experimental information makes the situation worse. Thus, the calculation of phase diagrams along the thermodynamic properties is significant for alloy development. Also, the development of computer programs has made the calculation much easier, sound and faster which ultimately helped the rapid progress in this field [2].

1.2 Motivation

Mg-Al based alloys are one of the most important alloys among all the Mg based alloys where the AM series, Mg-(2-6) % Al-(0.35-0.65) %Mn and AZ91, Mg-9%Al-1%Zn alloy can perform very well at room temperature. However, the existence of creep-induced precipitation of γ-$Al_{12}Mg_{17}$ phase is responsible to the poor creep property of the Mg-Al based alloys. Hence, a large of amount of effort have been made to increase the service temperature of these alloys. It was found that, the addition of Ca in Mg-Al-Zn

based alloys, forming Mg-Ca-Al-Zn quaternary system, can be beneficial not only to keep the costs low but also to improve the mechanical properties especially the creep resistance at elevated temperatures.

The quaternary Mg-Ca-Al-Zn system has complex phase relation containing many binary and ternary systems. The conventional empirical investigation on this system would be costly and time consuming in searching for optimal combinations of chemistry and processing procedure. Thereby, a self-consistent thermodynamic database on this quaternary system can act as a roadmap for such searching.

Four constituent ternary systems: Mg-Al-Zn, Mg-Al-Ca, Mg-Ca-Zn and Al-Ca-Zn are needed to construct the quaternary Mg-Ca-Al-Zn system. Figure 1.1 demonstrates how all these ternaries contribute in this regard. It is worth mentioning that among these ternaries, the Mg-Al-Zn system has been extensively studied by various researchers [5-8] both experimentally and by thermodynamic modeling and recently the Mg-Al-Ca system was modeled by Aljarrah [9].
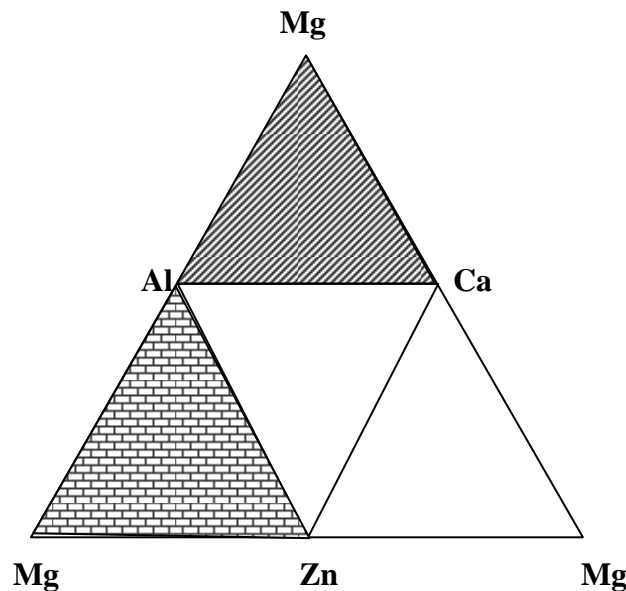
Figure 1.1: *Mg-Ca-Al-Zn quaternary system with the combination of the corresponding ternary systems*

Therefore, it is necessary to thermodynamically model the other two ternary systems: Mg-Ca-Zn and Al-Ca-Zn, in order to fully describe the Mg-Al-Ca-Zn quaternary system. In addition, both the Mg-Ca-Zn and Al-Ca-Zn ternary systems have some individual properties which can be very promising as well and will be described in the following chapters.

1.2.1 Importance of the Mg-Ca-Zn Ternary System

The main objective of adding alloying elements to pure magnesium is to increase the strength, to improve its corrosion resistance and to enhance the creep resistance which is important for commercial applications including automotive and aerospace sectors. It was found that alloying Mg with Ca increases the strength, castability and corrosion resistance and at the same time the presence of Zn in the binary Mg-Ca alloys enhances the precipitation hardening response [10]. Meanwhile, calcium also improves the oxidation resistance of magnesium at temperatures above 750 K [11]. Researchers also found that addition of Ca increases the ignition temperature of Mg. This will be helpful not only in the melting process, but also for potential automobile and aerospace application regarding the safety issues [12]. Calcium bearing Mg alloys show no sign of extensive combustion compared to non-Ca bearing Mg alloys as illustrated in Figure 1.2. On the other hand, the second major alloying element Zn has significant amount of solid solubility in Mg. This results in improving solid solution strengthening in Mg alloys. Zn also increases fracture toughness of wrought magnesium alloys [13].
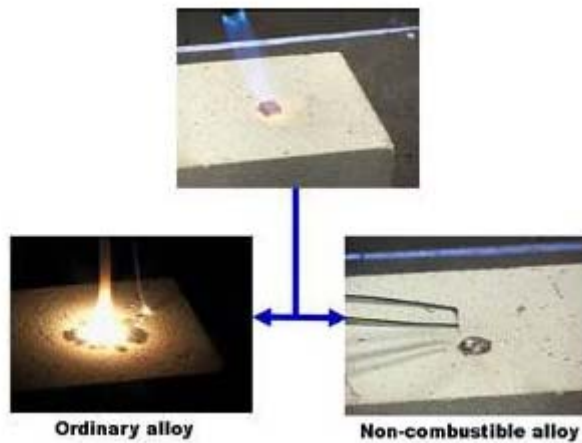
Figure 1.2: Non-combustible Ca bearing magnesium alloy [14]

Somekawa and Mukai [15] have recently shown that hot extrusion of Mg-0.3 at.% Ca-1.8 at.% Zn resulted in good balance of yield strength and fracture toughness which can be seen in Figure 1.3, where Mg-Ca-Zn alloys show improved mechanical properties than those of the conventional wrought magnesium alloys.
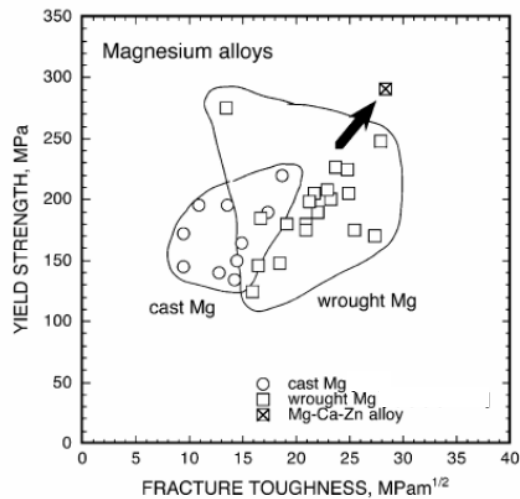
Figure 1.3: The relationship between fracture toughness and yield strength of magnesium alloys [15]

1.2.2 Importance of the Al-Ca-Zn Ternary System

In order to form complex shaped structures, superplasticity is regarded as a viable technique. The technique has the advantages of delivering exceptional formability and potentially giving good dimensional tolerance [16]. Al-based alloys have long standings

5

as the work metal for superplastic application due to their lightness and superior creep properties compared with those of the standard zinc-based alloys [17]. The Al-Zn eutectoid alloy and the Al-CaAl$_4$ eutectic alloy are known to be superplastic. However, sheets made of these alloys are brittle and cannot be cold rolled industrially, whereas, Al alloys containing Ca and Zn are more ductile and can be cold rolled to superplastic sheet using conventional rolling systems [18].

Another useful and important application of Al-based materials is as sacrificial anodes. In recent years, aluminum alloys are characterized by high current efficiency and long service life. Hence they are used for the protection of underground and underwater pipelines, reservoirs, oil storages, drilling rigs, municipal communications and continental shelf structures. But for the conventional aluminum protectors working in soils, it is necessary to use special activators (solutions of salts) to prevent the formation of passivating films on the surfaces of protectors in the process of operation [17]. Whereas, aluminum based protective materials including calcium and zinc do not require activating solutions and can withstand that difficulty.

1.3 Objectives of the present work

The exceptional properties of Mg alloys such as light weight, good castability and recyclability entice the automobile and aerospace manufacturers. Hence a complete and reliable thermodynamic database for these alloys is very necessary. The objective of this project is to thermodynamically model the Mg-Ca-Zn and Al-Ca-Zn ternary systems. The present work includes:

- Critical evaluation of all the available experimental data on Mg-Zn, Ca-Zn and Al-Zn binary systems and Mg-Ca-Zn and Al-Ca-Zn ternary systems.

6

- Thermodynamic modeling of all the phases present in the aforementioned systems. Remodeling of the Laves phase in the Mg-Ca system and improvement in the Al-Ca binary system are also carried out.

- Calculation of the phase diagrams and thermodynamic properties of the Mg-Zn, Ca-Zn and Al-Zn binary systems and comparing the results with the available experimental results reported in the literature.

- Construction of database for Mg-Ca-Zn and Al-Ca-Zn systems by combining the thermodynamic descriptions of the constituent binaries using a suitable extrapolation method.

- Calculation of ternary phase diagrams of the Mg-Ca-Zn and Al-Ca-Zn systems using the constructed databases.

- Thermodynamic modeling of the different ternary phases in the Mg-Ca-Zn and Al-Ca-Zn systems.

- Identification of the invariant points and the primary solidification regions of each field in the Mg-Ca-Zn and Al-Ca-Zn systems and comparing the results with the experimental data.

- Calculation of isoplethal sections as well as the isothermal sections from the constructed database and comparison with the corresponding experimental results.

CHAPTER 2

Literature Review

A brief description of different works found in the literature on the Mg-Ca-Zn and Al-Ca-Zn ternary systems and their constituent binary systems: Mg-Zn, Ca-Zn, Mg-Ca, Al-Zn and Al-Ca will be discussed in the current chapter. Emphasis is given on the critical evaluation of the phase equilibria, thermodynamic properties and crystallographic information of these systems.

2.1 Mg-Zn Binary System

2.1.1 Equilibrium Phase Diagram

The first work on the Mg-Zn system was carried out at the beginning of twentieth century by Boudouard [19] who determined the liquidus curve for the whole composition range using thermal analysis. But perhaps he had a contamination problem indicated by the low Mg melting point reported in his work [20]. Hence his reported experimental data will not be used in this work.

Grube [21] investigated the Mg-Zn system using thermal analysis for the whole composition. He determined the liquidus line with ± 1 K experimental error, one congruently melting compound $MgZn_2$ which melts at 868 K whilst the temperature of the two eutectics were given as 641 K on the Zn rich side and 617 K on the Mg rich side . His phase diagram did not show any solid solution area.

Later, Bruni *et al.* [22] studied the system from 66.7 to 100 at.% Zn and afterward, Bruni and Sandonnini [23] investigated it from 0 to 66.7 at.% Zn through thermal analysis. Both Bruni *et al.* [22] and Bruni and Sandonnini [23] reported only one intermediate compound, $MgZn_2$, which melts congruently at 862 K and two eutectics: one of them occurs at 28.7 at.% Zn and 613 K [23] and the other one at 92.5 at.% Zn and 636 K [22]. Similar to Grube [21], no solid solution was reported by Bruni *et al.* [22].

Chadwick [24] determined the liquidus across the whole composition using thermal and metallographic analysis with Mg containing 0.1% Si and no defectable amount of Fe or Al. He also confirmed the existence of $MgZn_2$, which was first detected by Grube [21], but reported a lower melting point than [21] by 10 K. A new compound $MgZn_5$ was discovered by Chadwick [24] and confirmed by Hume-Rothery and Rounsefell [25], but later was replaced by a more accurate composition of Mg_2Zn_{11} by Samson [26]. The eutectic temperature on the Zn rich side of Chadwick [24] was 641 K, same as Grube's [21] value which was higher of 4 K than those of later investigations [25, 32].

In the following year, Hume-Rothery and Rounsefell [25] used thermal analysis and microscopic examination of quenched specimens to investigate the system from 30 to 100 at.% Zn where their liquidus line agree well with those of Chadwick [24] and Grube [21]. They also reported a new compound MgZn formed by a peritectic reaction and later on, confirmed by Zaharov and Mladzeevskiy [27], Laves [28], Urazov *et al.* [29] and Savitskii and Baron [30]. The peritectic temperature for MgZn formation was 627 K measured by Hume-Rothery and Rounsefell [25], which was higher than those of Anderko *et al.* [31] and Park and Wyman [32] where the values were 622 ± 2 K and

620 ± 1 K respectively. Afterward, Clark and Rhines [33] placed the MgZn compound at 52.1 at.% Zn (74.5 wt.% Zn) rather than 50 at.% Zn(72.9 wt.% Zn) with a compound having 12:13 stoichiometric ratio and it was supported by Park and Wyman [32].

Takei [34] was the first who found the intermetallic compound Mg_2Zn_3 which occurs by a peritectic reaction between $MgZn_2$ and liquid at 683 ± 10 K and later on, established by Laves [28] who did micrographic and X-ray studies at the same peritectic temperature. The values reported by Anderko *et al.* [31] and Park and Wyman [32] for this transformation were 683 ± 5 K and 689 ± 1 K, respectively. Both Takei [34] and Laves [28] assumed that the Mg_2Zn_3 phase to be in equilibrium with the Mg terminal solid solution at room temperature which was later proved to be wrong by Clark and Rhines [33] who investigated the system in the composition range of 0 to 66.81 at.% Zn applying thermal, microscopic and powder X-ray diffraction analyses. They found that, MgZn, instead of Mg_2Zn_3, is in equilibrium with Mg terminal solid solution below 598 K and their result was confirmed by Anderko *et al.* [31] and Park and Wyman [32]. Clark and Rhines [33] also confirmed that the eutectoid decomposition of Mg_7Zn_3, which was first reported by Takei [34] and Ishida [35], was about 598 K. The peritectic formation of the compound Mg_7Zn_3 is somewhat obscure because of its close proximity to the Mg rich eutectic point as reported by different authors in the literature. Urazov *et al*. [29] located the formation of Mg_7Zn_3 on the Zn side of the eutectic (on the hyper-eutectic side) and later Koster and Muller [36] showed the compound to be on the high Mg side of the eutectic (on the hypo-eutectic side).

Anderko *et al.* [31] also tried to resolve this issue using thermal analysis, microscopic examination and X-ray diffraction on alloys made with Mg of 99.995 wt.%

purity and Zn of 99.9 wt.% purity in the composition range of 25 to 66.7 at.% Zn. They [31] found that Mg_7Zn_3 is formed at 30 at.% Zn in the peritectic temperature range of 617-621 K but they were not certain on which side of the eutectic it is located. Almost at the same time, Park and Wyman [32] also were working on this system using thermal, X-ray and metallographic methods and ended up by placing Mg_7Zn_3 on the right side of the eutectic with a peritectic temperature of 615 ± 1 K. After more than two decades, the intermetallic compound Mg_7Zn_3 was described with a stoichiometric ratio 51:20 suggested by Higashi *et al.* [37] after a careful crystal structure determination by single crystal X-ray diffraction. They suggested that, the crystal structure to be orthorhombic with lattice parameter a = 1.4083 nm, b = 1.4486 nm, c = 1.4025 nm. The new composition of $Mg_{51}Zn_{20}$ (28.169 at.%Zn) differs a little from that of Mg_7Zn_3 (30 at.%Zn) suggested by the previous authors [31, 32, 34, 35]. Higashi *et al.* [37] placed this compound on the hypo-eutectic side. Their results will be adopted in this work.

Chadwick [24] for the first time showed the solubility of Zn in Mg using microscopic examination of the quenched samples. However his results seem to show too high zinc content due to the presence of silicon as impurity, which was pointed out by Hansen [38]. Therefore his reported data was neglected in this work. Afterward, the Mg solvus curve was reported by several investigators such as Schmidt and Hansen [39] using metallography, Grube and Burkhardt [40] using electrical resistance measurements, Schmid and Seliger [41] using X-ray diffraction and Park and Wyman [32] using X-ray diffraction and microscopic examination and their values agree well with each other. Hence the results of [32, 39-41] will be used for the thermodynamic optimization of this system. Besides, Adenstedt and Burns [42] and Park and Wyman [32], studied the Mg

solidus curve where the solubility values of [42] are higher than the data of [32] who pointed out the experimental error in the dilatometric measurements of [42]. Park and Wyman [32] mentioned the maximum solubility of Zn in Mg is 2.5 at.% Zn at 613 ± 1 K and more emphasis is given on their work which appears to be more reliable considering the metal purity, sensitivity of the X-ray diffraction and microscopic examination used and the approach to equilibrium. The limited solubility of Mg in Zn was determined by Hume-Rothery and Rounsefell [25] applying metallographic analysis and reported that the maximum solubility of Mg in Zn is 0.3 at.% Mg at the eutectic temperature of 637 K, whereas no experimental points on the Zn solidus could be found in the literature.

Narrow homogeneity ranges have been reported for all the intermetallic compounds but detail quantitative investigations could not be found in the literature. Therefore all the intermetallic phases except $MgZn_2$ Laves phase were considered as stoichiometric phases. According to Chadwick [24], $MgZn_2$ forms a wide range of solid solution extending from 57 to 68 at.% Zn which he termed as γ solid solution though he was not sure about its stability at lower temperature. This discrepancy was due to the use of acid ferric chloride etching reagent as pointed out by Hume-Rothery and Rounsefell [25], according to whom $MgZn_2$ to be of fixed composition. However, later investigations [27, 34] indicated that this wide solubility encompassed other intermetallic phases such as Mg_2Zn_3. A much narrower solubility range for $MgZn_2$ was determined by Park and Wyman [32] who for the first time reported the homogeneity range to be from 66.0 at.% Zn at 689 K to 67.1 at.%Zn at 645 K and discarded any confusion about its instability at room temperature. Therefore, the data of [32] will be compared with the current findings. The crystal structure of this compound was first found by Friauf [43] and confirmed by

Komua and Tokunga [44] to be a C14 type Laves phase with hexagonal structure having a = 0.518 nm, c = 0.852 nm lattice parameters [45].

Clark *et al.* [46] assessed the Mg-Zn phase diagram based on the experimental work of Chadwick [24], Hume-Rothery and Rounsefell [25] and Park and Wyman [32]. They accomplished an excellent work by compiling all the experimental data that had been conducted prior to their work. However, they did not mention the details of the thermodynamic models used for different phases in their work. In fact, their work is more a review work rather than an optimization.

Agarwal *et al*. [20] also summarized the experimental work of Mg-Zn system and carried out a thermodynamic optimization for the Mg-Zn system based on the experimental data from the literature and their measured partial enthalpy of mixing data. Their calculated phase diagram is shown in Figure 2.1. Random mixing in the liquid phase was used in their [20] work and the Redlich-Kistler polynomial [47] to describe the liquid phase and the terminal solid solution. All the intermediate phases were regarded as stoichiometric phases in their work.
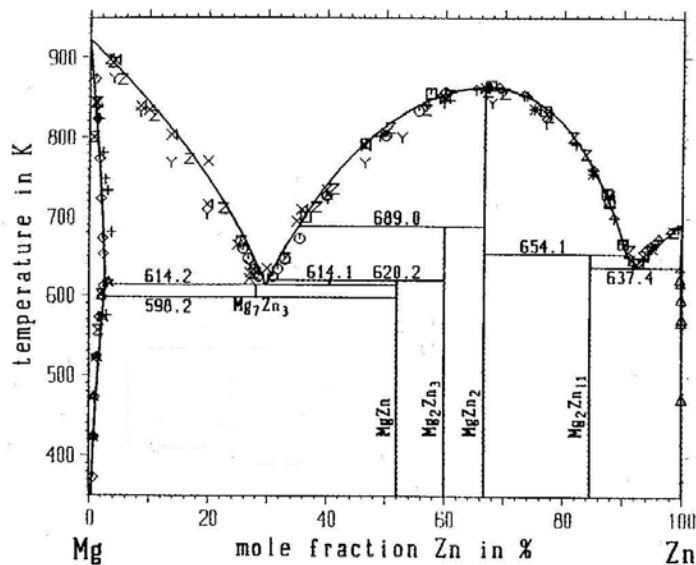
Figure 2.1: *Calculated Mg-Zn phase diagram [20]*

Later, Liang *et al.* [5] modeled this system based on the experimental data from literature but they did not show the calculated phase diagram. They also considered the liquid phase as random solution and used Redlich-Kistler polynomial to describe it and treated the intermediate Laves phase MgZn$_2$ as an ordered phase with narrow solubility range and modeled it by considering two sublattices using the compound energy formalism(sublattice model) [48]. They used the same number of Redlich-Kistler terms as [20] for both liquid and terminal solid solution phases.

2.1.2 Thermodynamic properties

The enthalpy of mixing of the Mg-Zn liquid was first measured by Kawakami [49] at 1073K using direct reaction calorimetry, but his experimental values were not very reliable in terms of experimental method and also very scattered and more exothermic in comparison with other experimental values [51, 52]. Hultgren *et al.* [50] also rejected the values of [49] because his values have been found to be wrong in other systems (Sn-Mg, Bi-Mg and Pb-Mg). Pyka [51] measured the enthalpy of mixing of the liquid Mg-Zn system at 862, 893 and 981 K using calorimetry where it shows a very slight temperature dependence for the enthalpy of mixing which was not pointed out by the author [51]. Later on, Agarwal and Sommer [52] performed calorimetric investigations to find out the enthalpy of mixing for the liquid phase at 773, 873, 933 and 940 K where alloys were prepared form Mg with 99.98 at.% purity and Zn with 99.995 at.% purity. Their measured values at 933 K show some deviation from other values at different temperatures especially in the Mg rich side but less in the Zn rich side and according to them this is due to the lower value of excess heat capacity at constant pressure (Δc_p^{excess}) in the Zn rich liquid alloys and predicted that this behavior occurs

because of the stabilization of one or more Mg rich intermediate phases and suggested that, it is an indication of short range ordering in the liquid phase.

Figure 2.2 shows the calculated enthalpy of mixing by Kim *et al.* [6] who used the association model to describe the thermodynamic properties of liquid in the Mg-Zn system at 981 K. It shows good agreement with the experimental values.
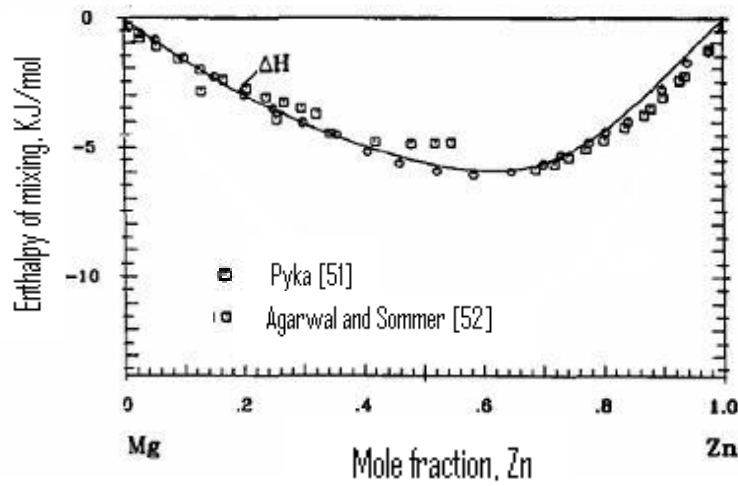
Figure 2.2: *Calculated enthalpy of mixing for liquid phase in Mg-Zn system at 981K with the experimental data [6]*

Terpilowski [53] and Chiotti and Stevens [54] measured electromotive force (EMF) of Mg in the liquid Mg-Zn alloy in order to determine different partial properties of the system in the liquid state. The partial enthalpy of Mg in the liquid phase was measured by Terpilowaski [53] at 923K in the composition range of 0.1 to 0.965 at.%Zn.

He also reported the activity values of Mg using $\Delta\overline{G}_{Mg} = RT.\ln a_{Mg}$ equation as shown in Figure 2.3. The activity values of Zn were calculated using Gibbs-Duhem equation at the same temperature. Agarwal *et al.* [20] also measured the partial enthalpy of Mg at 873 K using calorimetric method and their results will be compared with the values of [53] and those from the present work.

Later on the activity of Mg was measured by Moser [55] at 880 K and Pogodaev and Lukashenko [56] at 933 K and that of Zn by Pogodaev and Lukashenko [56] at 1073 K using electromotive force measurement. Moser [55] reported an error range of 1 to 6 percentage at the corresponding temperature. Kozuka *et al*. [57] used vapor pressure measurement to find out the activity of Zn in the liquid phase at 943 K.
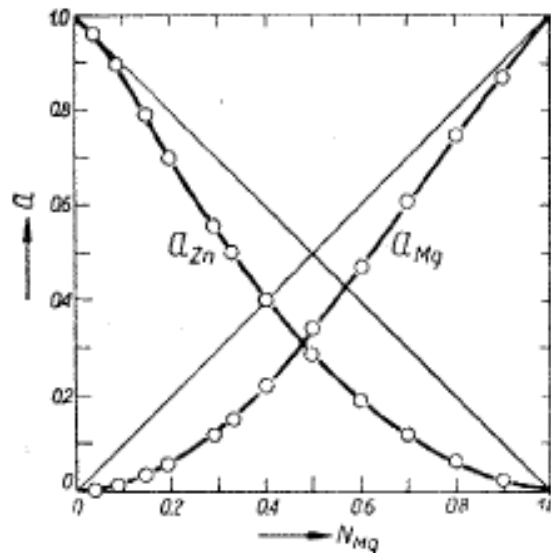
Figure 2.3: *Activity of Mg and Zn for liquid phase in Mg-Zn system at 923K [53]*

Schneider *et al*. [58] estimated the heat of formation at room temperature for three different compounds in the solid state namely: $Mg_{12}Zn_{13}$, $MgZn_2$ and Mg_2Zn_{11} using reaction calorimetry. Afterward, similar properties for $Mg_{12}Zn_{13}$ and $MgZn_2$ were determined by King and Kleppa [59] using tin solution calorimetry. More recent experimental values have been measured by Pedokand *et al*. [60] who determined the heat of formation for all the intermediate phases namely: $Mg_{51}Zn_{20}$, $Mg_{12}Zn_{13}$, Mg_2Zn_3, $MgZn_2$ and Mg_2Zn_{11} using EMF. Due to the different experimental techniques these values are not consistent.

2.2   Ca-Zn Binary System

2.2.1 Equilibrium Phase Diagram

Very limited amounts of experimental data have been found in the literature for the Ca-Zn system. The first experimental analysis of the Ca-Zn system was executed by Donski [61] using thermal analysis. In his experiment, the alloys were prepared in open glass tubes using materials that were impure by modern standards. The liquidus curve and three congruently melting compounds: $CaZn_{10}$, $CaZn_4$ and Ca_2Zn_3 which melted at 990, 953 and 961 K were reported. The incongruent melting of Ca_4Zn and a compound designated CaZn were also reported by the same author. Because of the use of highly contaminated alloys, his reported values were not considered in this work. Moreover, most of the intermediate phases reported by [61] were later replaced by new compositions based on the more accurate crystallographic investigations of [62-67].

Paris [68] also investigated the system by thermal and microscopic analysis where he studied the liquidus curve and mentioned a new compound Ca_5Zn_2 which was formed by a peritectic reaction at 684 K. However Ca_4Zn and CaZn were not detected by [68]. His experimental data were also abandoned in the present calculation because of the contradiction with the later experimental work of Messing *et al.* [69].

A through re-investigation on this system was done by Messing *et al.* [69], thirty years after Paris' [68] work, using differential thermal analysis (DTA) supplemented by X-ray diffraction analysis (XRD). Because of the high vapor pressure of the Ca-Zn alloys above 50 at.% Zn, Messing *et al.* [69] also used vapor effusion measurement for compound identification. The samples were prepared in tantalum crucible under helium atmosphere from refined 99.99 % Zn and twice sublimed Ca (with impurities of less than 0.1 wt% total Ba and Sr, 80 ppm other metals, 24ppm N_2 and 200 ppm H_2). According to

Messing *et al.*[69] the allotropic transformation α (Fcc_A1) ↔ β (Bcc_A2) of Ca took place at 718 K which is close to 716 K adopted by Itkin and Alcock [70]. They [69] reported eight intermetallic compounds: Ca_3Zn, Ca_7Zn_4, $CaZn$, $CaZn_2$, Ca_7Zn_{20}, $CaZn_5$, $CaZn_{11}$ and $CaZn_{13}$ all of which exist as stoichiometric compounds. Apart from $CaZn_2$, $CaZn_5$ and $CaZn_{11}$, all compounds undergo peritectic decomposition (incongruent melting). Their thermal analysis also showed three minima that belongs to eutectic reaction: at 27.4 at.%Zn and 667K, at 76.4 at.% Zn and 911K, and at 86.4 at.% Zn and 963K. The liquidus was determined with the accuracy of ±5 K which is very much reasonable for the used method and samples. Most of their reported experimental data, especially for the liquidus curve were taken into consideration in the current work.

Itkin and Alcock [70] assessed the Ca-Zn system where they made some changes by replacing Ca_7Zn_4 and Ca_7Zn_{20} designated by [69] with Ca_5Zn_3 and $CaZn_3$, respectively, based on the more accurate crystallographic investigation of Bruzzone et al. [62] and Fornasini and Merlo [63]. Their [70] calculated phase diagram was based mainly on the work of Messing *et al.* [69]. But they did not mention what kind of thermodynamic modeling they used during their calculation.

In 2002, Brubaker and Liu [71] calculated the system mainly based on the work of [69]. They assumed the liquid phase as substitutional solution phase and modeled it using sublattice model with all the intermetallic compounds. They proposed a new interpretation by reporting the $CaZn_3$ to undergo congruent melting which was reported to be incongruent melting by previous investigators. They based their decision on Messing *et al's*. [69] liquidus data and crystallographic data of [63]. The calculated phase diagram of [71] is shown in Figure 2.4.
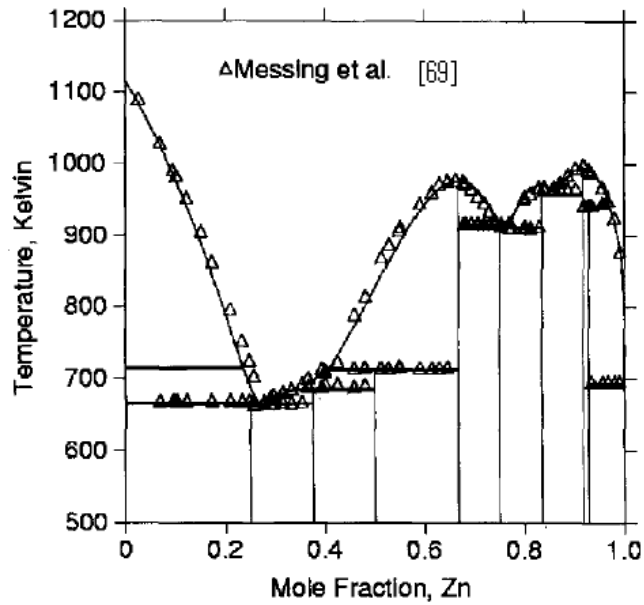
Figure 2.4: *Calculated Ca-Zn phase diagram [71]*

Most recently Spencer *et al.* [72] evaluated the experimental work of the Ca-Zn system and carried out a thermodynamic calculation of this system. They used the modified quasichemical model for the liquid phase and considered the $CaZn_3$ phase to be incongruently melted. The calculated phase diagram of [72] is shown in Figure 2.5 with experimental data of Messing *et al.* [69].
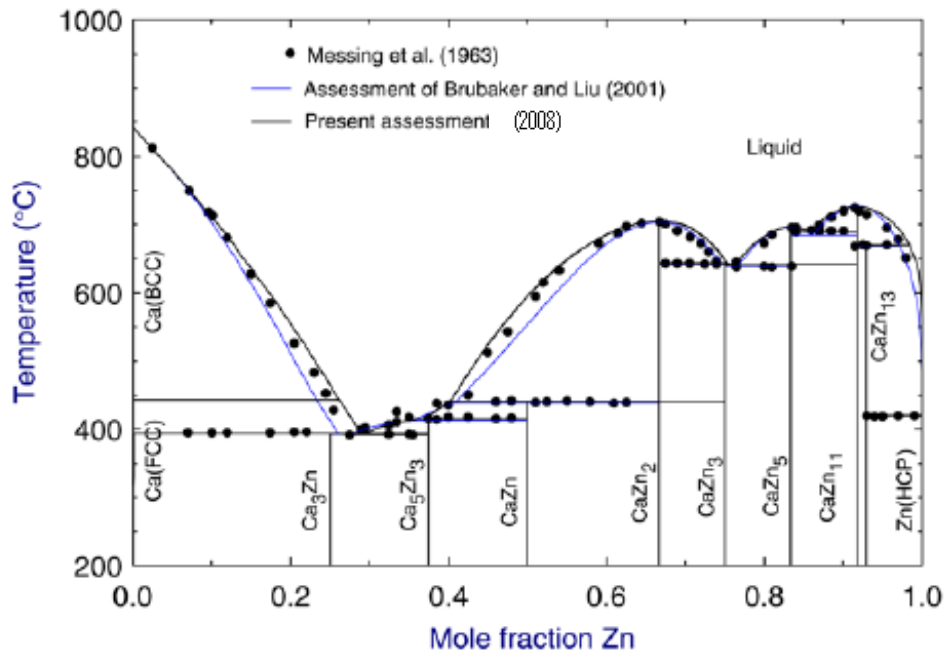
Figure 2.5: *Calculated Ca-Zn phase diagram [72]*

19

2.2.2 Thermodynamic properties

The amount of experimental data on the Ca-Zn system both for the solid and liquid states is very limited in the literature. The Zn vapor pressure was measured by Chiotti and Hecht [73] using the dewpoint method for samples greater than 50 at.%Zn and the Knudsen effusion method for lower Zn concentration. Later, Itkin and Alcock [70] evaluated the activity of Zn at 1073 K from the vapor pressure measurement data of [73]. Delcet and Egan [74] determined the activity of Ca at 1073 K using EMF measurements on CaF$_2$ solid electrolyte cells. The calculated value of Spencer *et al.* [72] showed reasonable consistency with the experimental data of [73] and [74] and calculated results of [71] as shown in Figure 2.6.
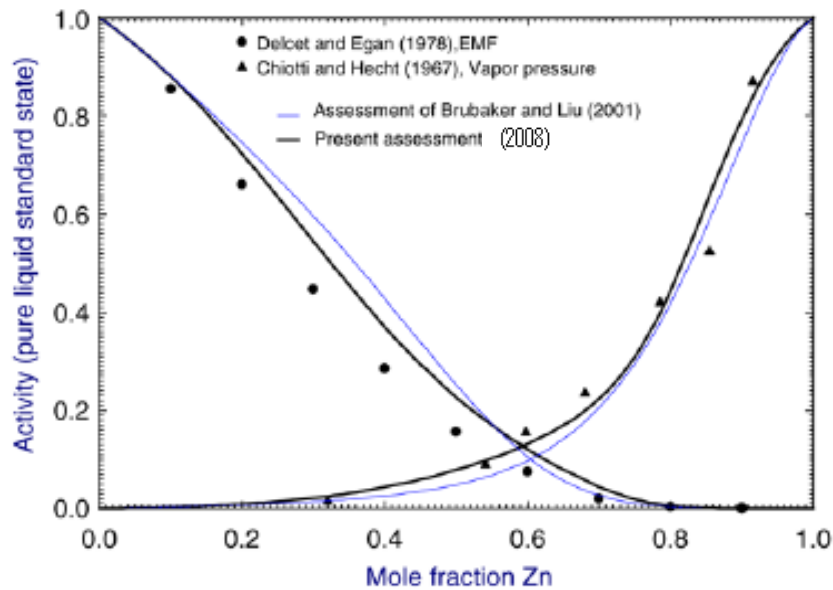
Figure2.6: *Activity of Ca and Zn in the liquid phase at 1073K [72]*

No experimental data for the enthalpy of mixing of the liquid phase could be found in the literature. The enthalpy of formation for all the intermediate phases was

calculated by Chiotti and Hecht [73] from the temperature dependence of the experimental Zn vapor pressure data and phase equilibrium condition.

2.3 Mg-Ca Binary System

2.3.1 Equilibrium Phase Diagram

The Mg-Ca is an important binary system in constructing a full description of the Mg-based alloy systems. Addition of Ca to Mg effectively increases the hardness and also these alloys have high specific strength [75]. In addition, it is an important part of the thermodynamic research of the Mg-Ca-Zn ternary system. As a result, a detailed thermodynamic description of this system is important.

The Mg-Ca binary system was studied by many researchers [76, 77] in the past. The most recent and complete thermodynamic description on this system was done by Aljarrah and Medraj [78] using CALPHAD approach [4]. They used the Modified Quasichemical Model [79-81] to account for the presence of short range ordering in the liquid phase. In their work, the Mg_2Ca phase was treated as stoichiometric compound, i.e. $(Mg)_2(Ca)_1$, for simplicity. However, for a multi component system containing Mg, Ca and Zn, the Mg_2Ca Laves C14 phase must be modeled using more complex sublattice model, $(Mg,Ca)_2 (Mg,Ca)_1$ so that both the $MgZn_2$ and Mg_2Ca phases having the same crystal structure, can be represented with one Gibbs energy function and this was accomplished in the present work.

Figure 2.7 shows the calculated phase diagram of Aljarrah and Medraj [78] where good consistency was achieved with the experimental data from literature.
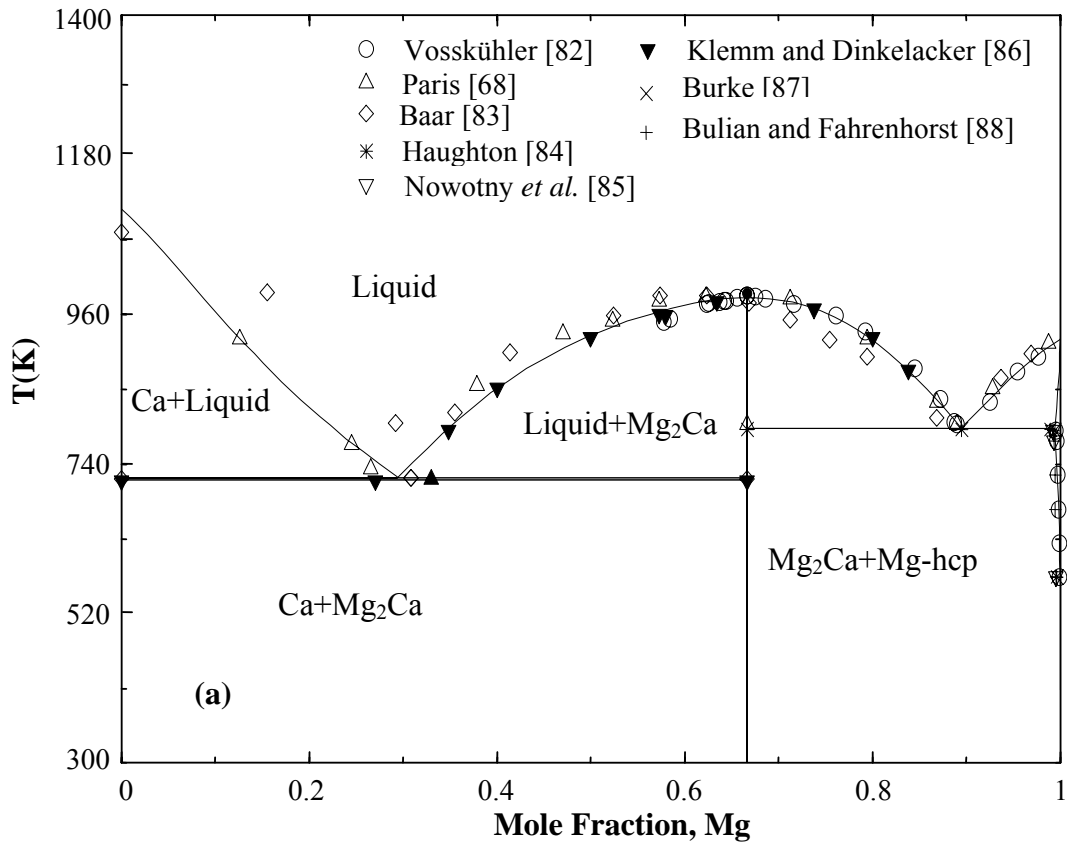
Figure 2.7: *Calculated Mg-Ca binary phase diagram [78]*

2.3.2 Thermodynamic properties

The calculated thermodynamic properties such as enthalpy of mixing, entropy of mixing and activities of both Mg and Ca in the liquid phase carried out by Aljarrah and Medraj [78] show reasonable agreement with the experimental results from the literature. All these properties with experimental data are shown in Figures 2.8 to 2.10. They [78] also made a comparison in the calculated results for enthalpy of mixing and entropy of mixing using the Modified Quasichemical Model and the Random Solution Model where the Modified Quasichemical Model shows better agreement with the experimental results of Sommer *et al.* [89] regarding enthalpy of mixing. Therefore their model parameters will be used in the present work.
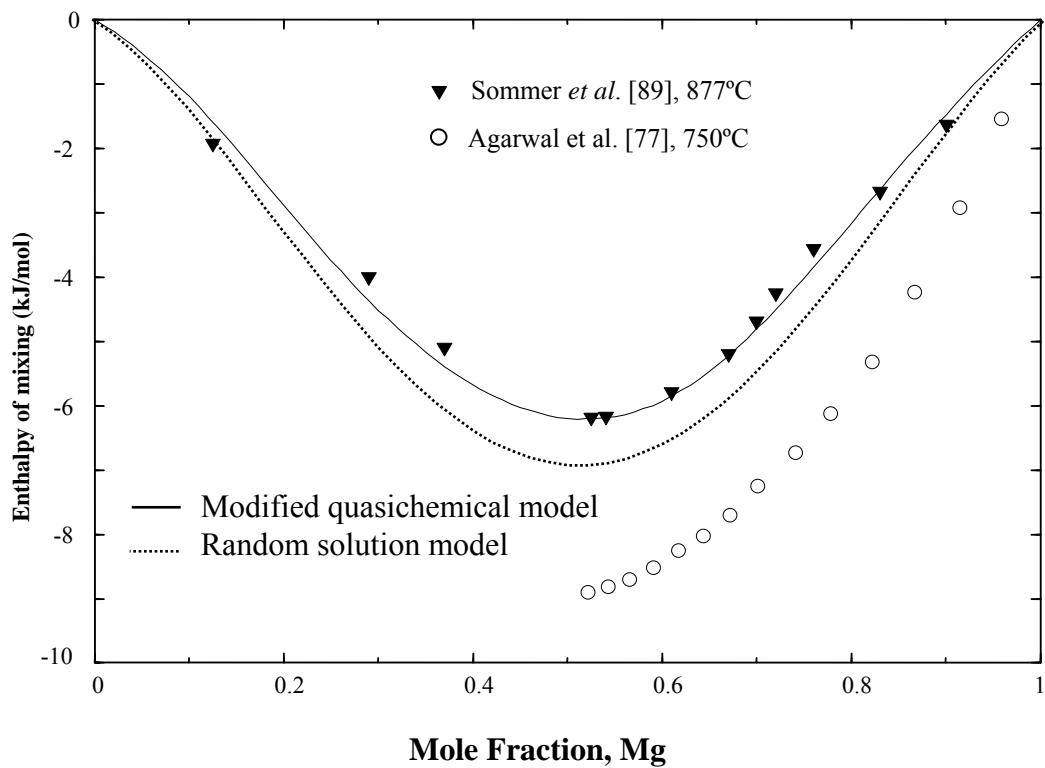
Figure 2.8: *Comparison between the calculated enthalpy of mixing of Mg-Ca liquid at 877ºC using the modified quasichemical model and random solution model along with the experimental data [78]*
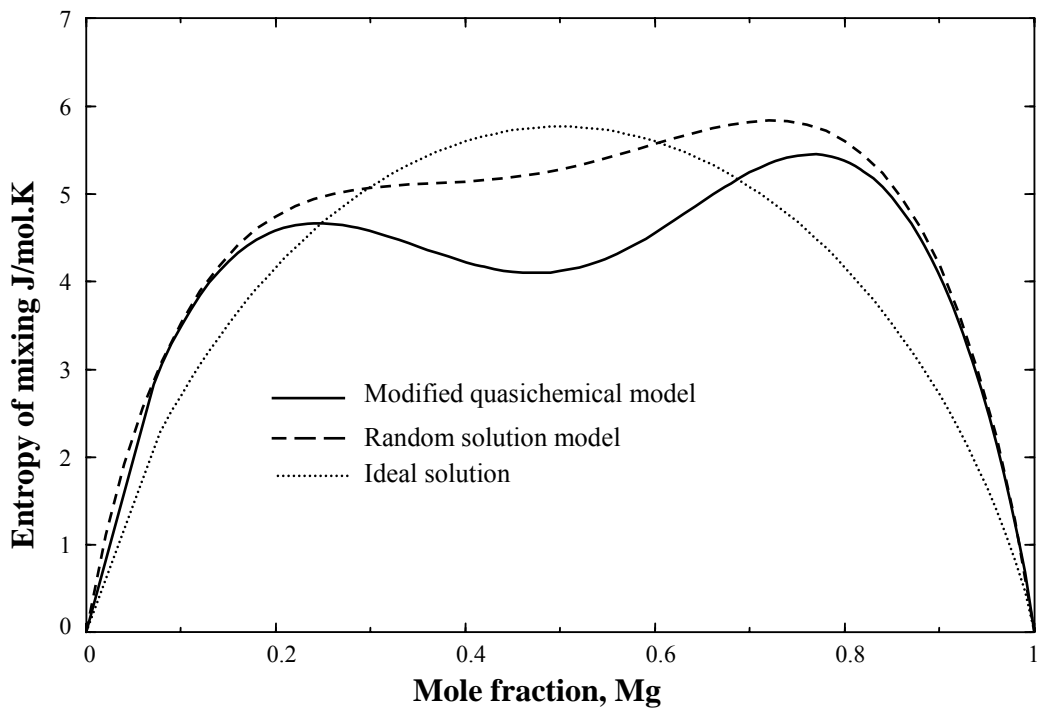
Figure 2.9: *Comparison between the calculated entropy of mixing of Mg-Ca liquid at 807ºC using the modified quasichemical model and random solution model [78]*
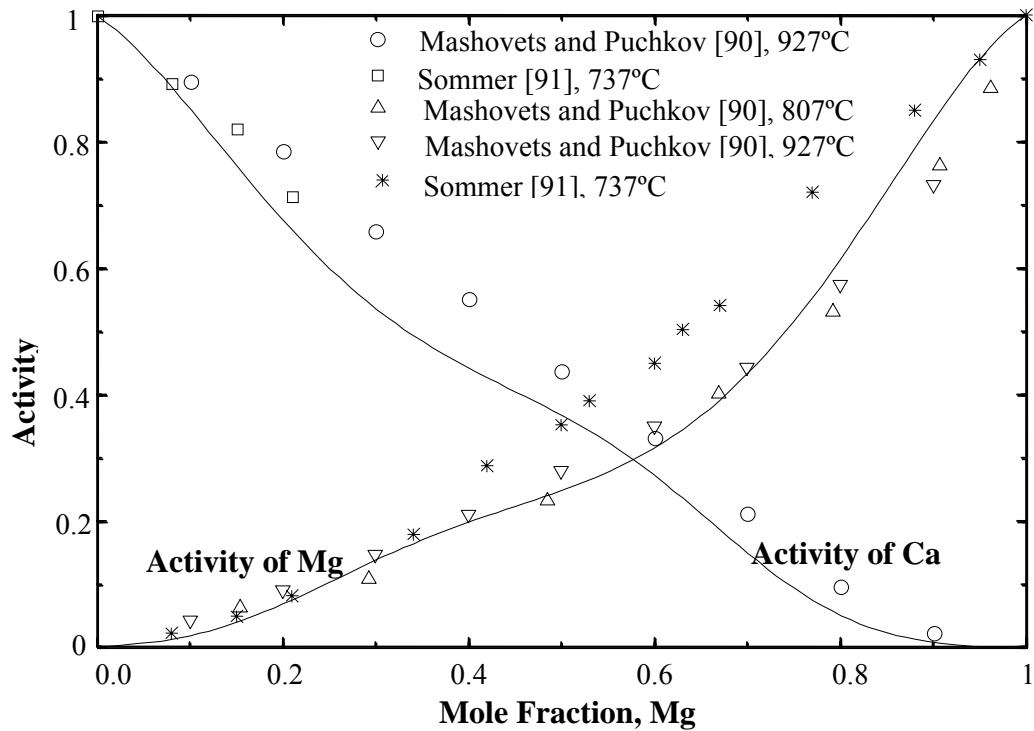
Figure 2.10: *Calculated activity of (a) Ca and (b) Mg in Mg-Ca liquid at 827ºC (Reference state: Ca-liquid and Mg-liquid) [78]*

2.4 Mg-Ca-Zn Ternary System

Despite the high potential of the Mg-Ca-Zn system as a source for structural alloys, a very limited amount of experimental work has been done on this system regarding the phase equilibrium diagram and thermodynamic properties. Paris [68] for the first time took the initiative to investigate the system in 1934. He studied the system by measuring the cooling curves of 189 different alloys. Paris chose the alloy composition in such a way so that the liquidus points could be plotted as sixteen isopleths which is shown in Figure 2.11. Although Paris' [68] samples might have had contamination problems, they were used during the optimization of the ternary Mg-Ca-Zn system because not many other experimental work on the liquidus curve could be found in the literature. Based on his thermal analysis and metallography, Paris reported one ternary compound with a composition of $Ca_2Mg_5Zn_5$ but did not provide any

24

crystallographic information for it. Figure 2.12 illustrates the liquidus projection reported by Paris [68].
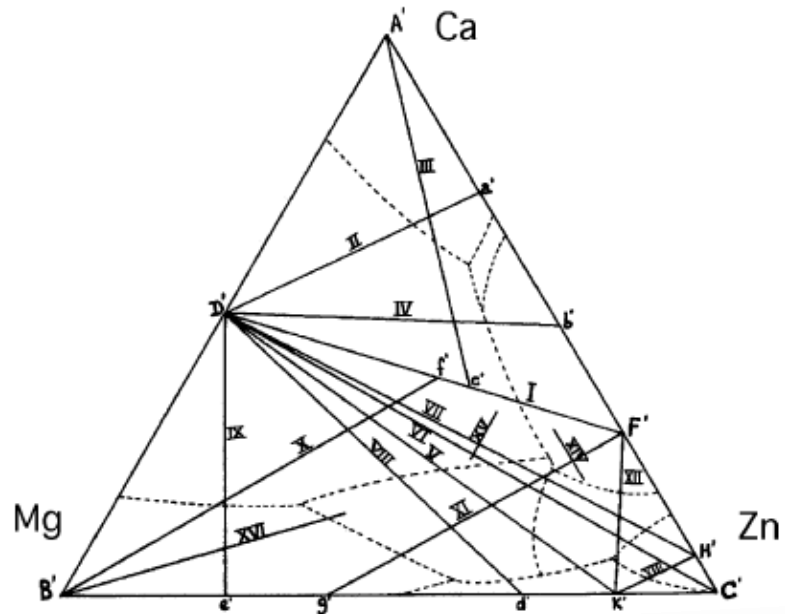
Figure 2.11: *The liquidus projection of the Mg-Ca-Zn ternary system with the location of the sixteen isopleths superimposed [68]*
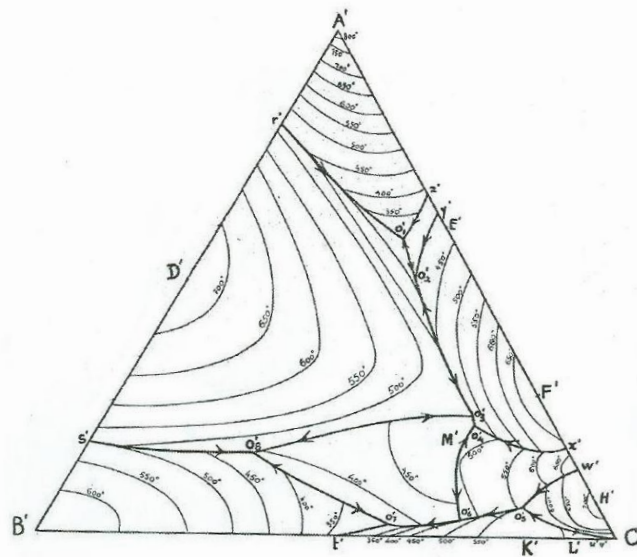
A=Ca	D=Mg$_5$Ca$_3$	G=w=CaZn$_4$	L=MgZn$_5$
B=Mg	E=Ca$_5$Zn$_2$	H=CaZn$_{10}$	M=Ca$_5$Zn$_5$C$_2$
C= Zn	F=Ca$_2$Zn$_3$	K=MgZn$_2$	

Figure 2.12: *The liquidus projection of the Mg-Ca-Zn ternary system with the solidification regions for different phases [68]*

25

Later, the isothermal section in the Mg-Zn side of the Mg-Ca-Zn system at 608 K was studied by Clark [92] using metallography and powder X-ray diffraction on seventy-six alloys searching for other ternary phases which is shown in Figure 2.13. This was performed using the diffusion couple method and two ternary compounds were reported, namely β and ω which were stable at room temperature under equilibrium conditions and disputed the composition of $Ca_2Mg_5Zn_5$ reported by Paris [68]. Later the compositions of the two ternary compounds were mentioned by Clark in the Joint Committee on Powder Diffraction Standards (JCPDS) [93, 94] as $Ca_2Mg_6Zn_3$ for β and $Ca_2Mg_5Zn_{13}$ for ω.

$\varepsilon = Mg\_Hcp$

$\rho = Mg_7Zn_3$

$\tau = MgZn$

$\psi = Mg_2Zn_3$

$\varphi = Mg_2Ca$

β and ω = ternary phase
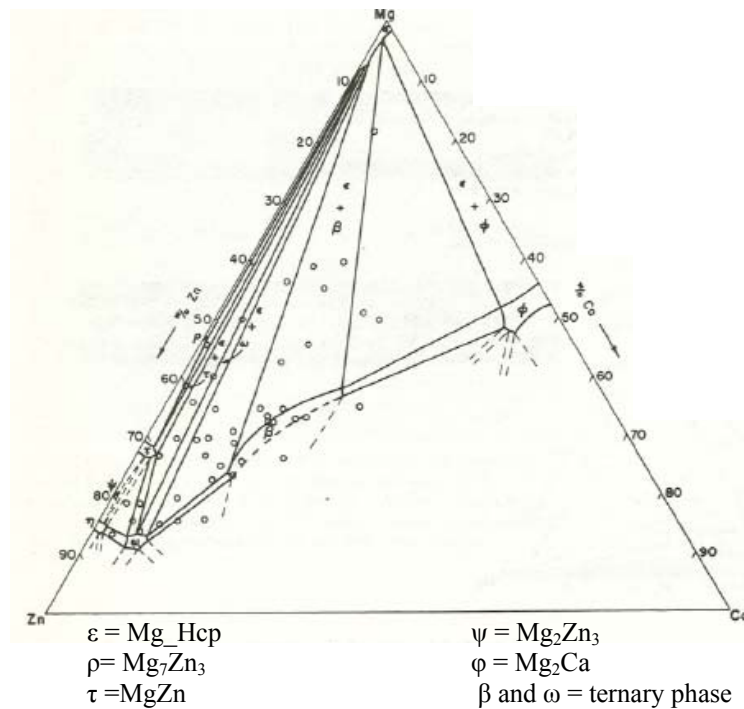
Figure 2.13: Isothermal section of the Mg-Ca-Zn system at 608 K [92]

Afterward, the potential advantage of the Mg-Ca-Zn alloys motivated researchers like Miyazaki *et al.* [75], Nie and Muddle [95], Horie *et al.* [96] to study this system but these studies were not conclusive regarding phase identification. Then recently, Larinova *et al.* [97] studied this system using XRD and Jardim *et al.* [98,99] used XRD,

transmission electron microscopy (TEM), energy dispersive X-ray spectroscopy (EDS) coupled with scanning transmission electron microscopy (STEM) and scanning electron microscopy (SEM). Both of them reported a ternary compound and determined with $Ca_2Mg_6Zn_3$ composition which is similar to the first compound given in the JCPDS card reported by Clark [92]. Larinova *et al.* [97] and Jardim *et al.* [98,99] prepared their samples in the form of ribbons using a melt spinning technique and heat treated those samples for almost one hour at 673 K and 473 K, respectively. Jardim *et al.* [99] also reported the crystallographic information of the compound $Ca_2Mg_6Zn_3$ which is presented in Table 2.1.

Table 2.1*: Crystallographic data for the Ca₂Mg₆Zn₃ phase*

Phase	Crystal structure	Pearson symbol	Space group	Lattice parameters(nm)		Ref.
				a	c	
$Ca_2Mg_6Zn_3$	Trigonal	hP22	$P\bar{3}1c$	0.97	1.0	[99]

A computational thermodynamic model on this system was reported by Brubaker and Liu [100] where they considered only the first ternary compound reported by Clark [92]. Their proposed model was based on the random mixing of atoms in the liquid phase, which cannot properly handle the presence of short range ordering. For these reasons, this system is being remodeled using the quasichemical model in this work. Figures 2.14 and 2.15 illustrate the calculated liquidus projection and isothermal section at 608 K of Brubaker and Liu [100] with the experimental data of Paris [68] and Clark [92].
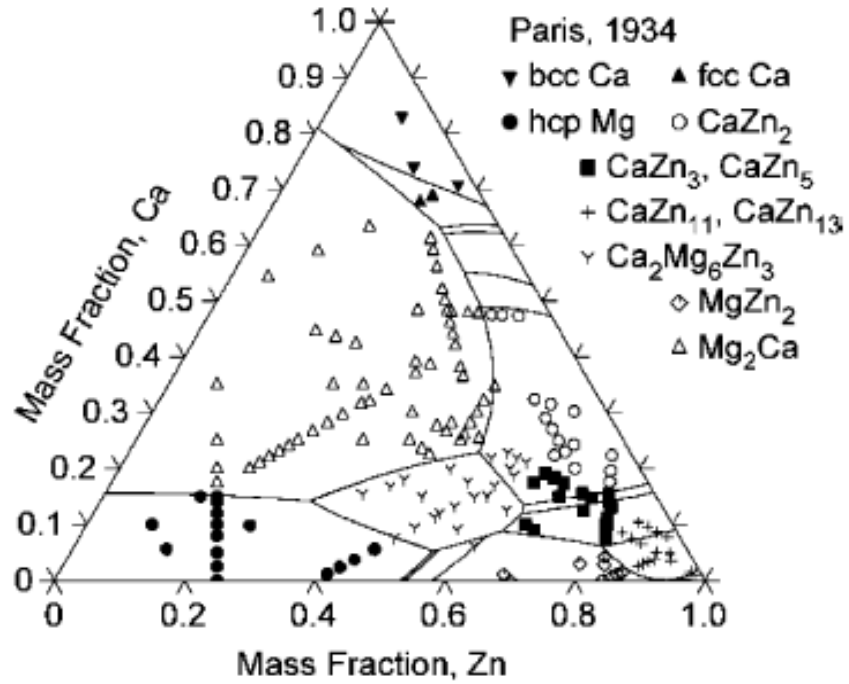
Figure 2.14: *The calculated liquidus projection of the Mg-Ca-Zn ternary system with experimental result form literature [100]*
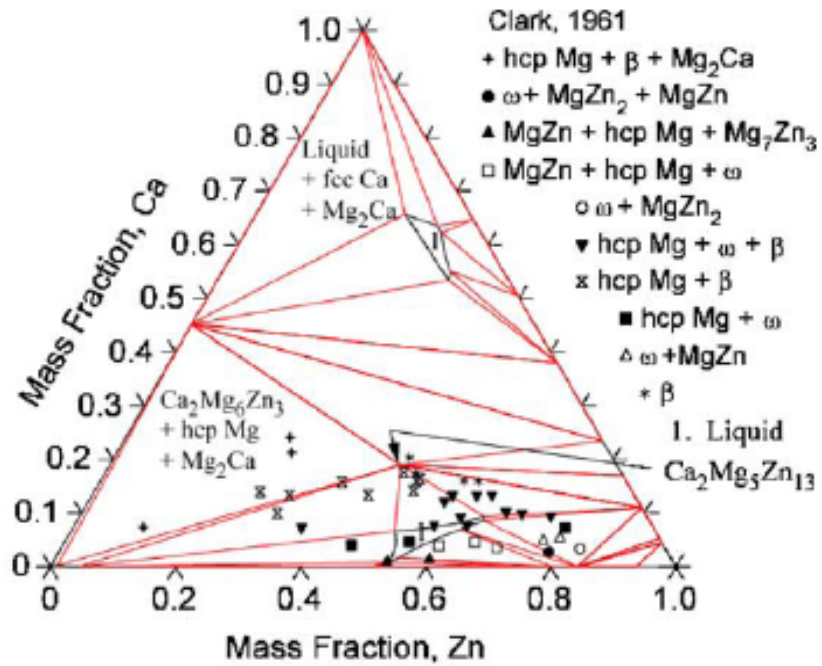
Figure 2.15: *The calculated isothermal section at 608 K of the Mg-Ca-Zn ternary system with experimental result form literature [100]*

2.5　Al-Zn Binary System

2.5.1　Equilibrium Phase Diagram

The Al-Zn system has been studied extensively in the literature and large amounts of experimental information were reported for the liquidus, solidus and solvus curves of the phase diagram. Heycock and Neville [101] first investigated the system using thermal analysis through cooling the samples. They determined the liquidus curve with the eutectic temperature 653.5K at 89 at.% Zn where the values of Tanabe [102] and Isihara [103] were 658 K at 88.7 at.% Zn and 653 K at 88.7 at.% Zn, respectively.

Tanabe [102] studied the system by means of thermal analysis, microstructure and the electric-resistance methods to determine the liquidus and Al-solidus curve. The Al-solidus curve of [102] was not considered in the present work due to the fact that he did the experiment by keeping the samples in the melt tube, so the phase change determination can not be accurate enough and this was pointed out by Isihara [103], who also used the same methods as [102] supplemented by the dilatometric method and X-ray diffraction analysis. From [103], the averages of the heating and cooling curves were chosen in the present calculation because of the greater discrepancy between heating and cooling and this discrepancy was also acknowledged by the author himself. Several data points of Isihara [103] were discarded during optimization because discrepancies between heating and cooling were too high (10 K).

The liquidus and the Al-solidus curve of the Al-Zn system were also determined by Gayler *et al.* [104] from 20 to 100 at.% Zn using thermal and microscopic analysis. They reported both the heating and cooling curves for the liquidus where the heating curve lies consistently higher than other measurements from the literature and that is why

only the cooling curve was considered in the present calculation. The eutectic temperature was reported as 654 K by [104]. Later, Pelzel and Schneider [105] studied the system from 30 to 100 at. % Zn using specific volume method and their data agreed fairly with the data of [104]. The eutectic point was determined by [105] to be at 88.7 at.% Zn and 653 K.

In 1945, Butchers and Hume-Rothery [106] investigated the liquidus and Al-solidus line of the Al-Zn system using the general cooling curve method for the liquidus and metallographic analysis for the solidus curve. Their reported data also agreed reasonably well with others. Afterward, almost at the same time, Pelzel [107] and Solet and Clair [108] worked separately on this system where their outcomes agree remarkably with each other. Pelzel [107] used thermal analysis to measure the liquidus and metallography for the solidus curve, whereas Solet and Claire [108] used thermal analysis to determine only the liquidus curve. They [108] took particular care in the chemical analysis of alloys, temperature measurements and choice of an optimal cooling rate.

The liquidus and solidus lines of this system were also studied by Peng *et al.* [109] using the acoustic emission method. In their experiment, they found different acoustic emission signals during solidification. They [109] reported higher liquidus temperatures than other researchers and concluded that the eutectic reaction occurs at 88.7 at.% Zn and 655 K. They also argued that their method is more precise than the conventional thermal analysis because of absence of the heat hysteresis phenomena.

The Al-solidus curve was also investigated by several researchers. Among them Morinaga [110] and Gebhardt [111] used microscopic analysis, Ellwood [112] used high temperature X-ray diffraction and recently Araki *et al.* [113] used electron-probe

microanalysis (EPMA) in order to determine the solidus line. Early works [102,103] showed lower values for solidus temperatures. Tanabe [102] and Isihara [103] found a series of thermal arrests between 713 K and 720 K, which they [102,103] attributed to a peritectic reaction, L + (Al)↔ solid solution (β). Later, Gayler *et al.* [104] and Morinaga [110] demonstrated that the thermal effect is the result of segregation. They [104, 110] found no evidence of any kind of phase change and this was supported by later investigators [112, 114]. Both Tanabe [102] and Ishihara [103] were unable to predict the miscibility gap rather they reported a solid solution which undergoes a peritectic reaction as discussed before.

The Fcc miscibility gap has also been studied by numerous groups of investigators [112, 114-119]. Fink and Willey [114] used electrical resistivity at elevated temperature and found two aluminum solid solutions in equilibrium at a temperature above 548 K. According to [114] the critical temperature is 626 K at 38.5 at.% Zn. Borelius and Larsson [115] and Muenster and Sagel [116] also used the electrical resistivity measurement to determine the miscibility gap. Borelius and Larsson [115] reported the eutectoid decomposition at 550 K with an uncertainty of about ± 0.5 K. On the other hand, Muenster and Sagel [116] used 29 alloys in their experiment and reported the composition of the critical temperature to be 614.5 ± 0.4 K at 39.5 ± 0.002 at.% Zn. The miscibility gap also studied by Ellwood [112], who used high temperature X-ray diffraction.

Later, Larsson [117] determined the boundary of the miscibility gap using electrical resistivity measurement on 28 different Al-Zn alloys in the composition range 1 to 65 at.% Zn. The results of Larsson [117] show slightly higher values in temperature in

comparison with the values of [112, 114, 116] above 50.0 at.% Zn. In order to determine the miscibility curve more accurately, X-ray diffraction and transmission electron microscopy was used by Simerska and Bartuska [118] who measured the Al solvus line and boundary of the miscibility gap upto 30.0 at.% Zn and were consistent with the other experimental works. Moreover, Terauchi *et al*. [119] reported the critical temperature to be 624 K at 39.16 at.% Zn and eutectoid temperature as 548 K using the small angle X-ray scattering method and cooling curve technique. The reported eutectoid temperate of [119] is close enough to the later investigation of Holender and Soltys [120], who used an electrical resistivity method and reported this value as 549 K. Peng *et al.* [109] also studied the miscibility gap during their investigation on this system using acoustic emission method and their results agree well with the earlier experimental works.

Early determinations of Ishihara [103] significantly overestimated the solubility of Zn in Al and will not be considered in the present work. The experimental results of Tanabe [102], Fink and Willey [114], Borelius and Larsson [115], Ellwood [112] and Araki *et al.* [113] are more or less consistent with each other except in the composition range 10 to 16.5 at.% Zn. The data of [102], [114] and [115] for the phase boundary Al_Fcc$_2$/ (Al_Fcc+Zn_Hcp) are consistent in the range 59 to 67 at.% Zn whereas the data of Larsson [117] show more scatter than the values of [102,114,115].

The experimental works of most of the researchers regarding the solubility of Al in Zn are in good agreement with each other. At first, Peirce and Palmerton [121] measured the solubility of Al in Zn using electrical resistivity measurements supplemented by microscopic analysis. Then Auer and Mann [122] used magnetic susceptibility to measure the same phenomena. Lattice parameters were measured by

Fuller and Wilcox [123], Burkhardt [124], Lohberg [125] and Hofmann and Fahrenhost [126], to detect the Zn solvus line. However, the data of Fuller and Wilcox [123] will not be considered in the present assessment due to impurity in the samples and inaccuracy in the experiment. Afterward, Pasternak [127] measured the same using electrical resistivity and they confirmed the earlier works of [121, 122, 124-126].

The thermodynamic and phase equilibrium data were critically assessed by Murray [128] in the early eighties where she attempted to develop a thermodynamic description for this binary system. Two sets of model parameters for the three phases were proposed. However, the calculated phase diagram was not in good accord with the experimental data available in the literature and she did not mention which types of model were used for the different phases. Mey and Effenberg [129] subsequently re-evaluated this system thermodynamically, but their calculated phase boundaries of Al_Fcc$_2$/(Al_Fcc+Zn_Hcp), as well as those for the miscibility gap of the Fcc phase, differ markedly from the experimental values.

Later, at the same time both Mey [130] and Chen and Chang [131] carried out the optimization on this system independently using newly available SGTE (Scientific Group Thermodata Europe) database for the lattice stabilities of the elements. Both of them achieved reasonable consistency with the experimental data. However, none of the aforementioned authors considered the short range ordering neither for the liquid nor for the Al-Fcc solid solution phase in their calculations. The calculated phase diagrams of [130] and [131] are shown in Figures 2.16 and Figure 2.17 respectively. The recent evaluation of this system was done by Mathon *et al*. [132] where they used Redlich-

Kistler polynomial [47] to describe the liquid phase along with the terminal solid solution

phases and did not account for the presence of short range ordering either.
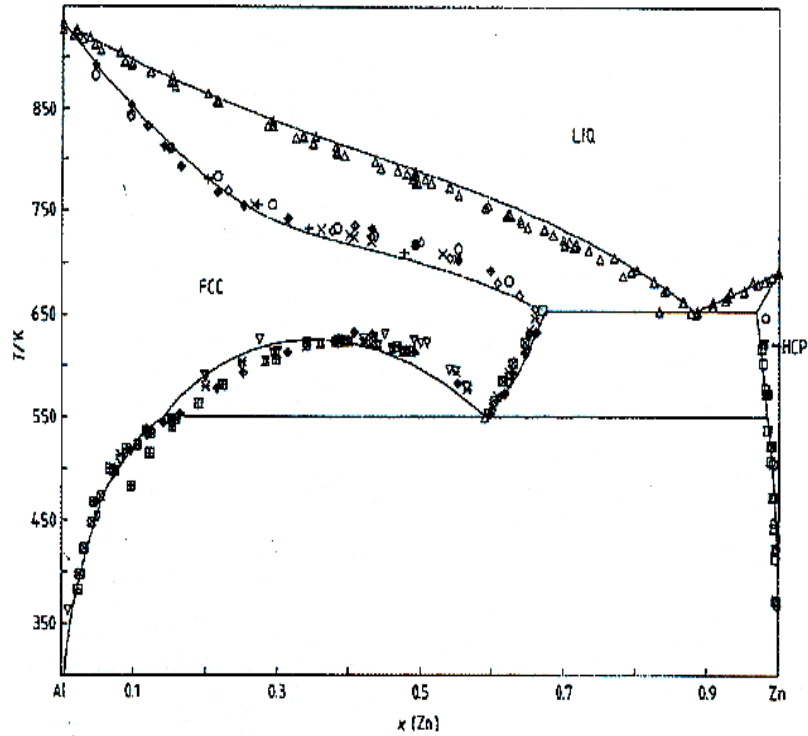
Figure 2.16: *Calculated Al-Zn phase diagram [130]*
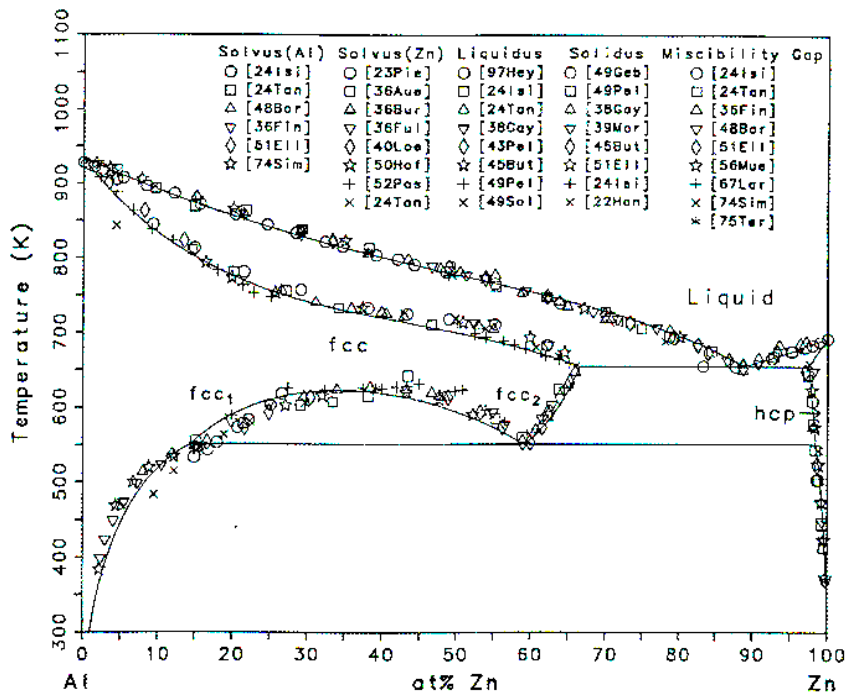
Figure 2.17: *Calculated Al-Zn phase diagram [131]*

2.5.2 Thermodynamic properties

Similar to phase equilibrium studies, a good amount of experimental works investigating the thermodynamic properties both for the liquid phase as well as for the extended solid solution of the Al_Fcc phase have been found in the literature. Enthalpy of mixing over the liquid Al-Zn alloy was performed by Wittig and Keil [133] calorimetrically at 953 K. The same property for the Al_Fcc phase was measured by Hilliard *et al.* [134], Corsepius and Munster [135], Wittig and Schoffl [136] and Connell and Downie [137] where the former two investigators used EMF measuremnts at 653 K and the later two authors [136, 137] used solution calorimeter at 643 K and 637 K, respectively. Poor agreement has been found between the calorimetric data and those from EMF studies, particularly in the composition range 0 to 40 at.% Zn. Although the agreement is better over 40 at.% Zn but the trends in composition of the two sets of data are quite different. Figure 2.18 illustrates the calculated enthalpy of mixing of Mey [130] both for the liquid and solid phase at 953 K and 643 K, respectively. The curve fits well with the experimental values of [133] in the liquid phase but deviates a lot both in terms of magnitude and trend from the experimental results of [136] and [137] for the Al_Fcc solid solution phase.
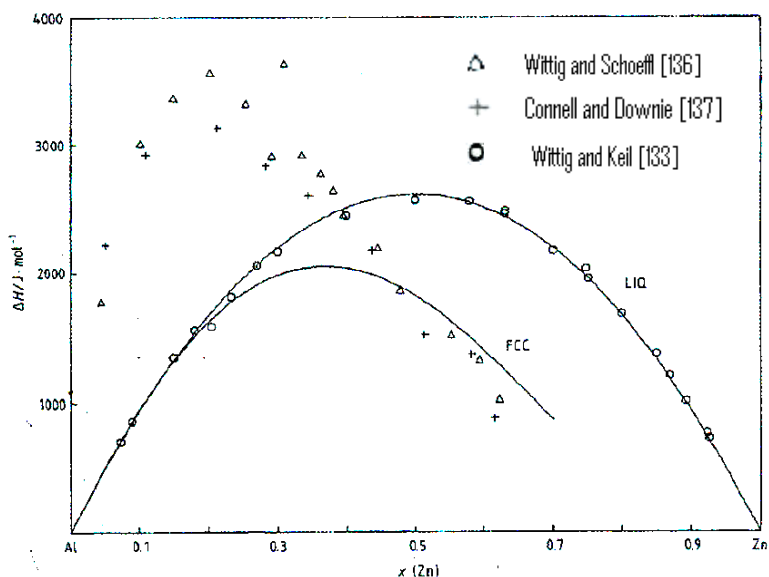
Figure 2.18: *Calculated enthalpy of mixing of liquid at 953K and Fcc phase at 643K [130]*

The activity of Al in the Al-Zn liquid alloys was measured by Batalin and Beloborodova [138] at 960 K, Predel and Schallner [139] at 1000 K and 1100 K and Sebkova and Beranek [140] at 973 K and 1073 K. All of them followed EMF method and their results agree fairly well with each other. The activity of Zn in the liquid phase was determined by Lutz and Voigt [141] at 1000 K, Bolsaitis and Sullivan [142] at 1076 K and later, by Yazawa and Lee [143] at 1073 K. Both Lutz and Voigt [141] and Yazawa and Lee [143] measured the vapor pressure over a number of liquid alloys using the dew point method. Whereas, the activity of Zn was determined by Bolsaitis and Sullivan [142] using the isopiestic technique. The activities both for the Al and Zn were calculated by Nayak [144] afterward, using iso-peribol calorimeter but did not provide any numerical values and hence will not be considered in the present calculation. Chen and Chang [131] calculated the partial Gibbs energy in the liquid phase at 1000 K and agree well with the experimental values as shown in Figure 2.19.
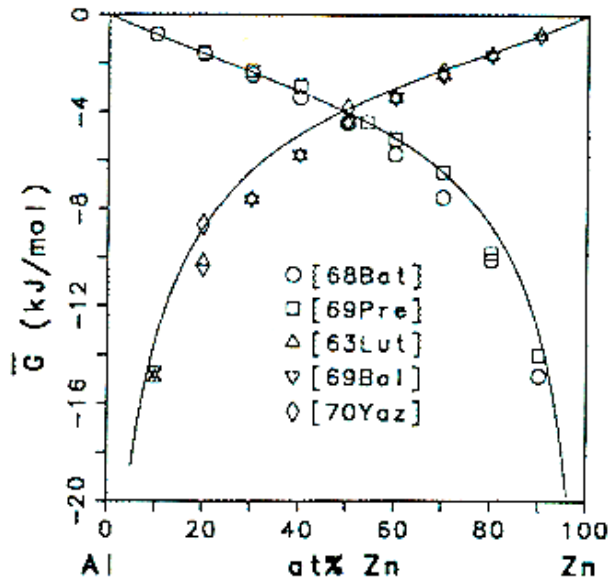
Figure 2.19: *Calculated partial Gibbs energy of liquid at 1000K with the experimental data of [131]*

The activity of Al in the solid Al_Fcc phase was measured by Ptak and Zabdyr [145] and Miller *et al.* [146] using EMF method at 653 K and 703 K, respectively, while that of Zn was determined by Piacente *et al.* [147] by measuring the partial pressure of Zn using a multiple rotating Knudsen source coupled with a mass spectrometer at 660 K, and by atomic absorption by Takahashi and Asano [148] at 653 K.

Earlier, both Hilliard *et al.* [134] and Corsepius and Munster [135] measured the partial Gibbs energy of Al in the Fcc solid solution phase at 653 K using the EMF method where their results show reasonable agreement with each other and will be used in the present work. In addition, Hilliard *et al.* [134] determined the partial enthalpy of Al in the solid phase at 653 K. Chen and Chang [131] calculated the partial Gibbs energy of the Al_Fcc solid solution phase at 653 K as shown in Figure 2.20. It can be seen form the same figure that their calculated results show good consistency with the experimental values for Al but show large deviation from those of [147] and [148] for Zn.
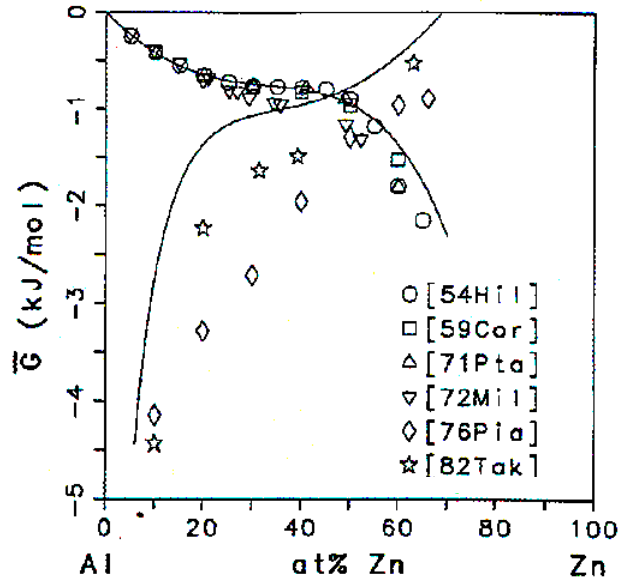
Figure 2.20: *Calculated partial Gibbs energy of* Al_Fcc solid phase *at 653K with the experimental data of [131]*

2.6   Al-Ca Binary System

The Al-Ca binary system is an important subsystem in the family of creep resistant Mg-based alloys. Several research groups [149, 150] worked on this system in the past performing both experimental and modeling studies. The most recent work has been done by Aljarrah and Medraj [151] by critically evaluating all the available experimental work. They used the modified quasichemical model for the liquid phase in order to account the presence of short range ordering. Some of their calculated invariant points deviate a bit from the experimental points and will be improved in the course of the present work by modifying the excess Gibbs energy parameters.

2.7   Al-Ca-Zn Ternary System

Limited amount of experimental data could be found in the literature for the Al-Ca-Zn ternary system. Kono *et al.* [152] studied the system using micrography, inverse rate thermal analysis, X-ray diffraction and EPMA analysis. They [152] reported two quasibinary sections between: Al-CaAlZn and Al-CaZn$_{13}$. But they indicated congruent melting of the compound CaZn$_{13}$ in the Al-CaZn$_{13}$ section. Their reported melting point for the CaZn$_{13}$ compound was higher by almost 60 K than the value found in the literature [69, 70] where it was reported as an incongruently melted compound. They also reported two ternary compounds: CaAlZn and CaZnAl$_3$ where the first one melted congruently and the latter formed by peritectic reaction from the liquid and the CaAlZn phase at 1129 K. Figures 2.21 and 2.22 show their quasibinary sections.
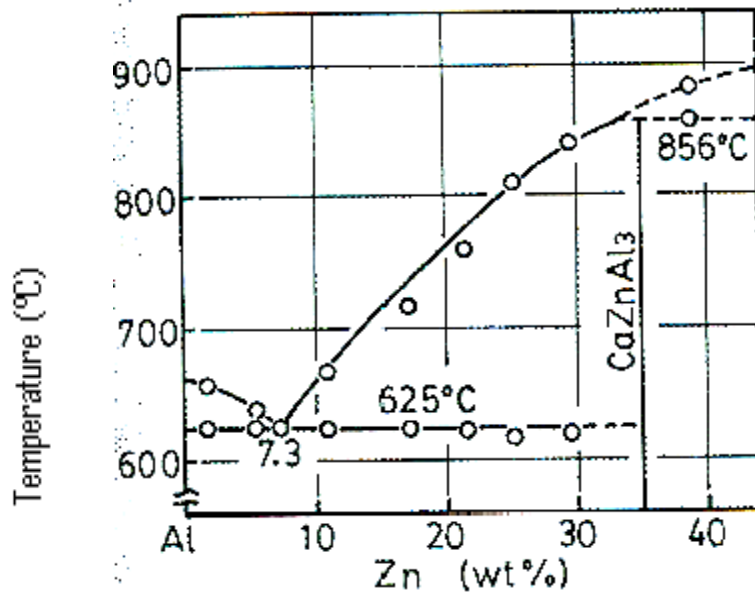
Figure 2.21: *The quasibinary section between Al and CaAlZn [152]*
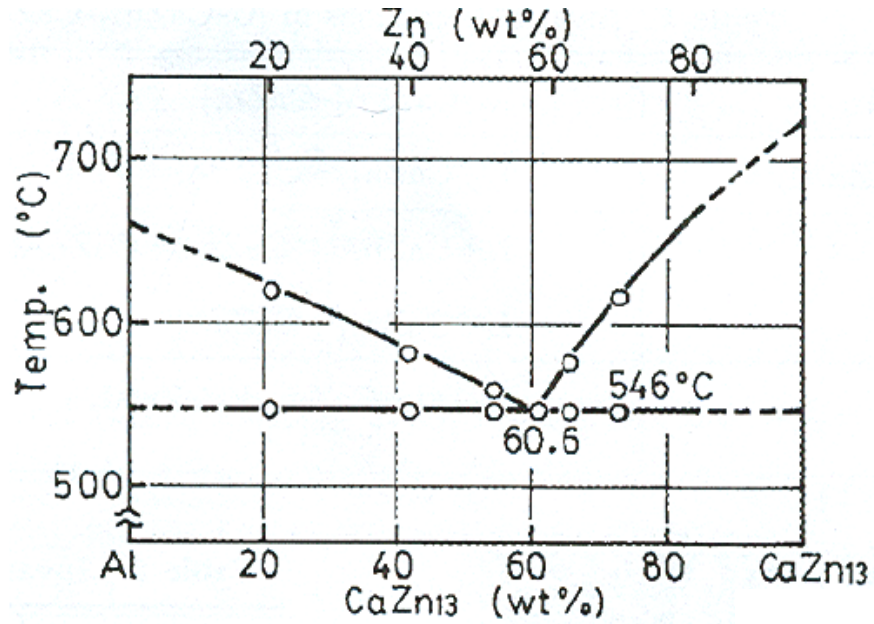
Figure 2.22: *The quasibinary section between Al and CaZn_{13} [152]*

Almost at the same time, Cordier *et al*. [153] determined the crystal structure of a new ternary compound $CaAl_2Zn_2$ which is different from $CaZnAl_3$ reported by [152]. The crystal structure of this new ternary compound is given in Table 2.2.

Table 2.2: *Crystallographic data for the CaAl_2Zn_2 phase*

Phase	Crystal structure	Pearson symbol	Space group	Lattice parameters(nm)		Ref.
				a	c	
$CaAl_2Zn_2$	Tetragonal	*tI*10	*I4/mmm*	0.4127	1.167	[153]

Later, Prince [154] assessed the system based on the work of Kono *et al*. [152] but he did not mention the details about the thermodynamic model in his work. He mainly focused on the Al-Zn side of the phase diagram. The tentative representation of liquidus surface reported by Prince [154] can be seen in Figure 2.23.

40
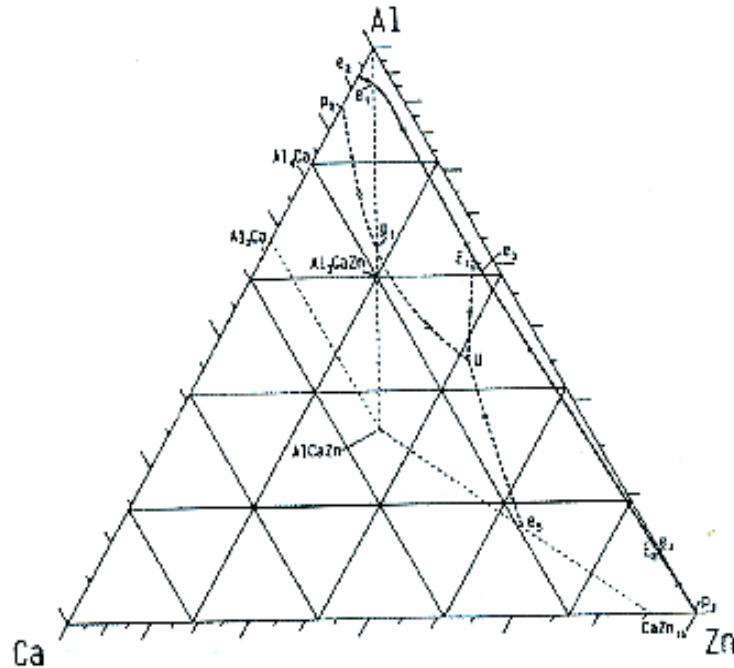
Figure 2.23: *A tentative Al-Ca-Zn liquidus projection [154]*

After that, Ganiev *et al*. [155] used differential thermal analysis (DTA), XRD and metallographic analysis to study the Al-Ca-Zn system and reported two compounds: $CaAlZn$ and $CaAl_2Zn_2$ which undergo congruent melting.

The most recent work on this system has been conducted by Gantsev *et al*. [156] using the metallographic analysis. They mentioned several pseudo-binary sections mainly located adjacent to the Al-Zn side. Like Ganiev *et al*. [155], they [156] reported two ternary compounds: $CaAlZn$ and $CaAl_2Zn_2$ in their work.

Since it is found that the existence of the ternary compound $CaAlZn$ has been confirmed by all the prior researchers, it will be considered in the current optimization. On the other hand, Kono *et al*. [152] reported a second ternary compound $CaZnAl_3$ which was different from $CaAl_2Zn_2$ reported by Ganiev *et al*. [155] and Gantsev *et al*. [156] in terms of composition. Moreover, the crystal structure of $CaAl_2Zn_2$ was also confirmed by Cordier *et al*.[153]. Hence $CaAl_2Zn_2$ compound is included in the Al-Ca-Zn system.

41

The only thermodynamic description of this system was reported by Zhong [157] who modeled the system by simply extrapolating the constituent binaries and did not consider any ternary compound in his work. Figure 2.24 shows the calculated liquidus projection of Zhong [157]
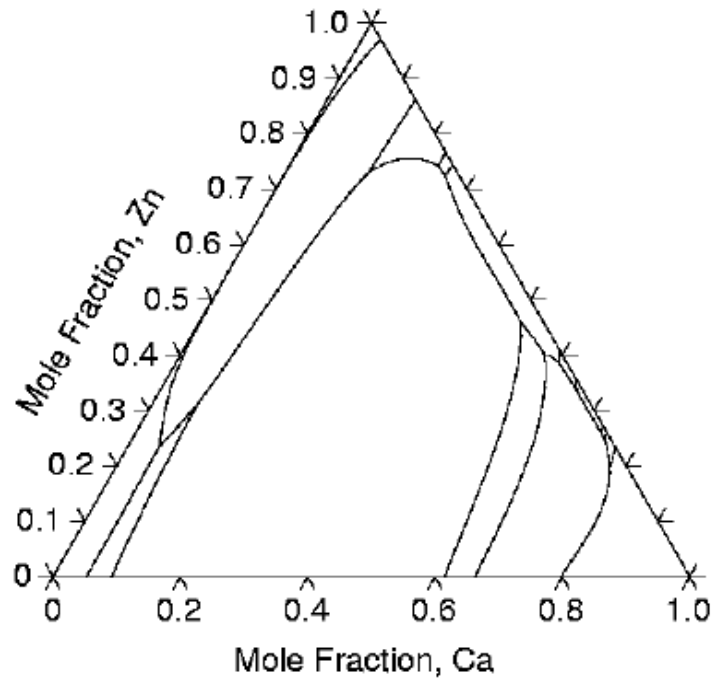
Figure 2.24: *Liquidus projection of the Al-Ca-Zn system [157]*

CHAPTER 3

Thermodynamic Modeling

3.1 Methodology of Thermodynamic Modeling

Thermodynamic modeling is a process of finding appropriate Gibbs energy equations for different phases in terms of temperature and composition of the constituent elements. The Gibbs free energy, G, is thus a function of T, P and the number of moles of all the species present in the system, i.e.,

$$G = G\ (T,\ P,\ n_i, n_j, n_k, \ldots\ldots\ldots) \quad \ldots\ldots\ldots\ldots\ldots\ldots\ldots\ldots\ldots\ldots\ldots\ldots \text{(3.1)}$$

Where T and P are temperature and pressure and $n_i, n_j,\ n_k \ldots..$ are the number of moles of the species $i, j, k, \ldots$ present in the system.

The minimization of the total Gibbs energy is imperative to calculate the phase equilibria in a multicomponent system [1] and it can be described as the sum of Gibbs energy of all phases multiplied by their mole fractions, i.e.,

$$G = \sum_{i=1}^{p} n_i G_i^{\phi} = \text{minimum} \quad \ldots\ldots\ldots\ldots\ldots\ldots\ldots\ldots\ldots\ldots\ldots.. \text{(3.2)}$$

Where n_i is the number of moles, p is the number of phases and G_i^{ϕ} is the Gibbs energy of phase i. G_i^{ϕ} for the multicomponent system can be defined as:

$$G_i^{\phi} = G^o + G^{ideal} + G^{ex} \quad \ldots\ldots\ldots\ldots\ldots\ldots\ldots\ldots\ldots\ldots\ldots\ldots.. \text{(3.3)}$$

Where G^0 corresponds to the mechanical mixing of pure components, G^{ideal} is the contribution of ideal mixing and G^{ex} is the excess Gibbs energy contribution due to the

interactions between the components. To expand the individual terms in equation 3.3, let us consider a binary system with components *A* and *B*. Thus the mechanical and ideal mixing contribution of this system can be expressed as follows:

$$G^0 = x_A G_A^0 + x_B G_B^0 \qquad \text{………………………………………} (3.4)$$

$$G^{ideal} = H_{mix}^{ideal} - T \, S_{mix}^{ideal} \qquad \text{………………………………………} (3.5)$$

Where x_A and x_B are the molar compositions of the components A and B, G_A^0 and G_B^0 are the Gibbs free energy of pure components A and B at standard state (298.15K and 1 bar).

For ideal mixing, the contribution of ideal enthalpy of mixing, H_{mix}^{ideal}, is zero since there is no change in bond energy or volume upon mixing. Hence equation 3.5 becomes,

$$G^{ideal} = -T \, S_{mix}^{ideal}$$
$$= -RT(x_A \ln x_A + x_B \ln x_B) \quad \text{…………………………………}. (3.6)$$

Where *R* is the universal gas constant. The mathematical expression of the excess Gibbs energy, G^{ex} is different for different models and will be described later in this chapter.

3.1.1 The CALPHAD Approach

The CALPHAD (CALculation of PHAse Diagram) approach pioneered by Kaufman and Bernstien [4], is based on the fact that a phase diagram is a representation of the thermodynamic properties of a system. Hence, if the thermodynamic properties are known, it would be possible to calculate the multicomponent phase diagrams. The CALPHAD method is considered to be not only completely general and extensible but also scientifically sound for optimization. The basic flowchart of this method is illustrated in Figure 3.1.
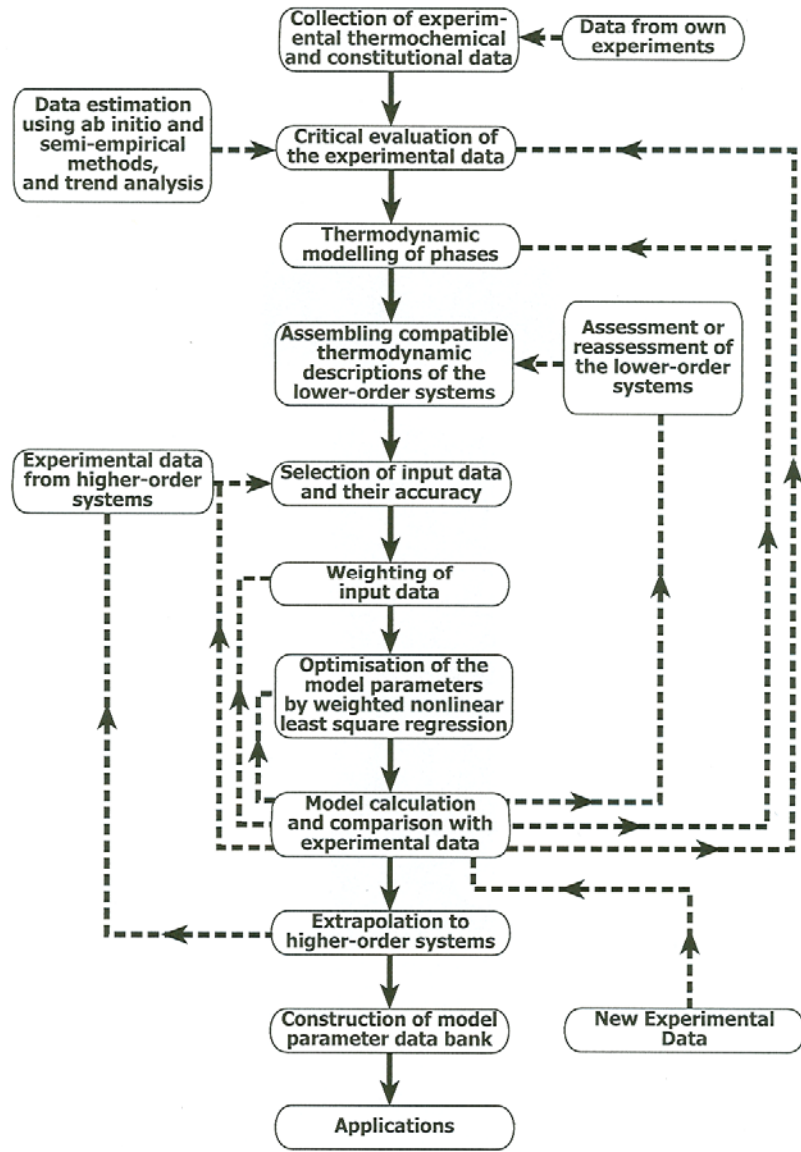
Figure 3.1: Flowchart of the CALPHAD method [158]

The initial step of thermodynamic modeling and optimization according to CALPHAD method is to collect and classify experimental data relevant to Gibbs energy as input. Literally, constitutional and thermochemical results are the data collected from the literature and used in this work. Crystallographic information is also useful for modeling the Gibbs energy especially for the order phases [158]. The second step is to critically evaluate the already collected experimental data to remove inconsistency and

contradiction. Also, unreliable experimental data should be identified and eliminated in this stage as discussed in the previous chapter. The following step is the selection of a suitable thermodynamic model for each phase in such a way that the selected model should be physically sound and it should be able to represent the *P-T-x* domain in which the phase is stable. In addition, the model should have reasonable extrapolation characteristics in the higher order systems. During optimization, it is important to select the initial input data set appropriately and it is better to assign a weighting factor based on the accuracy of the measurement technique and equilibrium condition.

The next step is to determine the model parameters using the experimental data through reproducing the phase diagram and thermodynamic properties and to verify the consistency between the calculations and the experimental data. Continuous iteration is needed until a reasonable agreement with the experimental points is achieved. After successful optimization of the binaries, the excess Gibbs energy parameters will be then used to calculate the higher order systems by extrapolation. If experimental data for higher order systems are available, then higher order model parameters with small magnitude may also be used to ensure consistency with the experimental data. It is important to select a suitable geometrical model for reliable extrapolation. Nowadays, several software packages are available to perform this thermodynamic calculation more easily and accurately. FactSage 5.5 program [159] has been used in the present work.

3.2 Analytical Description of the Thermodynamic Models Employed

Different models are used for different phases based on the characteristics of each individual phase. The mathematical expression of these models is described here.

3.2.1 Unary Phases

For pure element i, the Gibbs energy function in a certain phase ϕ is described as a function of temperature by the following equations [160]:

$$G_i^\phi(T) - H_i^{SER} = a + bT + cT \ln T + dT^2 + eT^3 + fT^{-1} + gT^7 + hT^{-9} \ldots\ldots\ldots (3.7)$$

Where the left hand side of the equation is defined as the Gibbs energy relative to a standard element reference state (SER), where H_i^{SER} is the enthalpy of the element in its stable state at 298.15 K. The values of the coefficients a to h are taken from the SGTE (Scientific Group Thermodata Europe) compilation of Dinsdale [160]

3.2.2 Stoichiometric Phases

Due to strong chemical bonding between atoms, most of the intermettalic phases appear in the phase diagram with highly ordered atomic orientation. The Gibbs energy function of the binary stoichiometric phase can be given by

$$G^\phi = x_i \, {}^0G_i^{\phi_1} + x_j \, {}^0G_j^{\phi_2} + \Delta G_f \quad \ldots\ldots\ldots\ldots\ldots\ldots\ldots\ldots\ldots\ldots\ldots\ldots (3.8)$$

Where x_i, x_j are the mole fractions of components i and j and are given by the stoichiometry of the compound, ${}^0G_i^{\phi_1}$ and ${}^0G_j^{\phi_2}$ represent the Gibbs energy in their standard state and $\Delta G_f = a + bT$ is the Gibbs energy of formation per mole of atoms of the stoichiometric compound where the parameters a and b are obtained by optimization using experimental results of phase equilibria and thermodynamic data.

3.2.3 Disordered Solution Phases

To describe the disordered solution phases present in all the sub-binaries of the Mg-Ca-Zn and Al-Ca-Zn ternary systems, two different types of solution model were used. For all the terminal solid solution phases except the Al_Fcc of Al-Zn system, the random solution model with Redlich-Kister polynomial [47] was used and the Modified Quasichemical Model (MQM) [79-81] was used to describe the liquid phase and Al_Fcc solid solution phase to account the presence of short range ordering.

3.2.3.1 Random Solution Model. Random solution model was used to describe the disorder terminal solid solution phases which can be expressed as:

$$G^\phi = x_i\,{}^0G_i^\phi + x_i\,{}^0G_j^\phi + RT\,[x_i \ln x_i + x_j \ln x_j] + {}^{ex}G^\phi \quad\text{.................. (3.9)}$$

Where ϕ denotes the phase in question and x_i, x_j denote the mole fraction of component i and j, respectively. The first two terms on the right hand side of equation 3.9 represent the Gibbs energy of the mechanical mixture of the components, the third term is the ideal Gibbs energy of mixing, and the fourth term is the excess Gibbs energy, which is described by the Redlich-Kister polynomial model in this work and can be represented as:

$$^{ex}G^\phi = x_i.x_j \sum_{n=0}^{n=m} {}^nL_{i,j}^\phi (x_i - x_j)^n \quad\text{…………………………………... .(3.10)}$$

$$\text{with } {}^nL_{i,j}^\phi = a_n + b_n \times T \qquad (n = 0,1\text{…..m})$$

Where $^nL_{i,j}^\phi$ is the interaction parameters, n is the number of terms, a_n and b_n are the parameters of the model that need to be optimized considering the experimental phase diagram and thermodynamic data.

3.2.3.2 Modified Quasichemical Model. In order to provide a good prediction for the thermodynamic properties of any system, it is necessary to choose the suitable model that describes the excess Gibbs energy. The random solution model is not able to properly represent the binary solutions with short range ordering (SRO) exhibit enthalpy and entropy of mixing functions. Moreover, in this model, the enthalpy and entropy are expressed using independent sets of model parameters without being coupled [161]. Alloy systems which show a strong compound forming tendency (i.e. Ca-Zn, Al-Ca and Mg-Zn system) in the solid state also display a pronounced minimum in the enthalpy of mixing of the liquid phase and this is caused due to the existence of short range ordering [72]. The "associate" or "molecular" model [162] was also proposed to deal with the short range ordering where the model assumes that the some molecules occupy specific atomic positions. But one of the important weaknesses of the "associate" model is its inability to predict the correct thermodynamic properties of ternary solutions when the binary sub-systems exhibit short range ordering [161].

The presence of short-range ordering can be taken into account with bond energy models by considering the interactions between atoms that extend beyond the nearest neighbors approximation. This problem has been treated using modified quasichemical model (MQM) [79-81]. The model is so-called because it has a mass-action equation that is typical in chemical reaction theory.

Some distinct characteristics of the modified quasichemical model are as follows [79-81]:

    i.   It permits the composition of maximum short range ordering in a binary system to be freely chosen.

ii.   It expresses the energy of pair formation as a function of composition which can be expanded as a polynomial in the pair fraction. Also, the coordination numbers are permitted to vary with the composition

iii.   The model can be extended to multicomponent systems.

Let us consider the following pair exchange reaction for further elaboration of the modified quasichemical model

$$(A\text{-}A)_{pair} + (B\text{-}B)_{pair} = 2 (A\text{-}B)_{pair} \; ; \; \Delta g_{AB} \quad \dots\dots\dots\dots\dots\dots \quad (3.11)$$
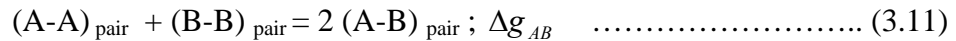
Where (A-B) represents a first-nearest neighbor pair and Δg_{AB} is the nonconfigurational Gibbs energy change for the formation of two moles of (A-B) pairs.

According to Pelton *et al.* [79-81] the molar Gibbs energy of a binary A-B solution is given by:

$$G = (n_A g_A^0 + n_B g_B^0) - T\Delta S^{config} + (\frac{n_{AB}}{2})\Delta g_{AB} \quad \dots\dots\dots\dots\dots\dots \quad (3.12)$$

Here n_A and n_B are number of moles of component *A* and *B*, n_{AB} is the number of moles of *(A-B)* pairs and g_A^o and g_B^o are the molar Gibbs energies of the pure components. The configurational entropy of mixing, ΔS^{config}, can be given by random distribution of the *(A-A)*, *(B-B)* and *(A-B)* pairs and expressed as equation 3.13

$$\Delta S^{config} = -R[n_A \ln(X_A) + n_B \ln(X_B)] - R[n_{AA} \ln(\frac{X_{AA}}{Y_A^2}) + n_{BB} \ln(\frac{X_{BB}}{Y_B^2}) + n_{AB} \ln(\frac{X_{AB}}{2Y_A Y_B})]$$

$$\dots\dots\dots\dots\dots\dots \quad (3.13)$$

Where,

X_A and X_B are the mole fractions of A and B and can be presented as:

$$X_A = \frac{n_A}{n_A + n_B} = 1 - X_B \quad\quad\quad \dots\dots\dots\dots\dots\dots \quad (3.14)$$

And, X_{AA}, X_{BB} and X_{AB} are the pair fractions and can be expressed as in equation 3.15

$$X_{ij} = \frac{n_{ij}}{n_{AA} + n_{BB} + n_{AB}}$$

…..…………............... (3.15)

Y_A and Y_B in equation 3.13 are the coordination equivalent fraction and can be expressed as in equation 3.16.

$$Y_A = \frac{Z_A n_A}{Z_A n_A + Z_B n_B} = \frac{Z_A X_A}{Z_A X_A + Z_B X_B}$$

$$= 1 - Y_B$$

……………………….. (3.16)

Where Z_A and Z_B are the coordination numbers of A and B respectively.

Pelton et al. [79] suggested a modification of equation 3.12 by expanding the term Δg_{AB} as a polynomial in terms of the pair fractions X_{AA} and X_{BB} which can be represented as equation 3.17

$$\Delta g_{AB} = \Delta g^o_{AB} + \sum_{i \geq 1} g^{i0}_{AB} X^i_{AA} + \sum_{j \geq 1} g^{0j}_{AB} X^j_{BB}$$

………………………....(3.17)

Where Δg^o_{AB}, g^{i0}_{AB} and g^{0j}_{AB} are the model parameters to be optimized and can be expressed as functions of temperature ($\Delta g^o_{AB} = a + bT$).

The further modification suggested by [79] is the composition-dependent coordination numbers in order to overcome the drawbacks of the constant coordination numbers. This modification can be expressed as follows:

$$\frac{1}{Z_A} = \frac{1}{Z^A_{AA}} \left(\frac{2n_{AA}}{2n_{AA} + n_{AB}} \right) + \frac{1}{Z^A_{AB}} \left(\frac{n_{AB}}{2n_{AA} + n_{AB}} \right)$$

………………………… (3.18)

$$\frac{1}{Z_B} = \frac{1}{Z^B_{BB}} \left(\frac{2n_{BB}}{2n_{BB} + n_{AB}} \right) + \frac{1}{Z^B_{BA}} \left(\frac{n_{AB}}{2n_{BB} + n_{AB}} \right)$$

..…………………………(3.19)

Here Z_{AA}^{A} and Z_{AB}^{A} are the values of Z_A when all nearest neighbors of an A atom are A's, and when all nearest neighbors of A atom are B's, respectively. Similarly for Z_{BB}^{B} and Z_{BA}^{B}.

The composition of maximum short range ordering is determined by the ratio $\dfrac{Z_{BA}^{B}}{Z_{AB}^{A}}$. Values of Z_{AB}^{A} and Z_{BA}^{B} are unique to the A-B binary system and should be carefully determined to fit the thermodynamic experimental data (enthalpy of mixing, activity etc.). In the case of solid solution, it is required that $Z_{AA}^{A} = Z_{BB}^{B} = Z_{AB}^{A} = Z_{BA}^{B}$ due to their rigid lattice structure. The values of Z_{AA}^{A} and Z_{BB}^{B} are common for all systems containing A and B as components. The coordination number of the pure elements in the metallic solution, $Z_{MgMg}^{Mg} = Z_{CaCa}^{Ca} = Z_{ZnZn}^{Zn} = Z_{AlAl}^{Al}$, were set to be 6. This gave the best possible fit for many binary systems and was also recommended by Pelton *et al*. [79].

For salt or oxide systems where a strong degree of short range ordering usually occurs, this model can be further extended. In these cases the solution can be treated with two sublattices, I and II. One of which is considered to have the species A, B, C……and the other have X, Y, Z…... In a salt system like NaCl-CaCl$_2$ all the cations (Na and Ca) are assumed to reside on sublattice I and the anion (Cl) on sublattice II. For metallic systems like this work only vacancies are considered to reside on the second sublattice and thus the model actually reduces to a single sublattice modified quasichemical model.

3.2.4 Ordered Solid Solution Phases

The Gibbs energy of an ordered solution phase is described by the compound energy formalism [48] which can be expressed as:

$$G = G^{ref} + G^{ideal} + G^{excess} \qquad \text{......................} (3.20)$$

$$G^{ref} = \sum y_i^l y_j^m ....y_k^{q\ 0}G_{(i:j:...:k)} \qquad \text{.......................} (3.21)$$

$$G^{ideal} = RT\sum_l f_l \sum_i y_i^l \ln y_i^l \qquad \text{.....................}(3.22)$$

$$G^{excess} = \sum y_i^l y_j^l y_k^m \sum_{\gamma=0} {}^{\gamma}L_{(i,j):k} \times (y_i^l - y_j^l)^{\gamma} \text{.....................}(3.23)$$

Where $i, j, ...k$ represent components or vacancy, l, m and q represent sublattices. y_i^l is the site fraction of component i on sublattice l. f_l is the fraction of sublattice l relative to the total lattice sites. ${}^0G_{(i:j:..k)}$ represents the energy of a real or hypothetical compound (end member). ${}^{\gamma}L_{(i,j):k}$ represent the interaction parameters between components i and j on one sublattice when the other sublattice is occupied only by k.

3.3 Extrapolation Method for the Ternary System

The thermodynamic phase equilibria of the ternary system can be calculated from the optimized parameters of its corresponding binaries using an extrapolation method. Different "geometric" extrapolation models have been proposed to obtain a constructive ternary system. Among them, the most widely used models are Kohler [163], Muggianu [164] and Toop [165] models where the first two are symmetric models and the last one is an asymmetric model. Where one component is singled out and treated differently. If the binary thermodynamic properties deviate significantly from the regular behavior then

different model will give completely different results. Hence, it is important to choose the right extrapolation model for the right system and it is a matter of experience. In particular, asymmetric models will give better results for some systems, while symmetric models are better for other systems. Figure 3.2 illustrates some of the aforementioned geometric models.
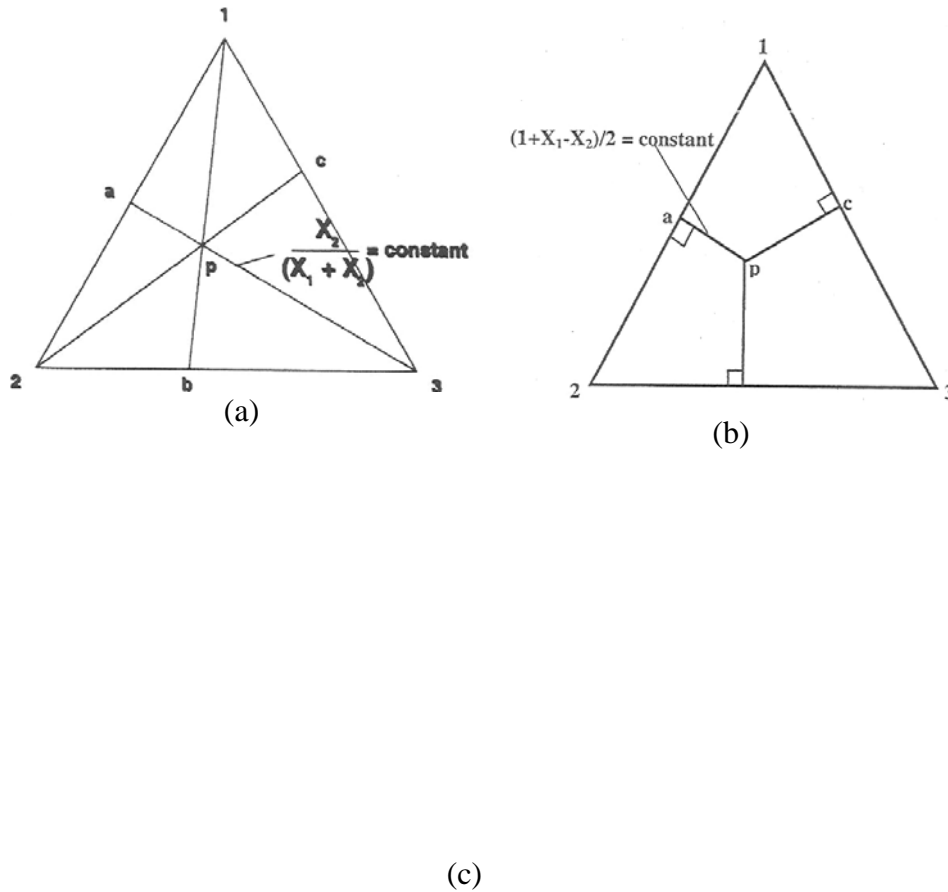
Figure 3.2: *Different "geometric" models for ternary extrapolation: (a) Kohler (b) Muggianu and (c) Toop [166]*

The mathematical expression of the Kohler Model [163], shown in Figure 3.2 (a) can be expressed as follows:
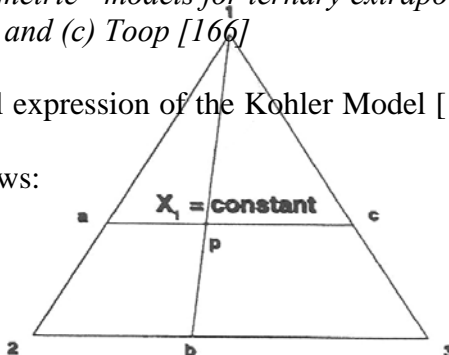
$$\Delta G^E = (x_1 + x_2)^2 \Delta G_{12}^E \left(\frac{x_1}{x_1 + x_2}; \frac{x_2}{x_1 + x_2} \right) + (x_2 + x_3)^2 \Delta G_{23}^E \left(\frac{x_2}{x_2 + x_3}; \frac{x_3}{x_2 + x_3} \right)$$

$$+ (x_3 + x_1)^2 \Delta G_{31}^E \left(\frac{x_3}{x_1 + x_3}; \frac{x_1}{x_1 + x_3} \right)$$

$$\text{.....................(3.24)}$$

Figure 3.2 (b) shows the Muggianu Model [164], which can be expressed by equation 3.24

$$\Delta G^E = \frac{4x_1 x_2}{(1 + x_1 - x_2)(1 + x_2 - x_1)} \Delta G_{12}^E \left(\frac{1 + x_1 - x_2}{2}; \frac{1 + x_2 - x_1}{2} \right)$$

$$+ \frac{4x_2 x_3}{(1 + x_2 - x_3)(1 + x_3 - x_2)} \Delta G_{23}^E \left(\frac{1 + x_2 - x_3}{2}; \frac{1 + x_3 - x_2}{2} \right)$$

$$+ \frac{4x_3 x_1}{(1 + x_3 - x_1)(1 + x_1 - x_3)} \Delta G_{31}^E \left(\frac{1 + x_3 - x_1}{2}; \frac{1 + x_1 - x_3}{2} \right)$$

$$\text{.....................(3.25)}$$

While Toop Model [165] illustrated in Figure 3.2 (c) uses the following expression:

$$\Delta G^E = \frac{x_2}{1 - x_1} \Delta G_{12}^E (x_1; 1 - x_1) + \frac{x_3}{1 - x_1} \Delta G_{13}^E (x_1; 1 - x_1)$$

$$+ (x_2 + x_3)^2 \Delta G_{23}^E \left(\frac{x_2}{x_2 + x_3}; \frac{x_3}{x_2 + x_3} \right)$$

$$\text{.....................(3.26)}$$

In equations 3.23 to 3.25, ΔG^E and ΔG_{ij}^E correspond to the integral molar excess Gibbs energy for ternary and binary systems, respectively, and x_1, x_2, x_3 are the mole fraction of components 1, 2 and 3, respectively.

3.3.1 Ternary Interaction Terms

Ternary model parameters can be included in the calculation if the ternary experimental data are available and identically these parameters do not influence the constituent binary systems. However, without ternary terms the extrapolation should

provide a reasonable first estimation of the ternary molar excess Gibbs energy. Chartland and Pelton [166] proposed the following equations to represent ternary terms for different geometrical models.

For the symmetric Kohler Model:

$$X_1 X_2 \left\{ q_{12(3)}^{ijk} \left(\frac{X_1}{X_1 + X_2} \right)^i \left(\frac{X_2}{X_1 + X_2} \right)^j X_3^k \right\} \qquad \ldots\ldots\ldots\ldots\ldots\ldots(3.27)$$

For the symmetric Muggianu Model:

$$X_1 X_2 \left\{ q_{12(3)}^{ijk} \left(\frac{1 + X_1 - X_2}{2} \right)^i \left(\frac{1 - X_1 + X_2}{2} \right)^j X_3^k \right\} \qquad \ldots\ldots\ldots\ldots\ldots\ldots(3.28)$$

And for the asymmetric Toop Model:

$$X_1 X_2 \left\{ q_{12(3)}^{ijk} (X_i)^i (1 - X_1)^j \left(\frac{X_3}{X_2 + X_3} \right)^k \right\} \qquad \ldots\ldots\ldots\ldots\ldots\ldots(3.29)$$

Where $i \geq 0, j \geq 0$ and $k \geq 1$. $q_{12(3)}^{ijk}$ represents the effect of a third component, 3, on the energy due to the pair exchange reaction (equation 3.11) between component 1 and 2. In the same way in any ternary system 1-2-3 another two terms may be included: terms giving the effect of component 1 upon Δg_{23} and terms giving the effect of component 2 upon Δg_{13}. Here Δg represents the energy for pair exchange reaction between two components.

CHAPTER 4

Results and Discussions

In order to describe the two ternary systems Mg-Ca-Zn and Al-Ca-Zn, in total five constituent binary systems, namely: Mg-Zn, Mg-Ca, Ca-Zn, Al-Zn and Al-Ca are required where the first three binaries contribute to model the ternary Mg-Ca-Zn system and the last three are needed for the Al-Ca-Zn ternary system. The thermodynamic models were kept as simple as possible during optimization by reducing the number of model parameters which eventually reduces the uncertainty during extrapolation to a higher order system. Also the magnitude of the parameters was kept within reasonable limits, not too high or low.

In this chapter, the obtained results regarding the phase diagram and the thermodynamic properties of the aforementioned systems which were optimized simultaneously using FactSage 5.5 software [159], have been described briefly.

4.1   Mg-Zn Binary System

4.1.1 Equilibrium Phase Diagram

Both Agarwal *et al*. [20] and Liang *et al*. [5] who calculated the system so far, did not consider the presence of short range ordering (SRO) during their calculations. According to Terpilowski [53], the maximum short range order in the liquid phase occurs near the composition of Laves phase $MgZn_2$ at around 60 at.% Zn where Hafner [167]

reported the tendency of glass formation in the Mg-Zn system in the composition range of $Mg_{51}Zn_{20}$ and $MgZn_2$ which also indicates the tendency for short range ordering in the liquid phase [168]. Hence it is imperative to re-optimize the system using the appropriate model which can take the presence of short range ordering into consideration.

The liquid phase was modeled using the modified version of the quasichemical model according to equation 3.12 to account the presence of the short range ordering. Therefore according to equation 3.17 the optimized Gibbs energy as a polynomial in terms of pair fraction can be expressed as:

$$\Delta^{ex}G_{MgZn}^{liq} = -8100.84 + 2.26\ T + (-146.3 - 3.55\ T)\ X_{MgMg} + (-79.42 - 4.24\ T)\ X_{ZnZn}\quad J.mol^{-1}$$

.... (4.1)

The tendency of the maximum short range ordering around the composition 60 at.% Zn was achieved by setting the coordination numbers of the pairs $Z_{MgZn}^{Mg} = 6$ and $Z_{MgZn}^{Zn} = 4$.

Since both Mg-hcp and Zn-hcp terminal phases have the same crystal structure which is hexagonal close-packed, both phases were modeled using one set of Gibbs energy description and The Redlich-Kister polynomial [47] was used in this regard. Stoichiometric model was used for all the intermediate phases except Laves phase $MgZn_2$ which was modeled using the compound energy formalism. All the optimized parameters for different phases are shown in Table 4.1. The Gibbs energies of the pure Mg and Zn were taken from Dinsdale's compilation [160] as mentioned earlier.

Table 4.1: *Optimized model parameters for different phases of the Mg-Zn binary system*

Phase	Terms	a (J/mol-atom)	b (J/mol-atom.K)
	Δg_{AB}^{0}	-8100.84	2.26
Liquid	g_{AB}^{i0}	-146.3	-3.55
	g_{AB}^{0j}	-79.42	-4.24
Hcp-phase	$^{0}L^{Mg-hcp,Zn-hcp}$	-2090.19	5.21
Mg$_{51}$Zn$_{20}$	ΔG_{f}	-5276.06	-0.54
Mg$_{12}$Zn$_{13}$	ΔG_{f}	-10440.03	-2.35
Mg$_{2}$Zn$_{3}$	ΔG_{f}	-10877.24	-0.92
Mg$_{2}$Zn$_{11}$	ΔG_{f}	-9882.95	-6.85
	$^{0}G_{Mg:Mg}$	3884.6	0
	$^{0}G_{Mg:Zn}$	-11432.4	0.57
	$^{0}G_{Zn:Mg}$	18991.13	0
	$^{0}G_{Zn:Zn}$	7507.28	0
MgZn$_{2}$	$^{0}L_{Mg,Zn:Mg}^{MgZn_{2}}$	11288.85	0
	$^{0}L_{Mg,Zn:Zn}^{MgZn_{2}}$	11288.85	0
	$^{0}L_{Mg:Mg,Zn}^{MgZn_{2}}$	1.4	0
	$^{0}L_{Zn:Mg,Zn}^{MgZn_{2}}$	1.4	0

The calculated Mg-Zn binary system is shown in Figure 4.1, which shows reasonable agreement with the experimental data from the literature. From the same figure, it can be seen that there are two eutectic points, four peritetic points and all the intermediate compounds melt incongruently except MgZn$_{2}$. A magnified view of Zn rich side of the phase diagram is shown in Figure 4.2 for better illustration with the same experimental data points as in Figure 4.1.
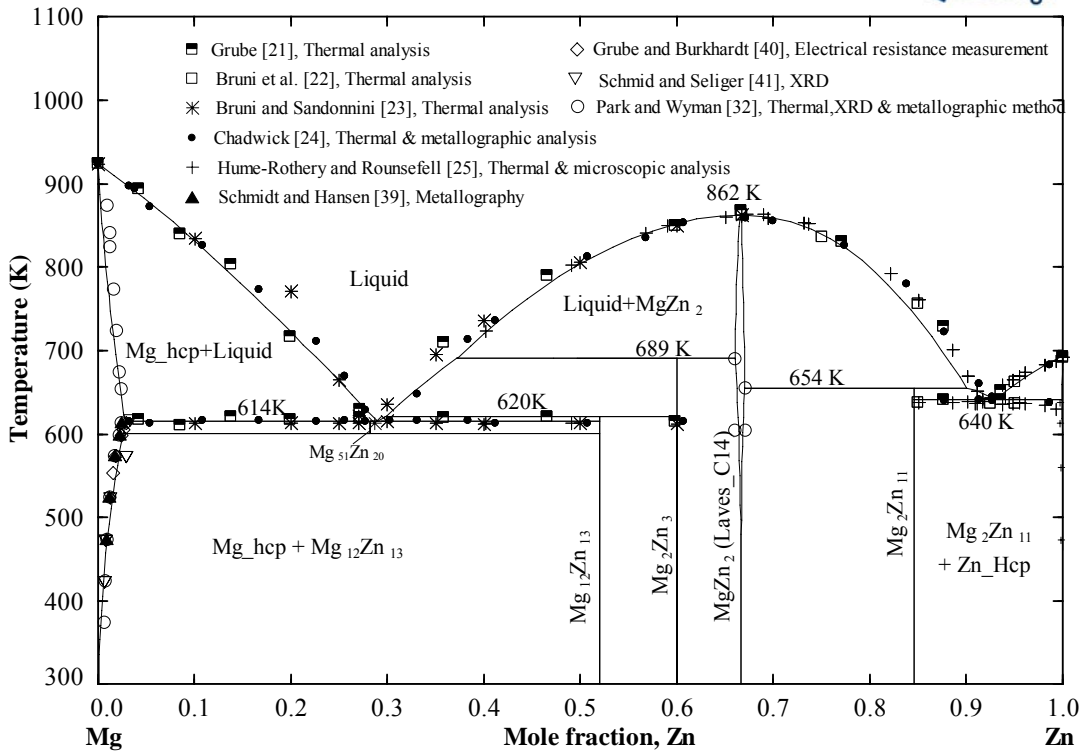
Figure 4.1: *Calculated Mg-Zn phase diagram in comparison with the experimental results from the literature*
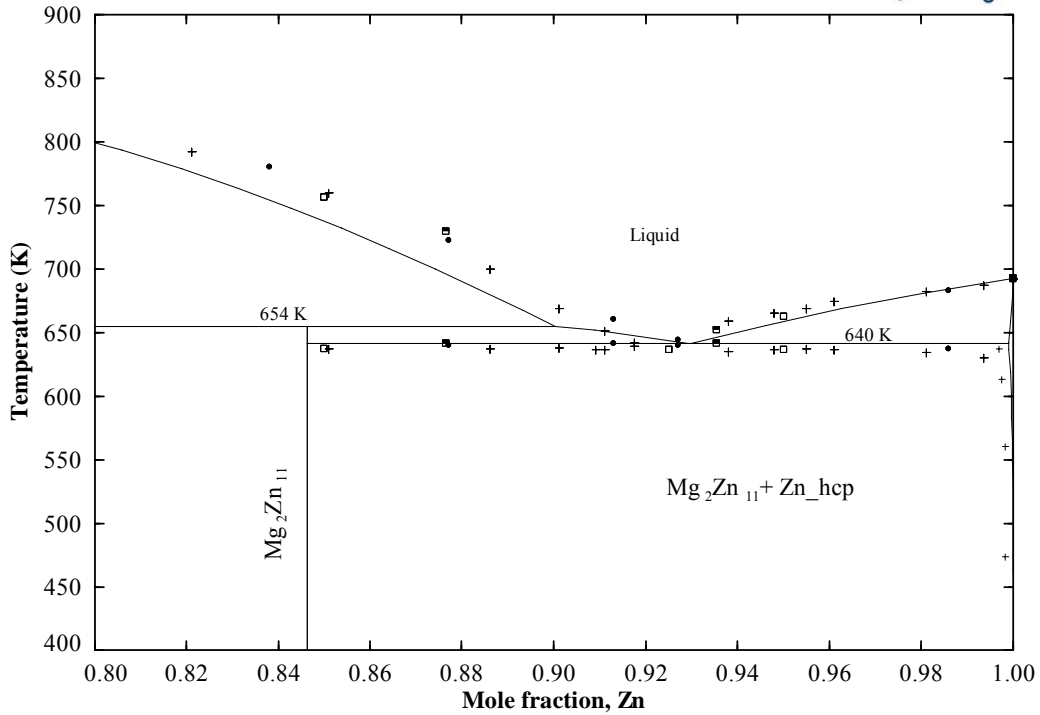
Figure 4.2: *Calculated Zn-rich side of the Mg-Zn phase diagram with experimental results from literature*

The maximum solubility of Zn in Mg was found to be 2.82 at.% Zn which is close to the experimental value of 2.9 at.% Zn reported by Grube and Burkhardt [40].. However, Park and Wyman [32] and Schmidt and Hansen [39] reported this as 2.5 at.% Zn and 2.4 at.% Zn, respectively. Hence, the value from the present calculation lies between the experimental values of [32, 39 and 40]. On the other hand, a very limited solubility of Mg in Zn (0.1 at.% Mg) was observed. This is in the same order of magnitude of the experimental value of Hume-Rothery and Rousefell [25] (0.3 at.% Mg). Moreover, it is worth noting that, both Agarwal et al. [20] and Liang et $al.$ [5] used two Redlich-Kister terms to describe the terminal solid solution whereas in the present work, one Redlich-Kister term was used.

A comparison between the invariant compositions and temperatures resulted from this work and the experimental data from the literature is shown in Table 4.2. The congruent melting temperature of the intermediate compound $MgZn_2$ was found to be 862 K which is in good agreement with most of the experimental data except those of Grube [21], according to whom the value was 868 K which is the highest among all the available experimental data.

Table 4.2: *Comparison between calculated and experimental values of the invariant reactions in the Mg-Zn system*

Reaction type	Reaction	Composition (at.% Zn)	Temperature (K)	Reference
Eutectic	$L \leftrightarrow Mg_{51}Zn_{20} + Mg_{12}Zn_{13}$	28.9	614.0	This work
		-	617.0	[21]
		28.7	613.0	[23]
		30.2	615.5	[24]
		28.1	613.0 ± 1.0	[32]
		30.0	616.0 ± 1.0	[31]
	$L \leftrightarrow Mg_2Zn_{11} + Zn\_Hcp$	92.9	640.0	This work
		-	641.0	[21]
		92.5	636.0	[22]
		-	641.0	[24]
		92.2	637.0	[25]
		92.2	637.0	[32]
Peritectic	$L + Mg\_Hcp \leftrightarrow Mg_{51}Zn_{20}$	28.9	614.0	This work
		28.3	615.0 ± 1.0	[32]
		-	617.0 to 621.0	[31]
	$L + Mg_2Zn_3 \leftrightarrow Mg_{12}Zn_{13}$	29.7	620.0	This work
		-	627.0	[25]
		29.0	620.0 ± 1.0	[32]
		-	622.0 ± 2.0	[31]
	$L + MgZn_2 \leftrightarrow Mg_2Zn_3$	37.1	689.0	This work
		-	683.0 ± 10.0	[34]
		-	689.0 ± 1.0	[32]
		-	683.0 ± 1.0	[31]
	$L + MgZn_2 \leftrightarrow Mg_2Zn_{11}$	90.0	654.0	This work
		-	654.0	[32]
		-	653.5	[25]
Congruent	$L \leftrightarrow MgZn_2$	66.7	862.0	This work
		66.7	868.0	[21]
		66.7	862.0	[23]
		66.7	858.0	[24]
		66.7	863.0	[25]
		66.7	861.0	[32]
Eutectoid	$Mg_{51}Zn_{20} \leftrightarrow Mg\_Hcp + Mg_{12}Zn_{13}$	28.1	599.0	This work
		-	598.0	[33]

4.1.2 Thermodynamic Modeling of the MgZn₂ (Laves_C14) phase

At first approximation, the Laves phase was modeled as a linear compound using the stoichiometric model. Once a satisfactory thermodynamic description was obtained for the whole system, especially the liquid phase, the Laves phase was again remodeled as a solid solution using sublattice model.

According to Hari Kumar and Wollants [158], attention should be given to the crystallographic information and the solubility range of the phase during modeling of a solid solution using the sublattice model. Only Park and Wyman [32] mentioned the homogeneity range for the phase. The crystallographic data of this phase is taken from [45] and summarized in Table 4.3.

Table 4.3: *Crystallographic data for the Laves_C14 phase [45]*

Phase	Crystal data		Atoms	WP[1]	CN[2]	PS[3]	Atomic position		
							X	Y	Z
Laves_C14 (MgZn$_2$)	Structure type	MgZn$_2$	Mg	4f	16	3m	0.333	0.666	0.063
	Pearson symbol	hP12	Zn1	2a	12	$\bar{3}$	0	0	0
	Space group	P6$_3$/mmc	Zn2	6h	12	mm2	0.830	0.660	0.250
	Space group no.	194							
	Lattice parameter (nm)	a=0.518 c=0.852							
	Angles: α=90, β=90, γ=120								

[1]*WP = Wyckoff Position,* [2]*CN = Coordination Number,* [3]*PS = Point Symmetry*

The coordination numbers shown in Table 4.3 are obtained in this work. It is defined as the number of nearest similar and dissimilar atoms around the atom of interest [169]. PowderCell software [170] along with the available crystallographic information from Table 4.3, are used to determine the substructure of the MgZn$_2$ phase as shown in Figure 4.3, in order to model this phase using sublattice model. The unit cell of the MgZn$_2$ phase is also shown in the same figure.

(a)

(b)   (c)   (d)

  = Mg   = Zn1   = Zn2   ★ = Atom of interest
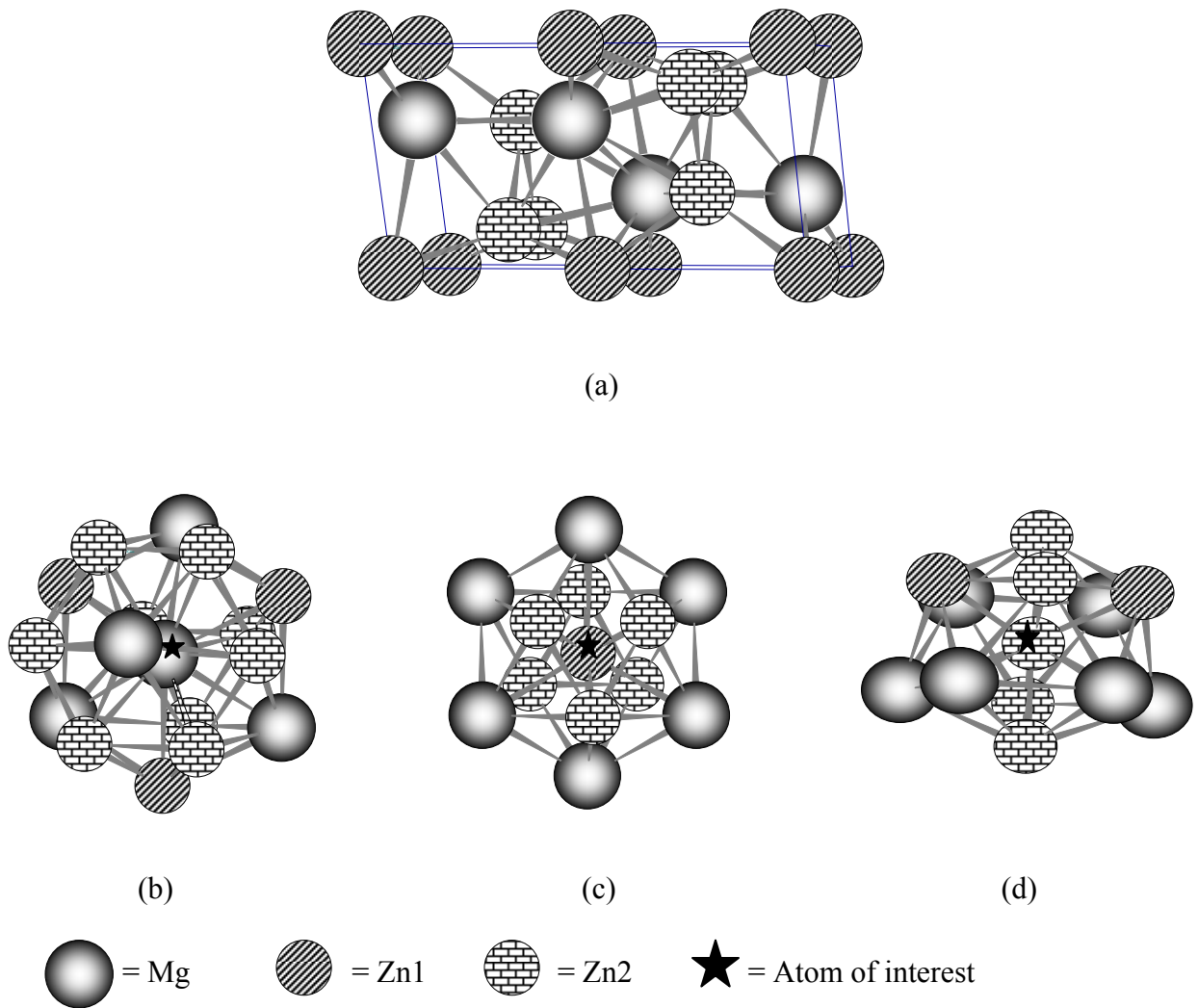
Figure 4.3: (a) Unit cell of MgZn₂, Substructure of (b) Mg atom with CN=16, (c) Zn1 atom with CN=12 and (d) Zn2 atom with CN=12

In the unit cell of $MgZn_2$ phase, as shown in Figure 4.3, atoms are distributed among the three crystallographically distinct lattice sites with 16, 12, 12 coordination numbers, respectively. Here the larger Mg atom prefer sites with higher coordination number (16) whereas smaller Zn atom prefer lattice sites with smaller coordination number (12).

An intermediate phase usually has ideal stoichiometry where each sublattice is occupied with only one constituent species. Hence, at first the sublattice model for the $MgZn_2$ phase can be represented by three sublattices:

$$(Mg)_4 :(Zn1)_2 :(Zn2)_6$$
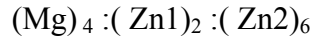
According to Hari Kumar and Wollants [158] the number of sublattices can be reduced by grouping the sublattices together with similar crystallographic characteristics such as same point symmetry criteria and/or same coordination number. As the simplified version is more practical from modeling point of view the sublattice Zn1 and Zn2 are combined as they have the same coordination number.

$$(Mg)_4 :(Zn)_8$$

$$(Mg)_1 :(Zn)_2$$
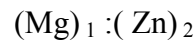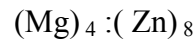
In reality, in order to model the homogeneity range some atoms in the sublattices should be allowed to mix. For an intermediate phase having a narrow homogeneity range like $MgZn_2$ phase, the mixing is performed by "defects" which may be vacancies or anti-structure atoms (i.e. atoms in the lattice sites belonging to the other kinds of atoms in the ideal structure). Because of the close packed structure of the $MgZn_2$ phase antistructure atoms are more appropriate as defects than vacancies [169]. Based on that the mixing of Zn atom in the Mg sublattice and Mg atom in the Zn sublattice has been allowed and the resulting model is:

$$(Mg\%,Zn)_{.3333}:(Mg,Zn\%)_{.6667}$$
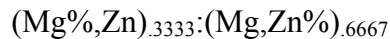
Here '%' denotes the major constituents of the sublattice. This intermediate phase having narrow solubility range can be modeled as Wagner-Schottky phase [171]. This model of two sublattices covers the whole composition range and therefore the

homogeneity range of $0.66 \le x_{Zn} \le 0.671$ which was reported by Park and Wyman [32] could be obtained from this model for $MgZn_2$ phase. Hence the Gibbs energy per mole of formula unit can be written as:

$$G_m^{MgZn_2} = y_{Mg}^I\, y_{Mg}^{II}\; ^0G_{Mg:Mg}^{MgZn_2} + y_{Mg}^I\, y_{Zn}^{II}\; ^0G_{Mg:Zn}^{MgZn_2} + y_{Zn}^I\, y_{Mg}^{II}\; ^0G_{Zn:Mg}^{MgZn_2} + y_{Zn}^I\, y_{Zn}^{II}\; ^0G_{Zn:Zn}^{MgZn_2}$$

$$+ RT\,(0.333 \sum_{i=Mg}^{Zn} y_i^I \ln y_i^I + 0.667 \sum_{i=Mg}^{Zn} y_i^{II} \ln y_i^{II}) + y_{Mg}^I\, y_{Zn}^I\,(y_{Mg}^{II}\; ^0L_{Mg,Zn:Mg}^{MgZn_2} + y_{Zn}^{II}\; ^0L_{Mg,Zn:Zn}^{MgZn_2})$$

$$+ y_{Mg}^{II}\, y_{Zn}^{II}\,(y_{Mg}^I\; ^0L_{Mg:Mg,Zn}^{MgZn_2} + y_{Zn}^I\; ^0L_{Zn:Mg,Zn}^{MgZn_2})$$

….…..………….... (4.2)

Where, the last two terms on the right hand side of equation 4.2 represents the excess Gibbs energy term, i is the lattice species and y_{Mg}^I, y_{Zn}^I, y_{Mg}^{II} and y_{Zn}^{II} are the species concentrations of Mg and Zn on sublattices I and II and $^0G_{Mg:Mg}^{MgZn2}$, $^0G_{Mg:Zn}^{MgZn_2}$, $^0G_{Zn:Mg}^{MgZn_2}$ and $^0G_{Zn:Zn}^{MgZn_2}$ can be visualized as the Gibbs energies of the end member phases. The end member phases are formed when each sublattices is occupied only by one kind of species and can be either real or hypothetical [1].

The interaction parameters within the sublattice can be expressed as:

$$^0L_{Mg,Zn:Mg}^{MgZn_2} = {}^0L_{Mg,Zn:Zn}^{MgZn_2} = \sum_{n=0}[(a_n + b_n T)(y_{Mg}^I - y_{Zn}^I)^n] \quad \text{.......................................(4.3)}$$

$$^0L_{Mg:Mg,Zn}^{MgZn_2} = {}^0L_{Zn:Mg,Zn}^{MgZn_2} = \sum_{n=0}[(a_n + b_n T)(y_{Mg}^{II} - y_{Zn}^{II})^n] \quad \text{.......................................(4.4)}$$

$^0G_{Mg:Mg}^{MgZn_2}, {}^0G_{Mg:Zn}^{MgZn_2}, {}^0G_{Zn:Mg}^{MgZn_2}, {}^0G_{Zn:Zn}^{MgZn_2}, {}^0L_{Mg,Zn:Mg}^{MgZn_2}, {}^0L_{Mg,Zn:Zn}^{MgZn_2}, {}^0L_{Mg:Mg,Zn}^{MgZn_2},$ and $^0L_{Zn:Mg,Zn}^{MgZn_2}$ are the parameters which were optimized using the sublattice model with the experimental data from the literature. The optimized values of the parameters are mentioned in Table 4.1.

4.1.3 Thermodynamic Properties

The calculated enthalpy of mixing of the Mg-Zn liquid at 981K, shown in Figure 4.4, is in good agreement with the experimental data from the literature except for the small deviation from the data of Agarwal and Sommer [52] at 933 K near the composition range 20 to 55 at.% Zn. However the current results agree well with those of Pyka [51]. It is also worth noting from the same figure that, the minimum value of enthalpy of mixing occurs near 60 at.% Zn which is very close to the value suggested by Terpilowski [53], where maximum short range ordering takes place.
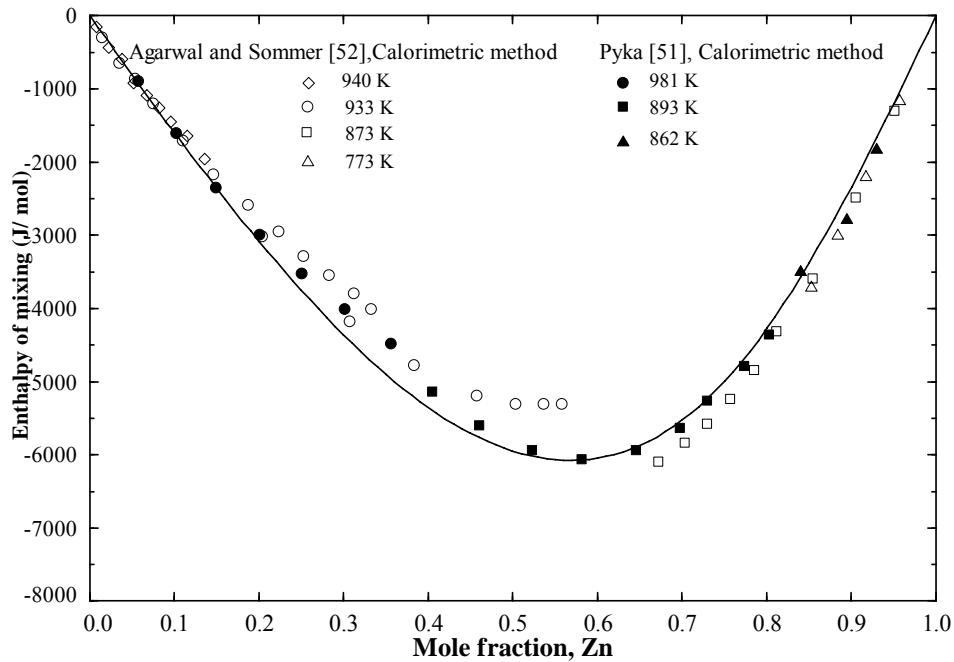
Figure 4.4: Calculated enthalpy of mixing of Mg-Zn liquid at 981 K

The calculated activities of Mg and Zn components over the liquid phase at 923 K and 1073 K are shown in Figure 4.5 where the activity of Mg shows good consistency with the experimental data. Some deviation can be seen between the calculated value and the experimental data of Pogodaev and Lukashenko [56] and Kozuka *et al.* [57] for the activity of Zn near 40 to 80 at.% Zn. This discrepancy is perhaps due to the less accurate

vapor pressure method used by [56] and [57]. However, the calculated activity curve of Zn shows reasonable agreement with the calculated results of Terpilowski [53] where he extracted the values from the activity of Mg using the Gibbs-Duhem equation.
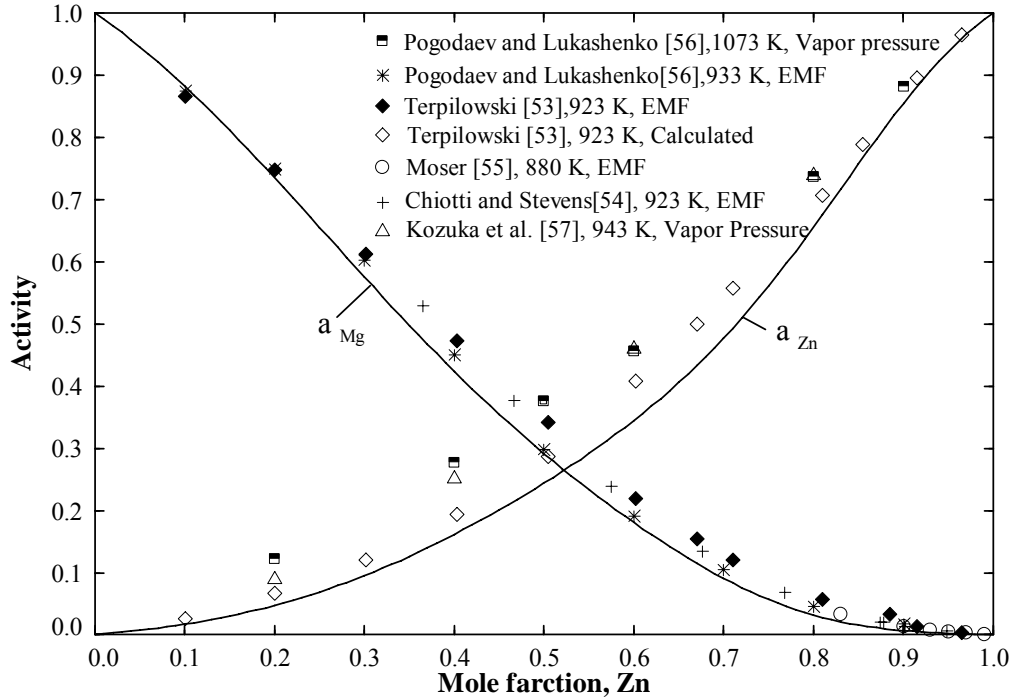
Figure 4.5: *Calculated activity of Mg and Zn (relative to pure liquid Mg and Zn) in Mg-Zn alloys at 923 K and 1073 K, respectively*

Figure 4.6 shows the partial enthalpy of mixing of Mg ($\overline{\Delta H}_{Mg}$) in the Mg-Zn liquid at 923 K in comparison with the experimental results from the literature where good consistency was accomplished.

A comparison between the enthalpy of formation for the intermediate phases and the experimental results from the literature is shown in Figure 4.7; in addition, Table 4.4 demonstrates the numerical values of enthalpy of formation compared with the experimental values. Reasonable consistency was achieved with the experimental values within the error limits. But the enthalpy of formation for Mg_2Zn_{11} phase measured by Pedokand *et al.* [60] is not consistent with the experimental value of Schneider *et al.* [58]

as well as the calculated value in this work. However, the data of Schneider *et al.* [58] is considered more reliable because of the use of reaction calorimetry.
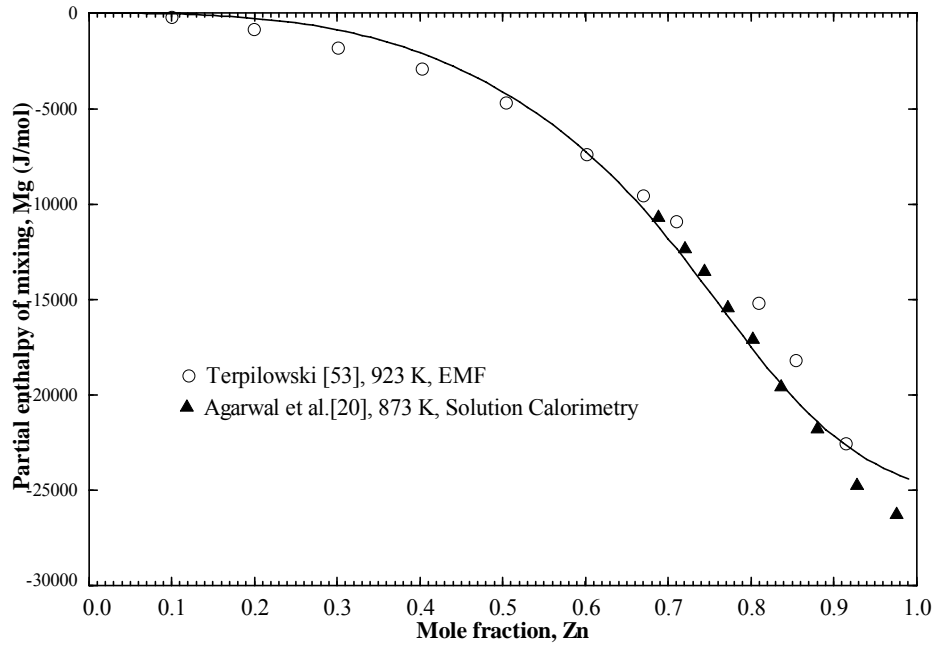
Figure 4.6: *Calculated partial enthalpy of mixing of Mg in the Mg-Zn liquid at 923 K*
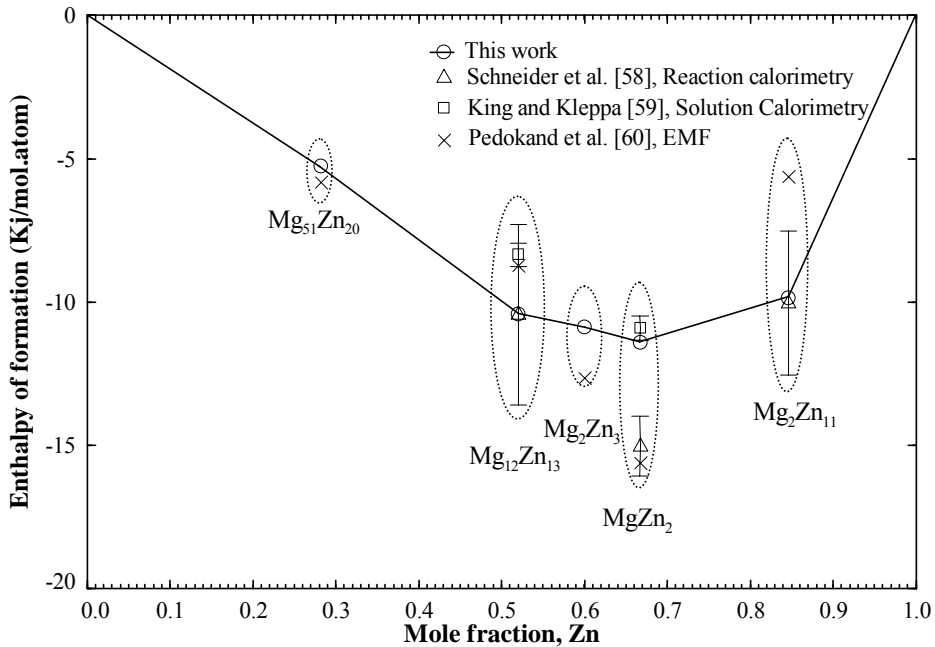
Figure 4.7: *Calculated enthalpy of formation for the intermediate phases of the Mg-Zn system at 298.15 K*

Table 4.4: *Enthalpy of formation for different intermediate phases in comparison with the experimental results*

Composition (at. % Zn)	Intermediate phases	Calculated enthalpy (KJ/mole-atom)	Experimental enthalpy (KJ/mole-atom)	
28.1	$Mg_{51}Zn_{20}$	-5.27	-5.85	[60]
52.0	$Mg_{12}Zn_{13}$	-10.44	-10.45 ± 3.135	[58]
			-8.36 ± 0.418	[59]
			-8.76	[60]
60.0	Mg_2Zn_3	-10.88	-12.67	[60]
66.67	$MgZn_2$	-11.43	-15.04 ± 1.045	[58]
			-10.91 ± 0.418	[59]
			-15.63	[60]
84.6	Mg_2Zn_{11}	-9.88	-10.03 ± 2.508	[58]
			-5.643	[60]

4.2   Ca-Zn Binary System

4.2.1 Equilibrium Phase Diagram

Brubaker and Liu [71] modeled the Ca-Zn system based on the experimental results of Messing *et al.* [69], which is regarded as the only reliable source of experimental data considering the experimental accuracy. They modeled all the phases using a sublattice model without accounting for the presence of short range ordering. They considered the intermediate phase $CaZn_3$ to be melted congruently by taking an assessment of the liquidus data of Messing *et al.* [69] but in that case, the liquidus of $CaZn_3$ on the Ca rich side becomes too flat and according to Okamoto and Massalski [172], this is thermodynamically improbable. In addition, according to Hafner [167], the Ca-Zn system belongs to the class of glass-forming binary metallic systems which indicates the tendency for short range ordering in the liquid phase [168].

Most recently, Spencer *et al.* [72] remodeled the system using modified quasichemical model for the liquid phase. However, their work has just appeared after this system has been modeled in this work. In addition, to build a self-consistent Mg alloy database, an independent re-optimization and thorough assessment on this system has been performed in the present work.

The Modified Quasichemical model was used to describe the liquid phase which accounts for the presence of short range ordering. The peritectic formation of the compound $CaZn_3$ was considered in the present work due to lack of adequate experimental work and also to avoid the unlikely thermodynamic behavior which is also supported by the recent work of Spencer *et al.* [72]. According to equation 3.17 the optimized Gibbs energy for the liquid phase can be written as:

$$\Delta^{ex}G_{CaZn}^{liq} = -17765 + 0.084\ T - 10282.8\ X_{CaCa} - 7942.0\ X_{ZnZn} \quad \text{J/mol} \quad \ldots\ldots\ldots\ldots (4.5)$$

The coordination number for the first nearest neighbors of Ca and Zn atoms ($Z_{CaCa}^{Ca}, Z_{ZnZn}^{Zn}$) were set equal to 6. The tendency of maximum short range ordering near the composition of most stable intermediate phase (in this case $CaZn_2$) was obtained by setting $Z_{CaZn}^{Ca} = 6$ and $Z_{CaZn}^{Zn} = 3$. These were determined by iterative process to get the optimum result.

A stoichiometric model was used for all the intermediate phases. For the liquid phase the reference state of the components are Ca-liquid and Zn-liquid and for the stoichiometric phases the reference states are Ca_Bcc and Zn_Hcp, respectively. Neither Ca nor Zn displays any solubility in one another and hence terminal solid solubility was not included in the present work. Table 4.5 shows all the optimized parameters for different phases.

Table 4.5: *Optimized model parameters for different phases of the Ca-Zn binary system*

Phase	Terms	a (J/mol-atom)	b (J/mol-atom.K)
Liquid	Δg_{AB}^{0}	-17765.0	0.084
	g_{AB}^{i0}	-10282.8	0
	g_{AB}^{0j}	- 7942.0	0
Ca_3Zn	ΔG_f	-11906.31	-3.82
Ca_5Zn_3	ΔG_f	-14486.92	-0.88
CaZn	ΔG_f	-17842.54	-0.53
$CaZn_2$	ΔG_f	-22728.35	-1.48
$CaZn_3$	ΔG_f	-21418.76	-2.66
$CaZn_5$	ΔG_f	-19997.51	-3.84
$CaZn_{11}$	ΔG_f	-14798.75	-3.62
$CaZn_{13}$	ΔG_f	-14149.64	-4.23

Figure 4.8 shows the optimized phase diagram of the Ca-Zn system along with the experimental results. The whole system has been split into two parts and is shown separately, for better understanding, in Figures 4.9 and 4.10 respectively. The calculated phase diagram shows reasonable agreement with the experimental data from the literature. The allotropic transformation α (Fcc_A1) ↔ β (Bcc_A2) of Ca takes place at 716 K which is the same as the value adopted by Itkin and Alcock [70] during their assessment of this system. The temperatures and phase composition of invariant reactions are presented in Table 4.6. It can be seen from the same table that the maximum difference of temperature between the experimental and calculated results is 6 K which is acceptable within the error limits.
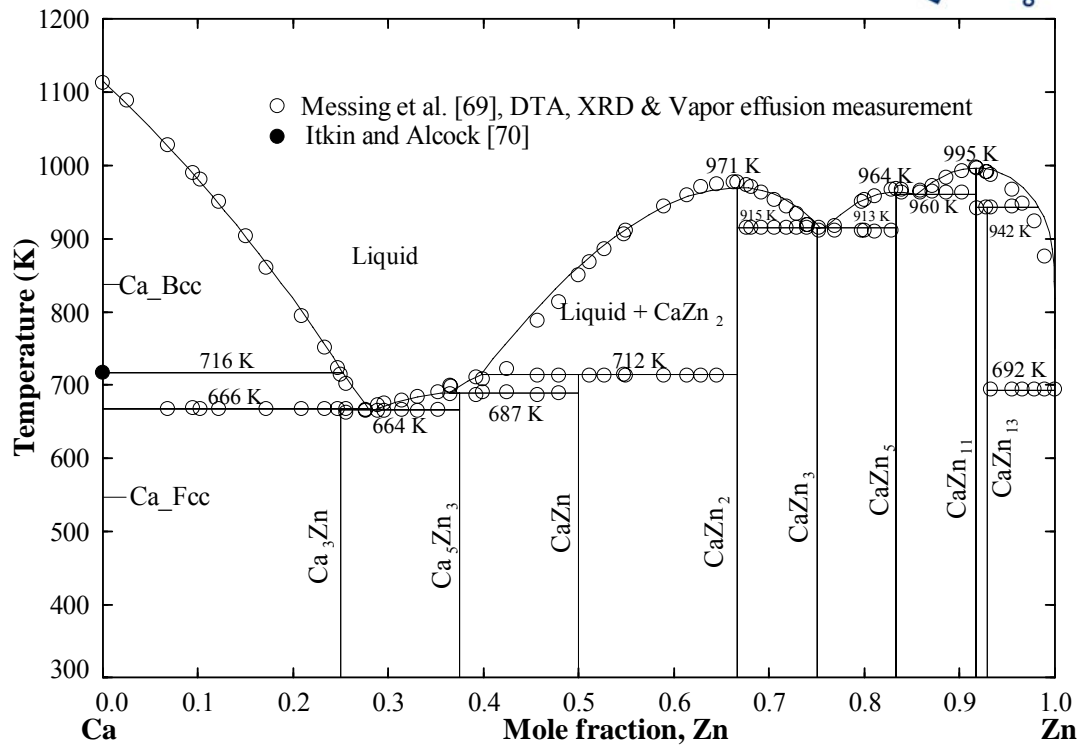
Figure 4.8: *Calculated Ca-Zn phase diagram in comparison with experimental results from the literature*
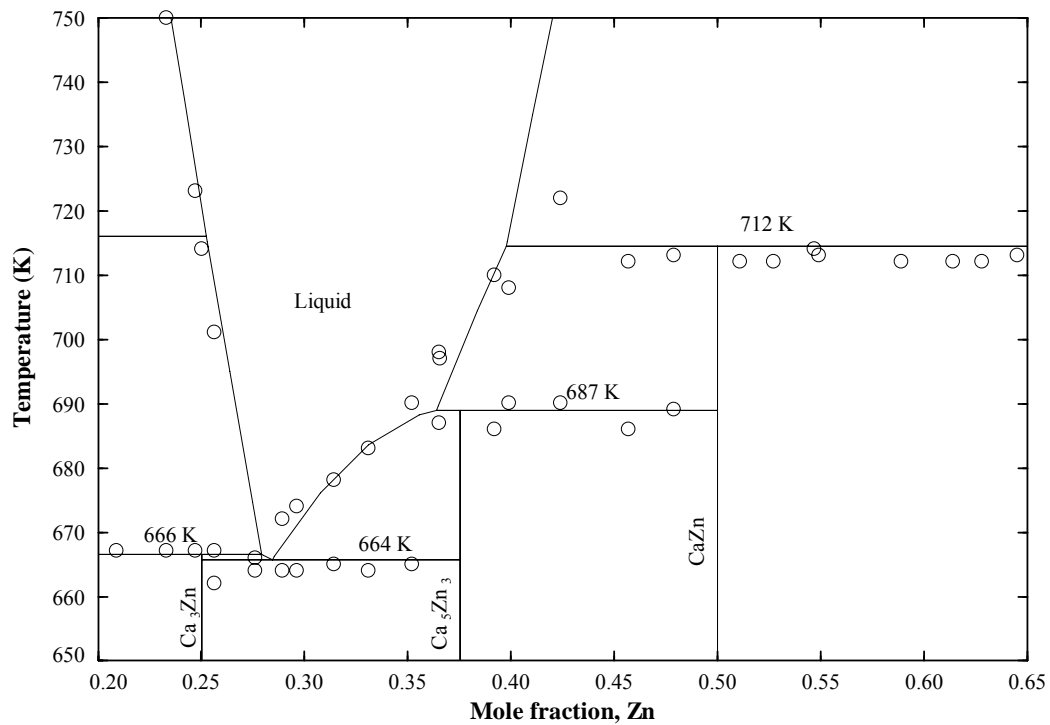
Figure 4.9: *Enlarged portion of the Ca-Zn phase diagram (Ca-rich side)*
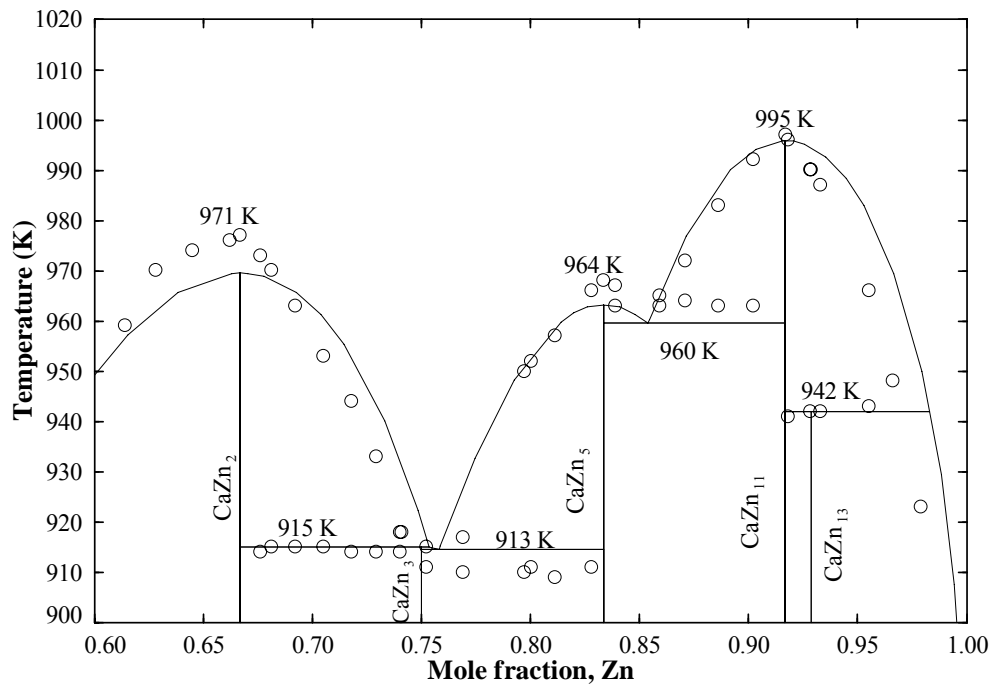
Figure 4.10: *Enlarged portion of the Ca-Zn phase diagram (Zn-rich side)*

Table 4.6: *Comparison between calculated and experimental values of the invariant reactions in the Mg-Zn system*

Reaction type	Reaction	Composition (at.% Zn)	Temperature (K)	Reference
Eutectic	L $\leftrightarrow$ Ca$_3$Zn + Ca$_5$Zn$_3$	28.4	664	This work
		27.4	664	[69]
	L $\leftrightarrow$ CaZn$_3$ + CaZn$_5$	76.0	913	This work
		76.4	911	[69]
	L $\leftrightarrow$ CaZn$_5$ + CaZn$_{11}$	85.4	960	This work
		86.4	963	[69]
Peritectic	L+Ca_Bcc $\leftrightarrow$ Ca$_3$Zn	27.9	666	This work
		-	667	[69]
	L+CaZn $\leftrightarrow$ Ca$_5$Zn$_3$	36.4	687	This work
		-	687	[69]
	L+CaZn$_2$ $\leftrightarrow$ CaZn	39.7	712	This work
		-	712	[69]
	L+CaZn$_2$ $\leftrightarrow$ CaZn$_3$	75.3	915	This work
		-	915	[69]
	L+CaZn$_{11}$ $\leftrightarrow$ CaZn$_{13}$	98.3	942	This work
		-	942	[69]]
Congruent	L $\leftrightarrow$ CaZn$_2$	66.7	971	This work
		66.7	977	[69]
	L $\leftrightarrow$ CaZn$_5$	83.3	964	This work
		83.3	968	[69]
	L $\leftrightarrow$ CaZn$_{11}$	91.7	995	This work
		91.7	997	[69]
Allotropic	Ca_Fcc $\leftrightarrow$ Ca_Bcc	0.0	716	This work
		0.0	718	[69]
		0.0	716	[70]

74

4.2.2 Thermodynamic properties

The calculated activities of Ca and Zn over the Ca-Zn liquid at 1073 K are shown in Figure 4.11 where a reasonable agreement was accomplished between the calculated curves and the experimental points. Comparison is also made with the assessment of Spencer *et al.* [72] in the same figure. Better agreement was not possible without deteriorating the liquidus curve.
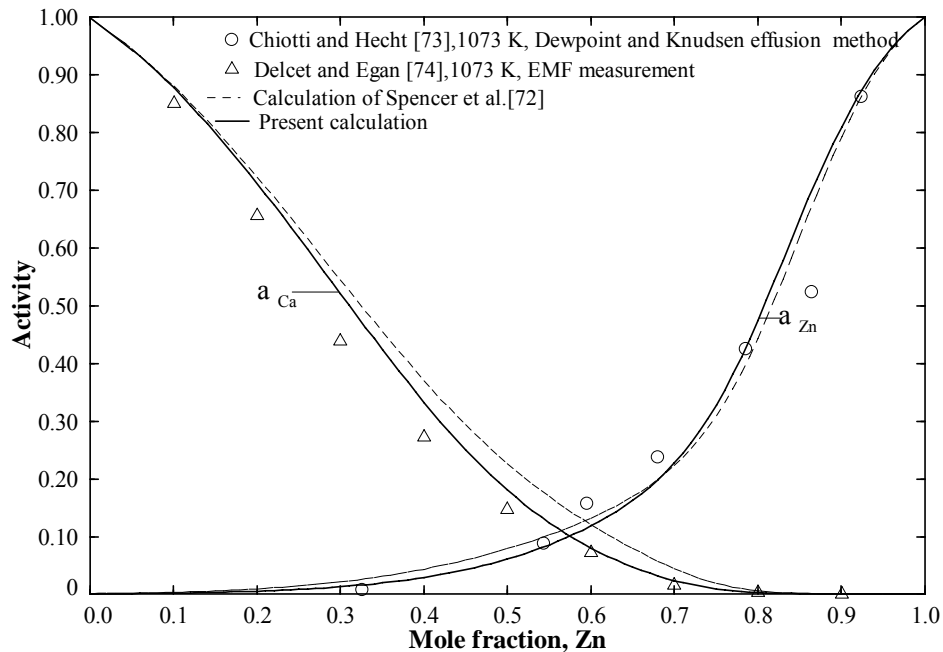
Figure 4.11: *Calculated activities of Ca and Zn in the Ca-Zn liquid at 1073 K*

Figure 4.12 shows a comparison between the calculated enthalpy of formation of all the intermediate phases and the experimental data. The consistencies for all the phases are reasonable except some mismatch exists for Ca_3Zn where the experimental value is more negative than the calculation. However, the calculations of [71] and [72] showed very similar results to the present calculation.
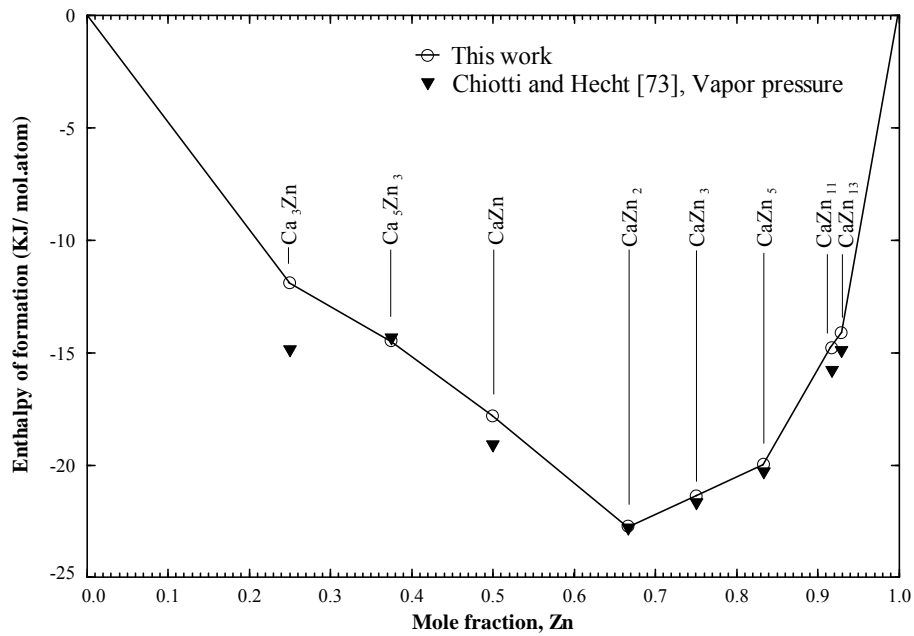
Figure 4.12: *Calculated heat of formation for the intermediate phases at 298.15 K with the experimental data*

The calculated enthalpy of mixing in comparison to the calculated curve of [72] over the Ca-Zn liquid phase at 1173 K is shown in Figure 4.13. The trend of these two curves is similar however, the results of [72] are more exothermic than the present calculation for the whole composition range.
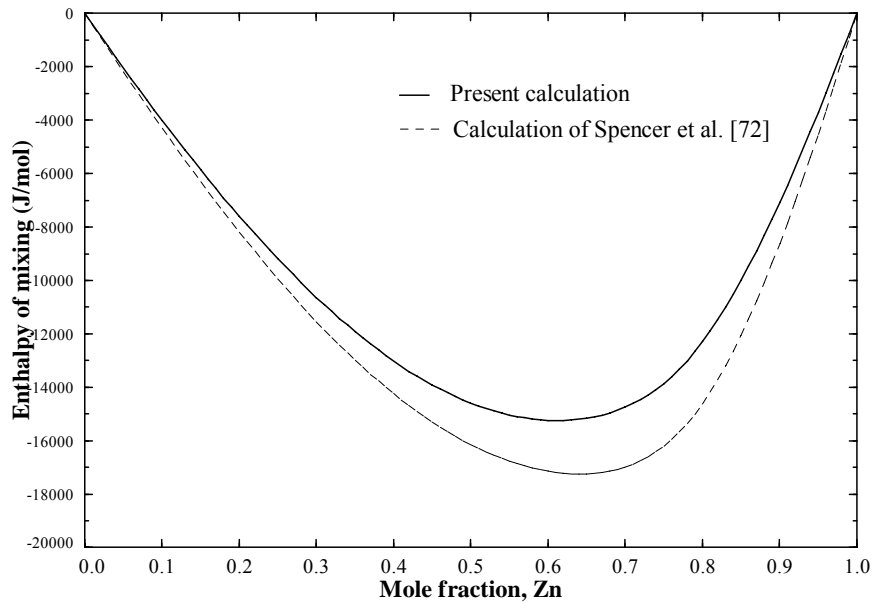
Figure 4.13: *Calculated enthalpy of mixing in the Ca-Zn liquid at 1173 K*

4.3 Mg-Ca Binary System

4.3.1 Equilibrium Phase Diagram

All the phases except Mg_2Ca compound of the Mg-Ca binary system were reproduced using the same model parameters reported by Aljarrah and Medraj [78]. The intermediate phase Mg_2Ca has the Laves C14 crystal structure which is similar to $MgZn_2$ phase in the Mg-Zn binary system. Hence it is decided to remodel Mg_2Ca phase using the sublattice model in order to represent both $MgZn_2$ and Mg_2Ca Laves C14 phase by one set of Gibbs energy parameters. This eventually makes both the phases as a single phase in the ternary Mg-Ca-Zn system with only one Gibbs energy description which is valid in all regions. The parameters for the remodeled Mg_2Ca phase are shown in Table 4.7.

Table 4.7: *Optimized model parameters for the Mg_2Ca phase of the Mg-Ca binary system*

Phase	Terms	a (J/mol-atom)	b (J/mol-atom.K)
Liquid	Δg_{AB}^{0}	-13187.9	7.98
	g_{AB}^{i0}	6908.55	-23.0
	g_{AB}^{0j}	8899.22	-15.93
Hcp-phase	$^{0}L^{Mg-hcp}$	1710.06	-12.32
Mg_2Ca	$^{0}G_{Mg:Mg}$	3884.6	0
	$^{0}G_{Mg:Ca}$	-11146.67	6.27
	$^{0}G_{Ca:Mg}$	5573.33	0
	$^{0}G_{Ca:Ca}$	42078.67	0
	$^{0}L_{Mg,Ca:Mg}^{Mg_2Ca}$	14006.43	0
	$^{0}L_{Mg,Ca:Ca}^{Mg_2Ca}$	14006.43	0
	$^{0}L_{Mg:Mg,Ca}^{Mg_2Ca}$	14006.43	0
	$^{0}L_{Ca:Mg,Ca}^{Mg_2Ca}$	14006.43	0

The remodeled Mg$_2$Ca phase using the parameters of Table 4.7, along with all other existing phases are in the complete Mg-Ca binary phase diagram shown in Figure 4.14.
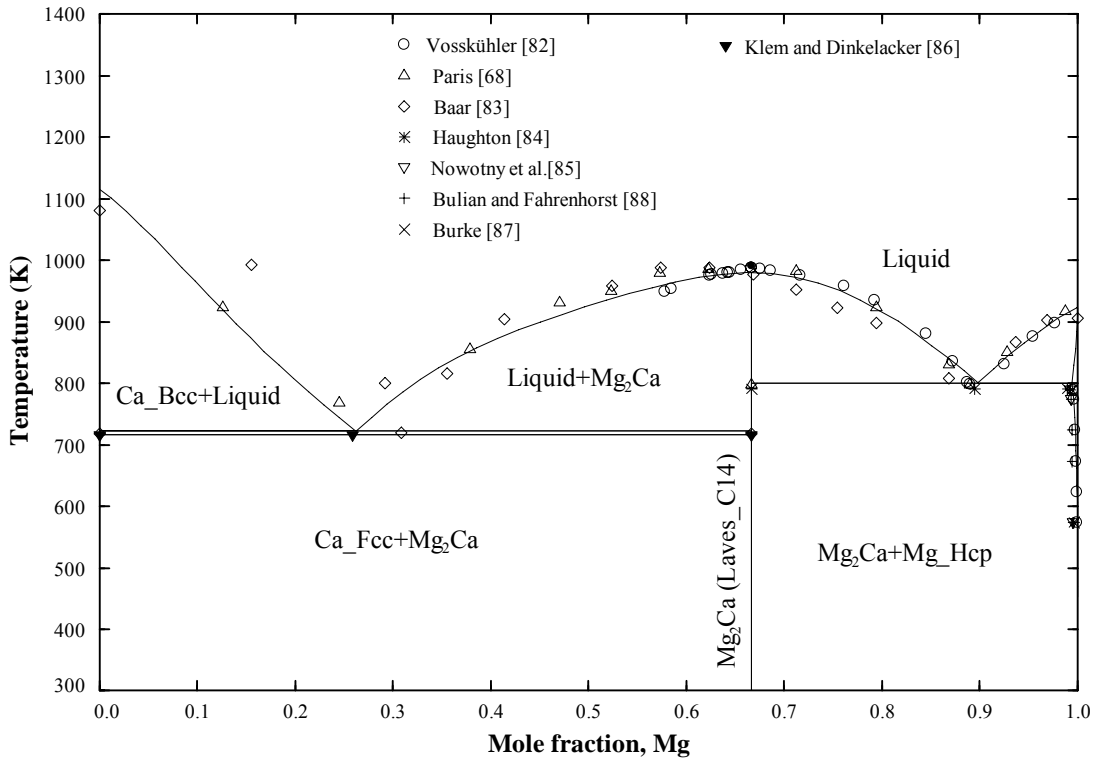
Figure 4.14: *Calculated Mg-Ca phase diagram in comparison with experimental results from literature*

4.3.2 Thermodynamic Modeling of the Mg$_2$Ca (Laves_C14) Phase

In order to model the Mg$_2$Ca (Laves_C14) phase, sublattice model was used in this work. This was accomplished by following the same approach used to model MgZn$_2$ as described earlier in detail. The crystallographic information and the substructure of the Mg$_2$Ca phase are shown in Table 4.8 and Figure 4.15, respectively.

Table 4.8: *Crystallographic data for the Laves_C14 phase [45]*

Phase	Crystal data		Atoms	WP[1]	CN[2]	PS[3]	Atomic position		
							X	Y	Z
Laves_C14 (Mg₂Ca)	Structure type	Mg₂Ca	Mg1	2a	12	$\bar{3}$ m	0.0	0.0	0.0
	Pearson symbol	hP12	Ca	4f	16	3m	0.333	0.666	0.062
	Space group	P6₃/mmc	Mg2	6h	12	mm2	0.830	0.660	0.250
	Space group no.	194							
	Lattice parameter (nm)	a=0.6225 c=1.018							
	Angles:α=90, β=90, γ=120								

[1]WP = Wyckoff Position, [2]CN = Coordination Number, [3]PS = Point Symmetry

(a)

(b)   (c)   (d)

= Ca   = Mg1   = Mg2   = Atom of interest
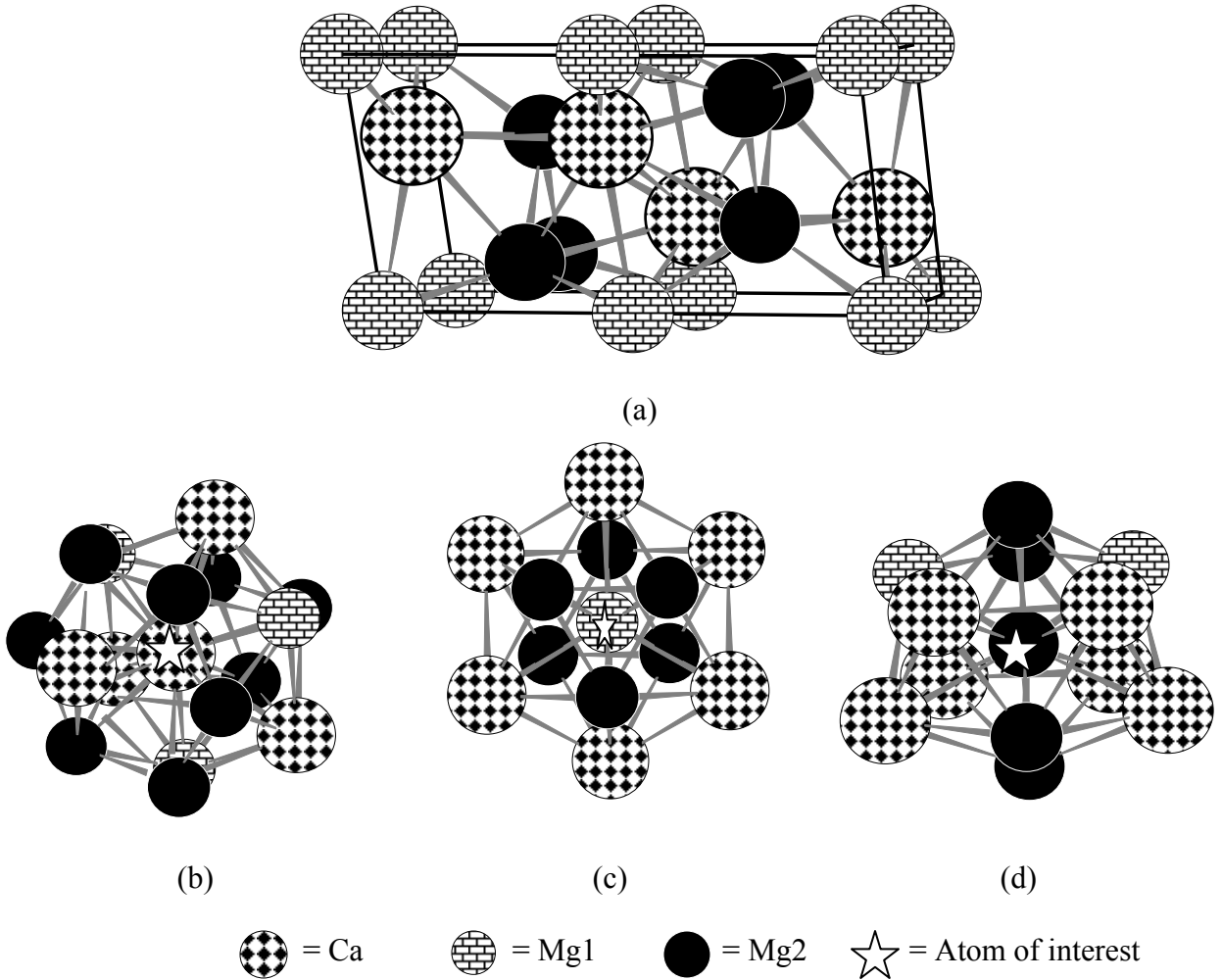
Figure 4.15: *(a) Unit cell of Mg₂Ca, Substructure of (b) Ca atom with CN=16, (c) Mg1 atom with CN=12 and (d) Mg2 atom with CN=12*

4.4 Mg-Ca-Zn Ternary System

A self-consistent thermodynamic database for the Mg-Ca-Zn system has been constructed by extrapolating the three constituting binaries Mg-Zn, Ca-Zn and Mg-Ca. Ternary interaction parameters were used in order to achieve consistency with the available experimental data from the literature. These ternary terms were kept as small numerically as possible which was also suggested by Chartland and Pelton [166]. The symmetric Kohler geometric model [163] was used for extrapolation since none of the constituent binaries show extreme dissimilarity in their thermodynamic properties. The different ternary compounds reported in the literature were considered during the present optimization.

4.4.1 Ternary Phase Diagram

The main features of the Mg-Ca-Zn ternary system will be discussed in this section by means of polythermal projections, isoplethal analysis and isothermal section. The optimized ternary parameters both for the liquid phase and ternary compounds are represented in Table 4.9.

Table 4.9: *Optimized model parameters for different phases of the Mg-Ca-Zn ternary system*

Phase	Terms	a (J/mol-atom)	b (J.mol-atom.K)
Liquid	$L_{MgCa(Zn)}$	-12540.0	0
	$L_{MgZn(Ca)}$	-12540.0	0
	$L_{CaZn(Mg)}$	4180.0	0
$Ca_2Mg_6Zn_3$	ΔG_f	-14801.83	-0.17
$Ca_2Mg_5Zn_{13}$	ΔG_f	-16740.51	-0.10

4.4.1.1 Polythermal Projection. The polythermal or liquidus projection is a two dimensional representation of the ternary liquidus surface on the Gibbs triangle which is mainly composed of several constant temperature lines called liquidus isotherms. The liquidus projection of the Mg-Ca-Zn system is shown in Figure 4.16 where the heavier solid lines represent the univariant valleys and the arrows on these lines indicate the directions of decreasing temperature. There are six ternary eutectic (E_1 to E_6) points, eleven quasi-peritectic (U_1 to U_{11}) points, one ternary peritectic and eight maximum (m_1 to m_8) points present in this system. The ternary invariant reactions are summarized in Table 4.10. The calculated liquidus projection shows reasonable consistency with the experimental results for most of the primary solidification regions except some deviation in the Zn-rich side. This is perhaps due to the fact that, Paris [68] reported two different compounds namely $CaZn_{10}$ and $CaZn_4$ in that region. But later investigation proved four other compounds: $CaZn_3$, $CaZn_5$, $CaZn_{11}$ and $CaZn_{13}$. It is not clear from Paris' results which data points correspond to $CaZn_3$ and which ones would correspond to $CaZn_5$. The same applies to the $CaZn_{11}$ and $CaZn_{13}$ compounds. Hence in Figure 4.16, based on Paris' work [68] one common symbol was used to mark $CaZn_3$ and $CaZn_5$ and another one for $CaZn_{11}$ and $CaZn_{13}$. It is also worth noting that, assuming the existence of a second ternary compound ($Ca_2Mg_5Zn_{13}$) during optimization, resulted in a better consistency with the experimental points of Paris [68] and Clark [92]. More details about this assumption in comparison with the other possibilities will be discussed in the following section.
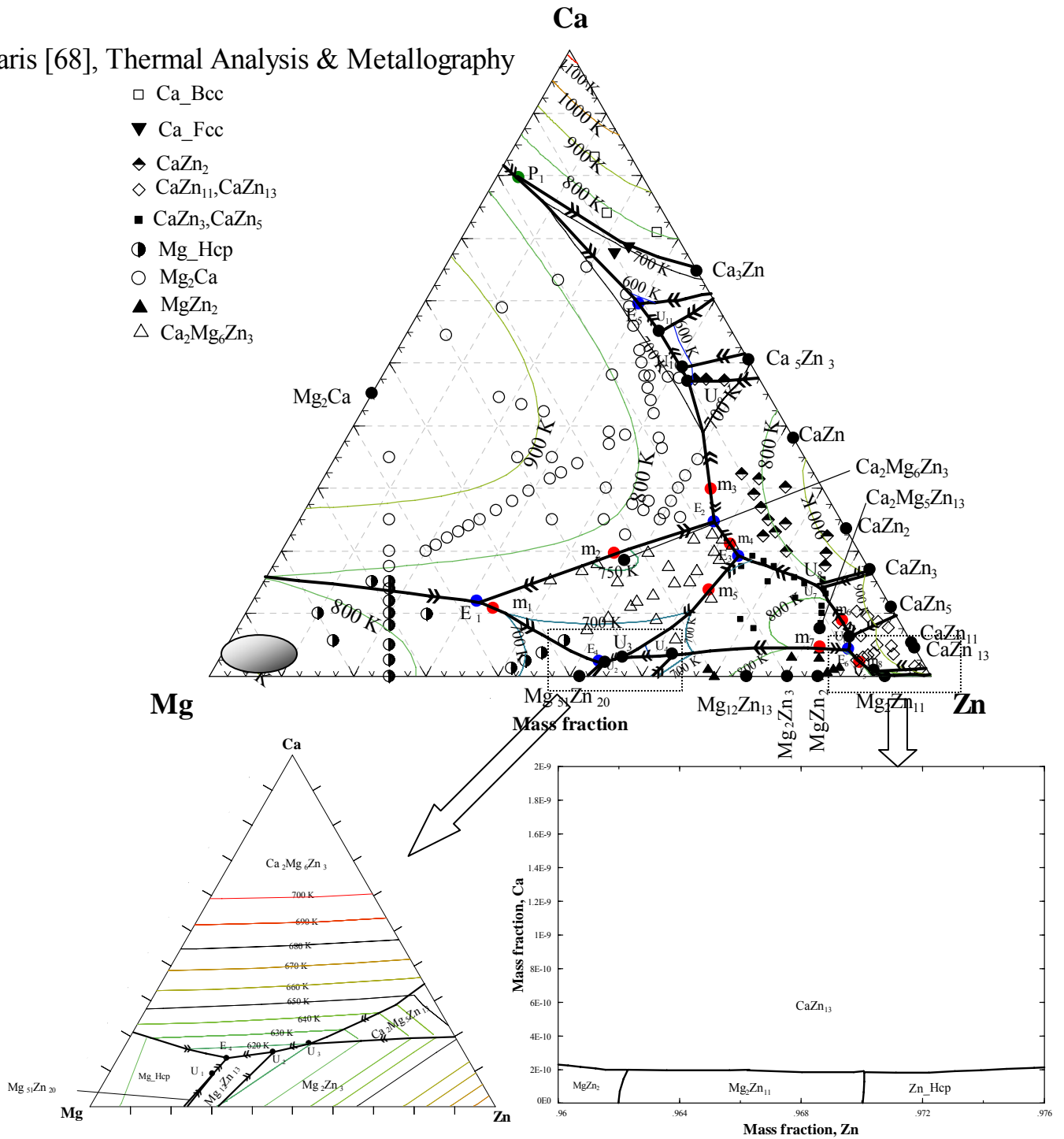
Figure 4.16: *Calculated liquidus surface of the Mg-Ca-Zn system in comparison with the experimental data of Paris [68]. The shaded area in the Mg-rich region of the liquidus surface shows the location of the compositions used in [97] and [98]*

Table 4.10: *Calculated invariant reactions and special points in the Mg-Ca-Zn system*

Type	Reaction	Composition (wt.%)			Temp (K)	Reference
		Mg	**Ca**	**Zn**		
E_1	L $\leftrightarrow$ Mg_Hcp+Ca$_2$Mg$_6$Zn$_3$+Mg$_2$Ca	55.6	11.5	32.9	701.5	This work
		55.5	16.0	28.5	673.0	[68]
E_2	L $\leftrightarrow$ Mg_Hcp+Ca$_2$Mg$_6$Zn$_3$+CaZn$_2$	17.6	24.7	57.7	720.0	This work
		13.5	24.0	62.5	723.0	[68]
E_3	L $\leftrightarrow$ CaZn$_2$+Ca$_2$Mg$_6$Zn$_3$+Ca$_2$Mg$_5$Zn$_{13}$	17.1	19.2	63.7	720.0	This work
E_4	L $\leftrightarrow$ Mg_Hcp+Ca$_2$Mg$_6$Zn$_3$+Mg$_{12}$Zn$_{13}$	44.5	2.1	53.4	610.0	This work
E_5	L $\leftrightarrow$ Mg$_2$Ca+Ca_Fcc+Ca$_3$Zn	10.5	59.5	30.0	580.0	This work
		8.0	59.0	33.0	592.0	[68]
E_6	L $\leftrightarrow$ Ca$_2$Mg$_5$Zn$_{13}$+MgZn$_2$+CaZn$_{11}$	9.1	4.0	86.9	800.0	This work
P_1	L+Mg$_2$Ca+Ca_Bcc $\leftrightarrow$ Ca_Fcc	17.0	78.7	4.3	708.0	This work
U_1	L+Mg$_{51}$Zn$_{20}$ $\leftrightarrow$ Mg_Hcp+Mg$_{12}$Zn$_{13}$	46.4	1.0	52.6	599.0	This work
U_2	L+Mg$_2$Zn$_3$ $\leftrightarrow$ Mg$_{12}$Zn$_{13}$+Ca$_2$Mg$_6$Zn$_3$	44.7	1.5	53.8	615.0	This work
U_3	L+Ca$_2$Mg$_5$Zn$_{13}$ $\leftrightarrow$ Mg$_2$Zn$_3$+Ca$_2$Mg$_6$Zn$_3$	43.7	1.8	54.5	620.0	This work
U_4	L+MgZn2 $\leftrightarrow$ Mg$_2$Zn$_3$+Ca$_2$Mg$_5$Zn$_{13}$	35.3	2.2	62.5	682.0	This work
U_5	L+CaZn$_{11}$ $\leftrightarrow$ MgZn$_2$+CaZn$_{13}$	7.9	0.9	91.2	790.0	This work
U_6	L+CaZn$_5$ $\leftrightarrow$ CaZn$_{11}$+Ca$_2$Mg$_5$Zn$_{13}$	7.8	6.7	85.5	810.0	This work
U_7	L+CaZn$_5$ $\leftrightarrow$ CaZn$_3$+Ca$_2$Mg$_5$Zn$_{13}$	8.0	14.3	77.7	780.0	This work
U_8	L+CaZn$_3$ $\leftrightarrow$ CaZn$_2$+Ca$_2$Mg$_5$Zn$_{13}$	8.5	14.8	76.7	770.0	This work
U_9	L+CaZn$_2$ $\leftrightarrow$ Mg$_2$Ca+CaZn	10.0	47.4	42.6	598.0	This work
U_{10}	L+CaZn $\leftrightarrow$ Mg$_2$Ca+Ca$_5$Zn$_3$	10.0	49.5	40.5	588.0	This work
U_{11}	L+Ca$_5$Zn$_3$ $\leftrightarrow$ Mg$_2$Ca+Ca$_3$Zn	10.2	55.2	34.6	580.0	This work
m_1	L $\leftrightarrow$ Mg_Hcp+ Ca$_2$Mg$_6$Zn$_3$	54.5	10.8	34.7	711.2	This work
m_2	L $\leftrightarrow$ Mg$_2$Ca+ Ca$_2$Mg$_6$Zn$_3$	34.8	19.3	45.9	776.3	This work
m_3	L $\leftrightarrow$ Mg$_2$Ca+ Ca$_2$Mg$_6$Zn$_3$	15.6	30.0	54.4	723.7	This work
m_4	L $\leftrightarrow$ CaZn$_2$+Ca$_2$Mg$_6$Zn$_3$	17.1	21.0	61.9	722.3	This work
m_5	L $\leftrightarrow$ Ca$_2$Mg$_6$Zn$_3$+ Ca$_2$Mg$_5$Zn$_{13}$	23.6	13.7	62.7	740.3	This work
m_6	L $\leftrightarrow$ CaZn$_5$+ Ca$_2$Mg$_5$Zn$_{13}$	8.0	8.8	83.2	834.4	This work
m_7	L $\leftrightarrow$ MgZn$_2$+ Ca$_2$Mg$_5$Zn$_{13}$	13.4	4.5	82.1	824.7	This work
m_8	L $\leftrightarrow$ MgZn$_2$+ CaZn$_{11}$	8.6	2.6	88.8	804.9	This work

4.4.1.2 The Approach Followed to Include the Ternary Compounds in the Mg-Ca-Zn System

As mentioned earlier, the experimental data reported in the literature by Paris [68] and Clark [92] regarding the number of ternary compounds in the Mg-Ca-Zn system are self-contradicting. Therefore several scenarios combining these two works were tried in order to find out the most probable description of this system. In this method, the ternary phase diagram was calculated and compared with all the experimental data for the following cases:

- Considering only the compound ($Ca_2Mg_5Zn_5$) reported by Paris [68]

- Considering only one ($Ca_2Mg_6Zn_3$) of the two compounds reported by Clark [92]

- Considering only the two ternary compounds ($Ca_2Mg_6Zn_3$ and $Ca_2Mg_5Zn_{13}$) reported by Clark [92]

- Considering Paris' compound ($Ca_2Mg_5Zn_5$) with one of Clark's compounds ($Ca_2Mg_5Zn_{13}$)

Several vertical sections (Sections V, VI, and VII in Figure 2.11) which passed through the regions of probable compound formation have been chosen and presented in Figures 4.17 to 4.20, for better clarification and comparison.
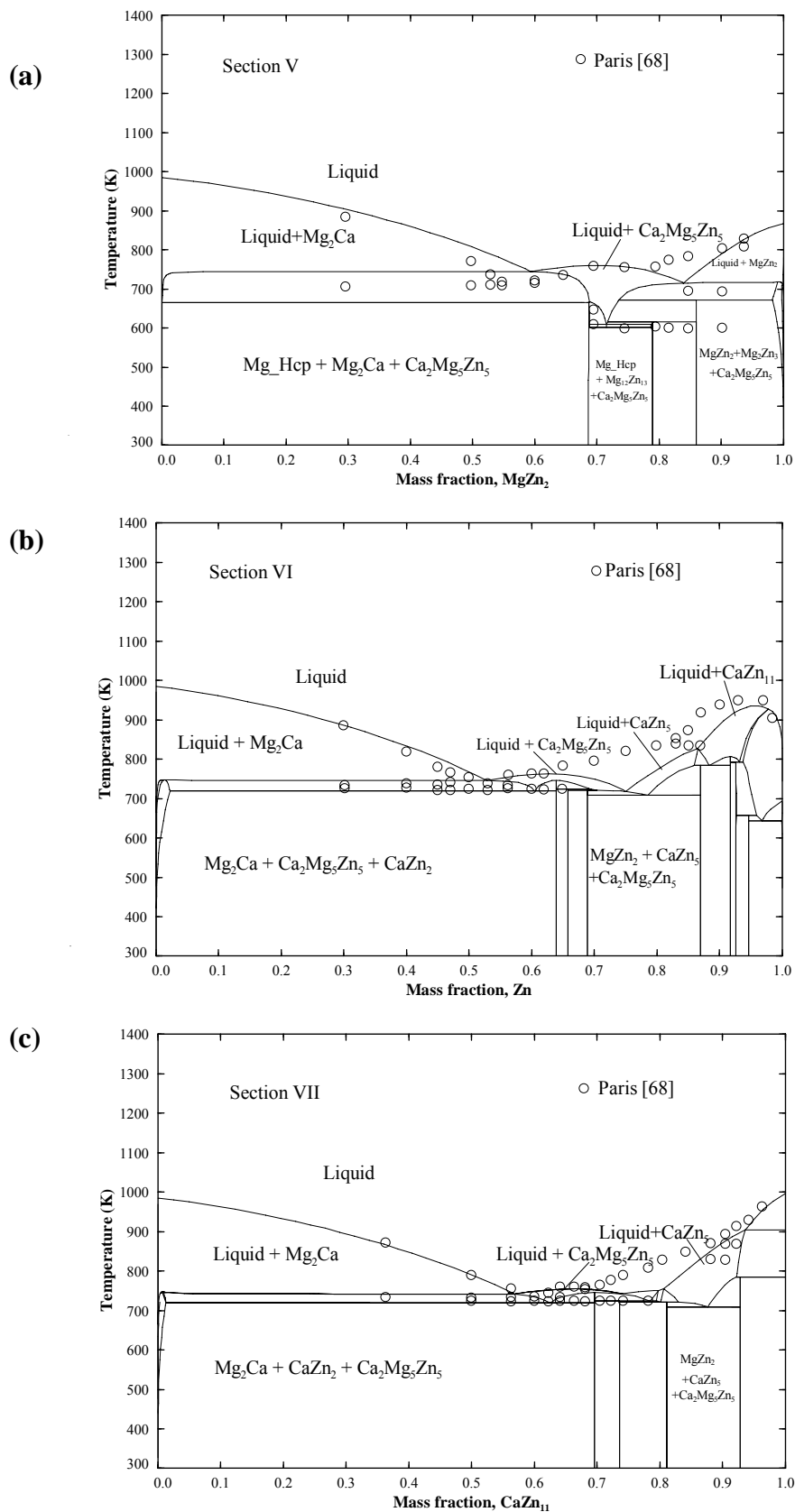
Figure 4.17: *Calculated isoplethal analysis of section (a) Mg₂Ca-MgZn₂, (b) Mg₂Ca-Zn and (c) Mg₂Ca-CaZn₁₁ in comparison with the experimental data of [68]*
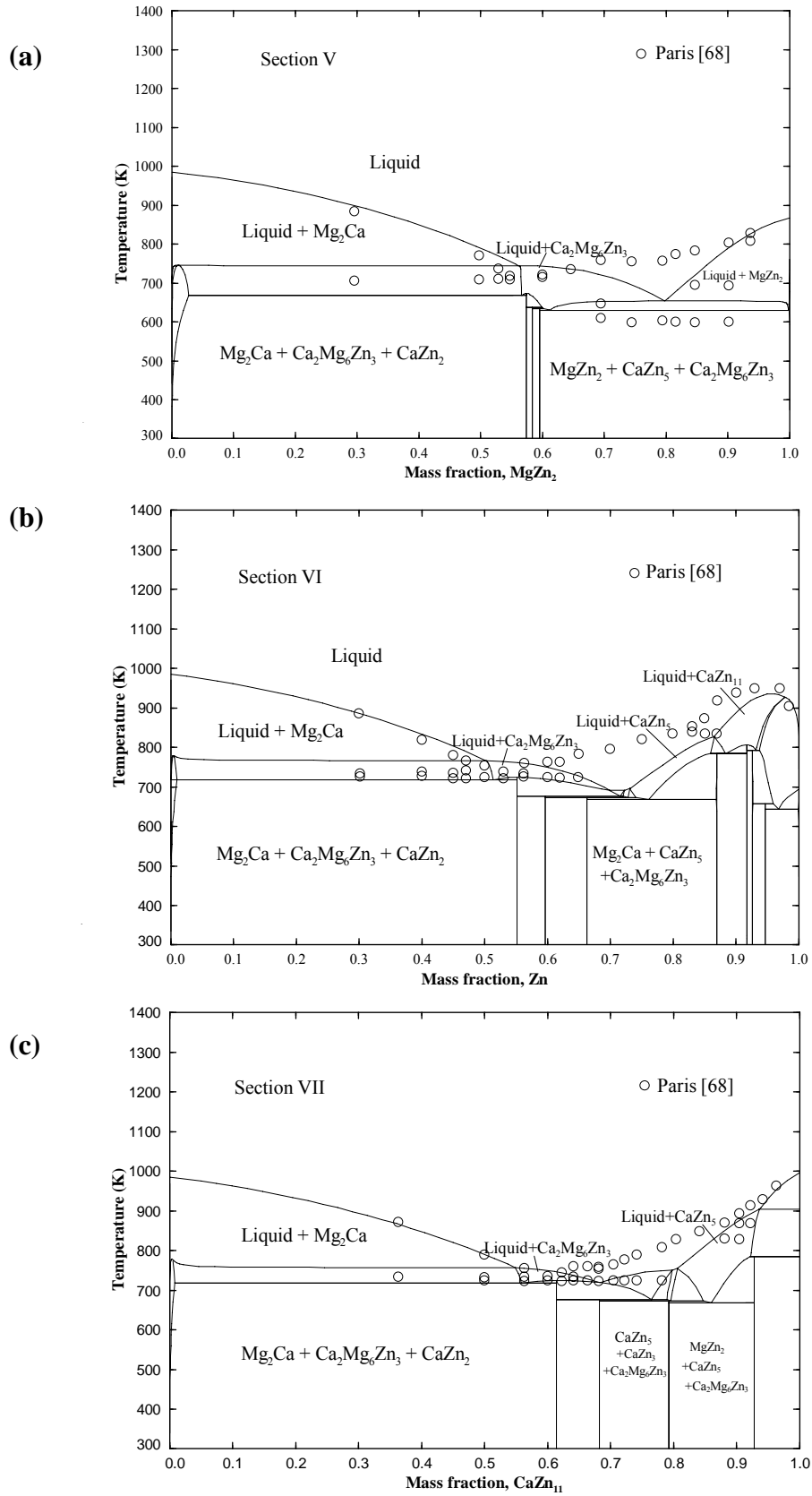
Figure 4.18: *Calculated isoplethal analysis of section (a) Mg_2Ca-$MgZn_2$, (b) Mg_2Ca-Zn and (c) Mg_2Ca-$CaZn_{11}$ in comparison with the experimental data of [68]*

(a)

Section V

○ Paris [68]

Liquid

Liquid + Mg$_2$Ca

Liquid+Ca$_2$Mg$_6$Zn$_3$

Liquid+Ca$_2$Mg$_5$Zn$_{13}$

Mg$_2$Ca + CaZn$_2$+ Ca$_2$Mg$_6$Zn$_3$

Ca$_2$Mg$_6$Zn$_3$+Ca$_2$Mg$_5$Zn$_{13}$+Mg$_{12}$Zn$_{13}$

Temperature (K)

Mass fraction, MgZn$_2$

(b)

Section VI

○ Paris [68]

Liquid

Liquid+CaZn$_{11}$

Liquid + Mg$_2$Ca

Liquid+Ca$_2$Mg$_5$Zn$_{13}$

Liquid+Ca$_2$Mg$_6$Zn$_3$

Mg$_2$Ca + CaZn$_2$ + Ca$_2$Mg$_6$Zn$_3$

Ca$_2$Mg$_5$Zn$_{13}$+CaZn$_2$
+Ca$_2$Mg$_6$Zn$_3$

Temperature (K)

Mass fraction, Zn

(c)

Section VII

○ Paris [68]

Liquid

Liquid+Mg$_2$Ca

Liquid+CaZn$_5$

Liquid+Ca$_2$Mg$_5$Zn$_{13}$

Liquid+Ca$_2$Mg$_6$Zn$_3$

Mg$_2$Ca + Ca$_2$Mg$_6$Zn$_3$+CaZn$_2$

CaZn$_2$+Ca$_2$Mg$_6$Zn$_3$
+Ca$_2$Mg$_5$Zn$_{13}$

CaZn$_5$
+CaZn$_{11}$
+Ca$_2$Mg$_5$Zn$_{13}$

Temperature (K)

Mass fraction CaZn$_{11}$

Figure 4.19: *Calculated isoplethal analysis of section (a) Mg$_2$Ca-MgZn$_2$, (b) Mg$_2$Ca-Zn and (c) Mg$_2$Ca-CaZn$_{11}$ in comparison with the experimental data of [68]*
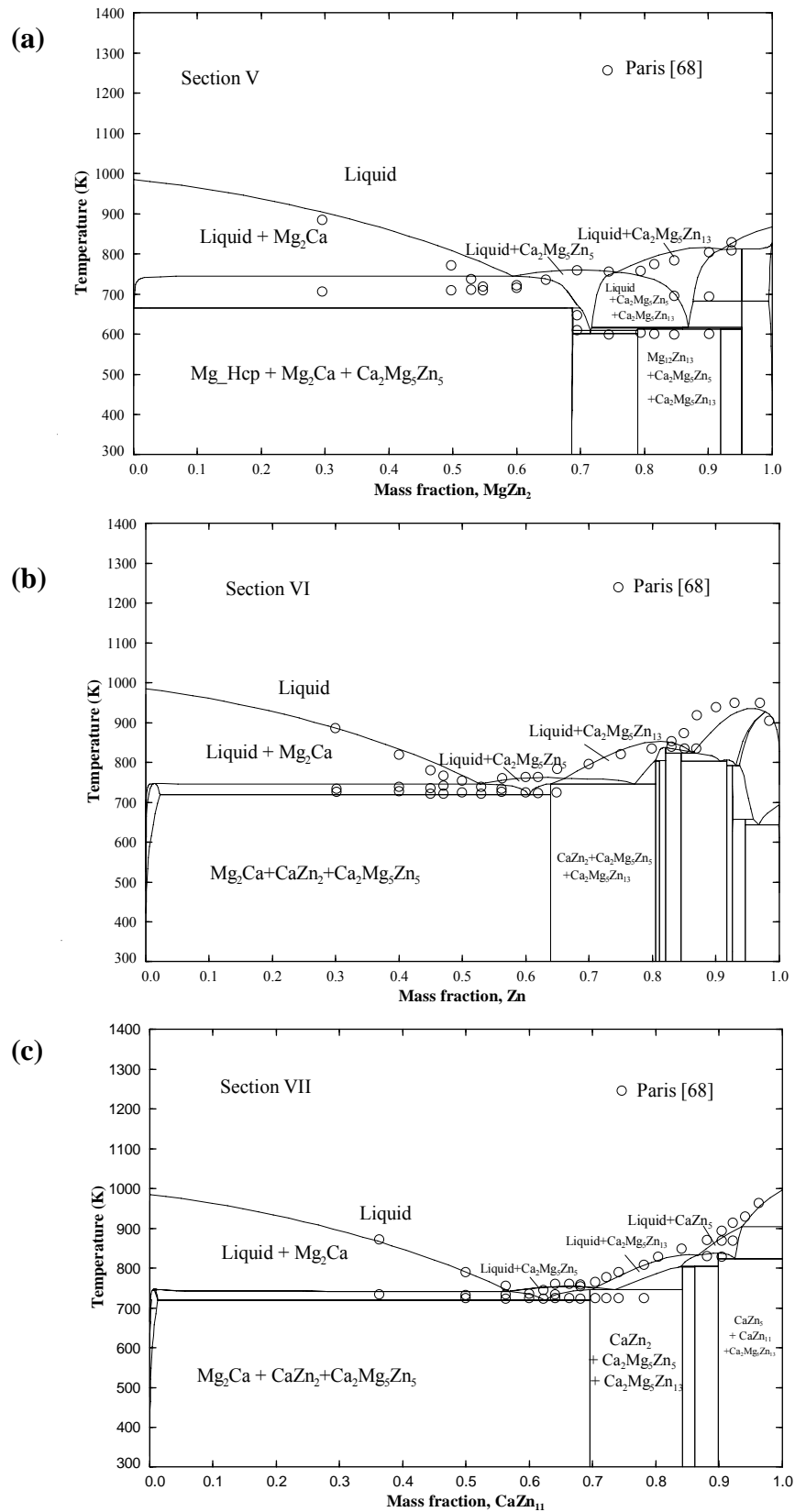
Figure 4.20: *Calculated isoplethal analysis of section (a) Mg$_2$Ca-MgZn$_2$, (b) Mg$_2$Ca-Zn and (c) Mg$_2$Ca-CaZn$_{11}$ in comparison with the experimental data of [68]*

Figure 4.17 illustrates the calculated vertical sections V, VI, and VII by considering only the ternary compound reported by Paris [68]. It shows reasonable consistency except some deviation in the region belonging to $CaZn_5$ especially in Figures 4.17 (b) and (c) (sections VI and VII) which might be an indication of the presence of a second compound.

By considering one of the two ternary compounds reported by Clark [92] almost similar liquidus curves like the first case have been obtained and demonstrated in Figure 4.18. Again the presence of a second ternary phase near the primary solidification region of $CaZn_5$ especially in Figures 4.18 (b) and (c) (sections VI and VII) becomes markedly apparent.

Based on the aforementioned observations, it is decided to consider the two ternary compounds reported by Clark [92]. Figure 4.19 illustrates the outcome of this consideration through different vertical sections. It can be seen from this figure that these calculated vertical sections are considerably closer to the experimental data points than those calculated without considering the second ternary compound.

Finally, the system was modeled considering two ternary phases where one of them was reported by Paris [68] ($Ca_2Mg_5Zn_5$) and the other one reported by Clark [92] ($Ca_2Mg_5Zn_{13}$). Figure 4.20 shows the calculated vertical sections in relation to the experimental data. Liquidus curves similar to those in the previous case have been obtained for all the verticals.

There are other two possibilities which can be considered regarding the ternary compounds in this system. One by including only the second compound ($Ca_2Mg_5Zn_{13}$) reported by Clark [92]. Second, considering the compound reported by Paris [68]

(Ca$_2$Mg$_5$Zn$_5$) with the first compound reported by Clark [92] (Ca$_2$Mg$_6$Zn$_3$). These scenarios were not pursued because of the following reasons: (1) The presence of the ternary compound Ca$_2$Mg$_6$Zn$_3$ was confirmed by later investigators [97-99], so it should be included in the Mg-Ca-Zn ternary system. (2) Paris' [68] compound and Clark's [92] first compound are similar in composition and Clark's first compound is thought of as a replacement of that of Paris.

Therefore, among the four feasible cases which were discussed earlier, it can be seen that the last two where two ternary compounds were considered provided better consistency with the experimental points of the ternary phase equilibria than the first two. In the last two feasible scenarios, the second phase (Ca$_2$Mg$_5$Zn$_{13}$) as reported by Clark [92] is common. The only difference between these two cases is the composition of the first ternary compound which is Ca$_2$Mg$_6$Zn$_3$ (reported by Clark [92]) for the third case and Ca$_2$Mg$_5$Zn$_5$ (reported by Paris [68]) for the last one. Clark [92] heat treated the alloys using a diffusion couple for almost three weeks and this method is thought to be more reliable for phase identification than that of Paris [68] who used thermal and metallographic analysis. In addition, Paris' liquidus curves suggested the presence of the second ternary compound which he was unable to detect. It is also worth mentioning that, the works of Larinova *et al.* [97] and Jardim *et al.* [98] mainly concentrated on the primary solidification region of Mg-rich solid solution and the locations of their alloy compositions are shown in Figure 4.16. For this reason perhaps they were unaware about the existence of the second ternary phase. Hence more emphasis has been given for the result of Clark [92]. All the other isopleths of Paris [68] shown in Figure 2.11 were also

reproduced concurrently during optimization considering the two ternary compounds of Clark and found to be consistent. Those vertical sections are presented in figure 4.21.

(a)

(b)

(c)

(d)

(e)

(f)

(g)

(h)

(i)

(j)

(k)

(l)

92
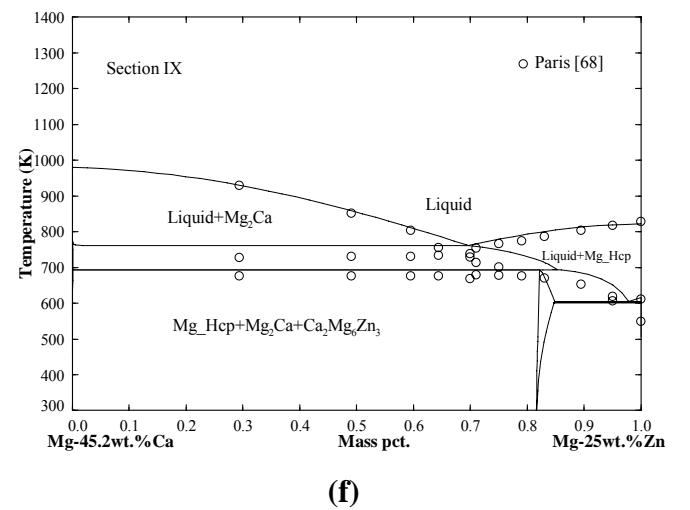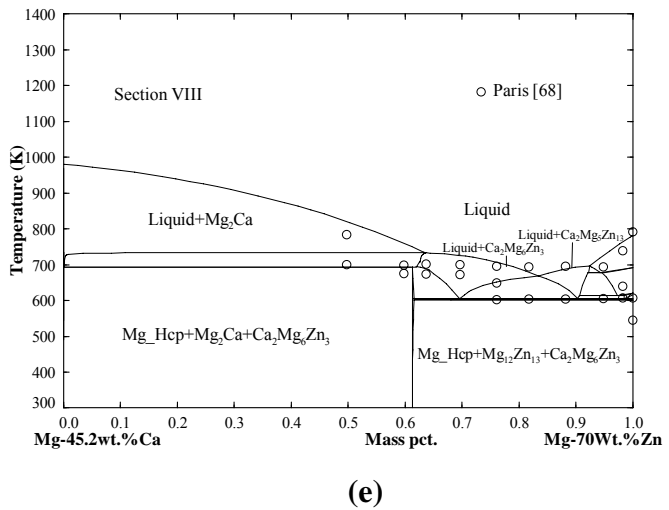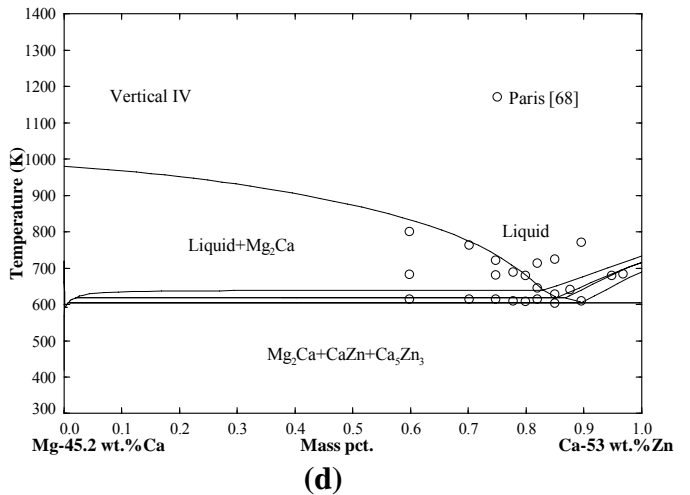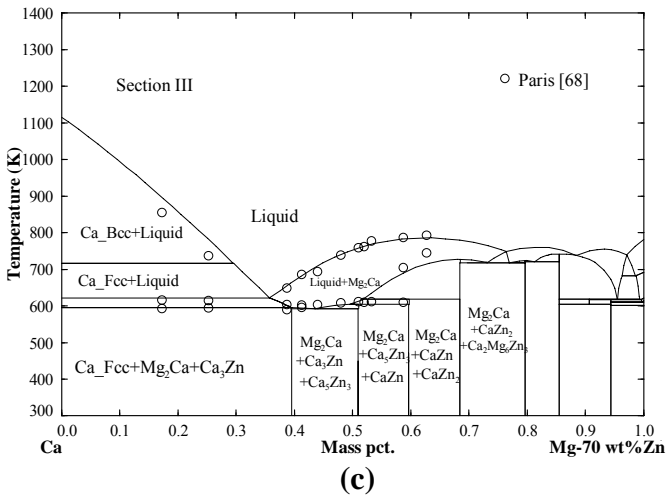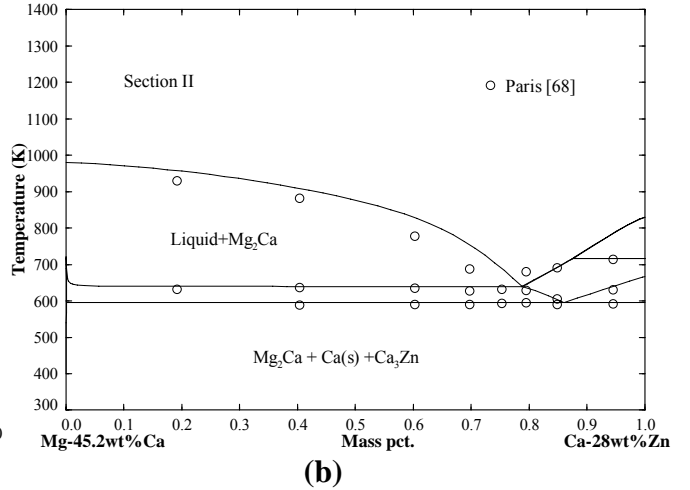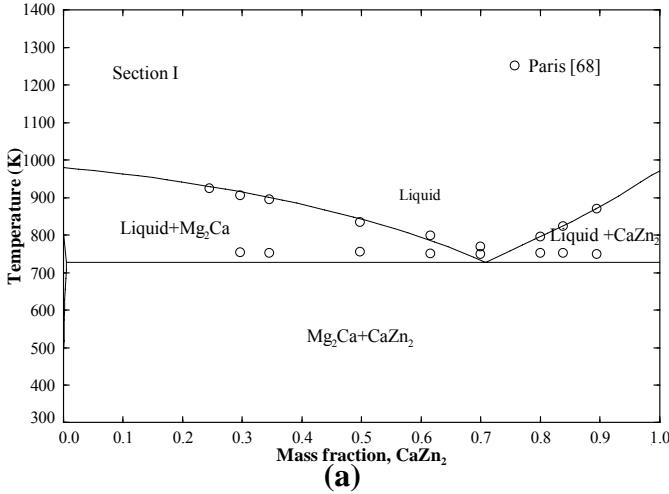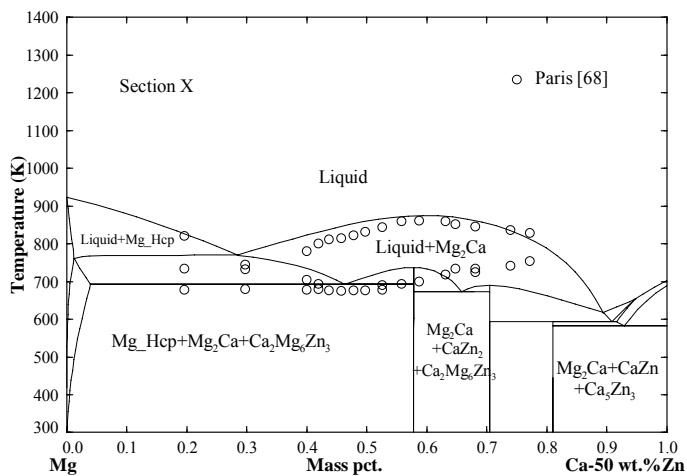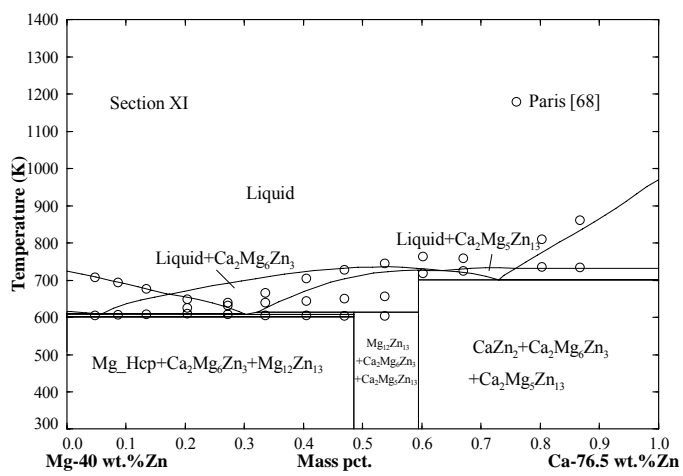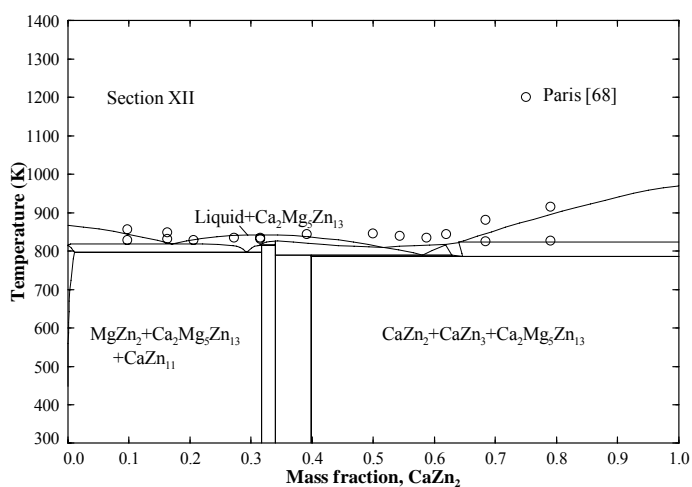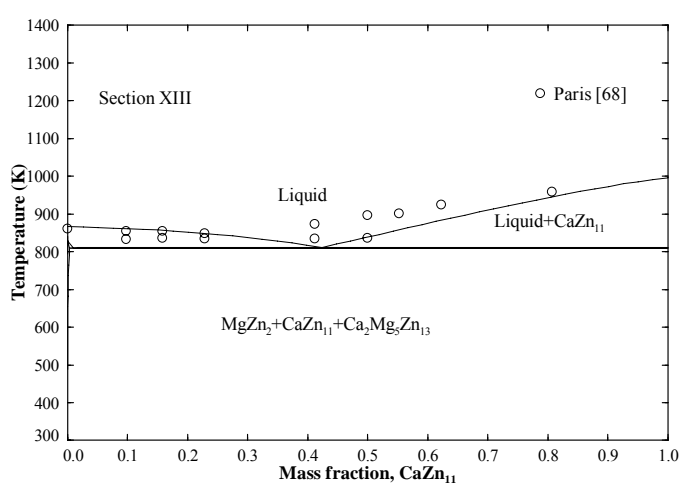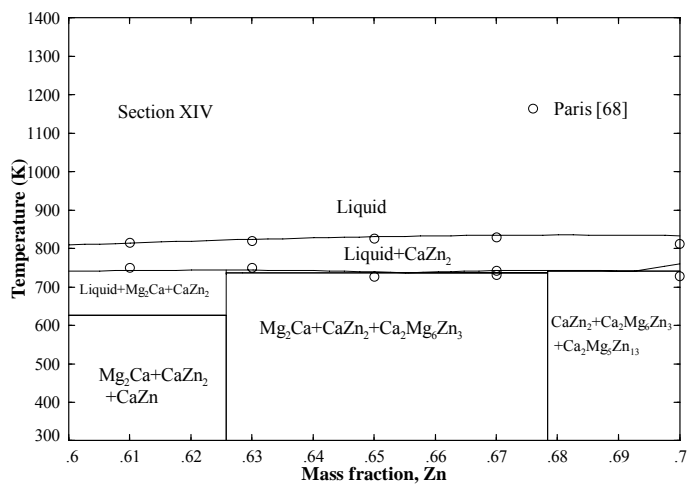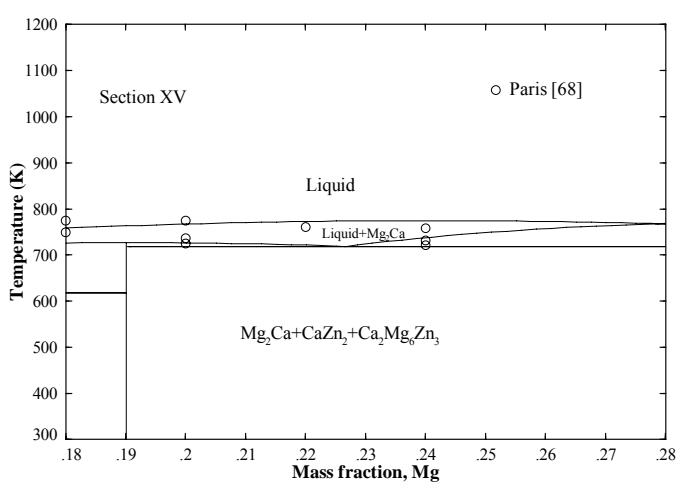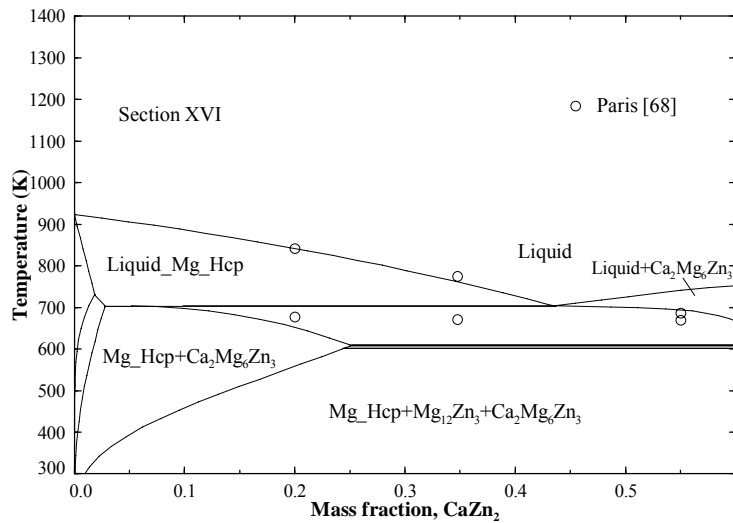
(m)

Figure 4.21: *Calculated isoplethal analysis of sections (a) Mg₂Ca-CaZn₂, (b) Mg-45.2 wt.%Ca----Ca-28.0 wt.%Zn, (c) Ca----Mg-70.0 wt.%Zn, (d)Mg-45.2wt.%Ca---Ca-53.0wt.%Zn,(e)Mg-45.2wt.%Ca---Mg-70.0wt.%Zn,(f)Mg-45.2wt.%Ca---Mg-25.0 wt.%Zn,(g)Mg---Ca-50wt.%Zn,(h)Mg-40.0wt.%Zn---Ca-76.5wt.%Zn,(i)MgZn₂-CaZn₂,(j)MgZn₂-CaZn₁₁, (k) At 10.0 at.%Mg, (l)At 50.0 at.%Zn and (m)Mg-CaZn₂ in comparison with the experimental data of [68]*

4.4.1.3 Isothermal Section. One way to show the phase relation between different phases of a ternary system is using isothermal sections which is basically a horizontal slice constructed through the three dimensional diagram. It represents both solid and liquid stable phases for different compositions at constant temperature. Figure 4.22 shows the calculated isothermal section of the Mg-Ca-Zn system at 608 K where reasonable agreement with the experimental data of Clark [92] was achieved by considering two ternary compounds. Some discrepancy can be observed around the ternary phase $Ca_2Mg_6Zn_3$ because it was modeled as stiochiometric phase whereas, Clark [92] speculated homogeneity in that phase but he was unable to determine its limits. It can also be seen from the same figure that a small region of liquid phase appears in the Ca-rich side of the ternary phase diagram at 608 K even though Clark [92] did not report any

liquid phase at this temperature. This is perhaps due to the fact that, he did the experiment in the Mg-Zn side of the ternary system.
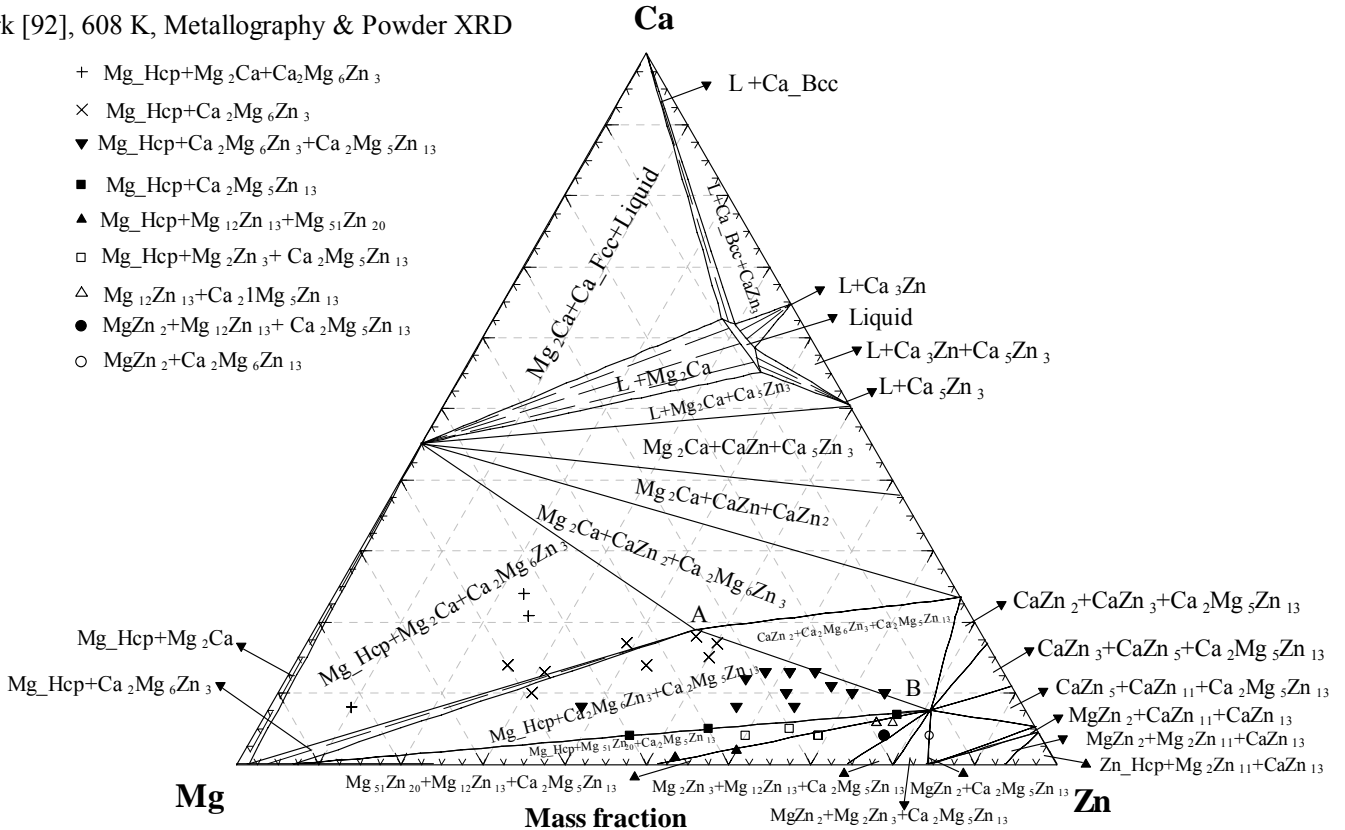
Figure 4.22: *Calculated isothermal section of the Mg-Ca-Zn system at 608 K with two ternary compounds and compared with experimental data [92] where A denotes: $Ca_2Mg_6Zn_3$ and B denotes: $Ca_2Mg_5Zn_{13}$*

4.5 Al-Zn Binary System

4.5.1 Equilibrium Phase Diagram

All the previous works [128-132] regarding thermodynamic modeling did not consider the presence of short range ordering neither for the liquid phase nor for the

Al_Fcc solid solution in the Al-Zn binary system. In order to model the Al_Fcc terminal solid solution the sublattice model will not be an appropriate model because the sublattice model has been extensively used to describe the intermediate interstitial solid solution with ordered crystal structure where in Al-Zn system the Al_Fcc phase is a terminal substitutional solid solution with random orientation of atoms [173] but with short range ordering. The random Redlich-Kister polynomial [47] had also been applied to describe the solid phase by Mey [130] but failed to be consistent with the experimental points for the enthalpy of mixing.

It is important to note that, Rudman and Averbach [174] found the evidence of the short range ordering in the Al_Fcc solid solution during their experiment on this system. Hence, the modified quasichemical model will be employed in the Al_Fcc substitutional solid solution with evidence of short range ordering and also for the liquid phase in this work. For the Zn_Hcp solid solution the Redlich-Kister polynomial [47] is used. According to equation 3.17, the optimized Gibbs energy for the liquid phase can be written as:

$$\Delta^{ex}G_{AlZn}^{liq} = 4057.94 - 1.463T \quad \text{J/mol} \qquad \qquad \text{............... (4.6)}$$

The coordination number for the first nearest neighbors of Al and Zn atoms ($Z_{AlAl}^{Al}, Z_{ZnZn}^{Zn}$) were set equal to 6. The values of Z_{AlZn}^{Al} and Z_{AlZn}^{Zn} were set equals to 5.

For the Al-fcc solid solution the optimized Gibbs energy can be expressed as:

$$\Delta^{ex}G_{AlZn}^{Al-fcc} = 3803.8 + 0.25\ T + (313.83 - 1.34\ T)\ X_{AlAl} + (-3347.34 - 0.418\ T)\ X_{ZnZn} \quad \text{J/mol}$$
$$\text{............... (4.7)}$$

For the very rigid lattice structure of solid solutions, all the coordination numbers must be equal. Clearly, in this case, $Z_{AlAl}^{Al} = Z_{ZnZn}^{Zn} = Z_{AlZn}^{Al} = Z_{AlZn}^{Zn} = 6$. Table 4.11 listed all

the optimized model parameters for different phases in the Al-Zn binary system. Using

these parameters the Al-Zn phase diagram is drawn and shown in Figure 4.23.

Table 4.11: Optimized model parameters for different phases of the Al-Zn binary system

Phase	Terms	a (J/mol)	b (J/mol.K)
Liquid	Δg_{AB}^{0}	4057.94	-1.463
Zn-hcp	$^{0}L^{Zn-hcp}$	13377.88	0.438
Al-fcc	Δg_{AB}^{0}	3803.8	0.25
	g_{AB}^{i0}	313.83	-1.34
	g_{AB}^{0j}	-3347.34	-0.418
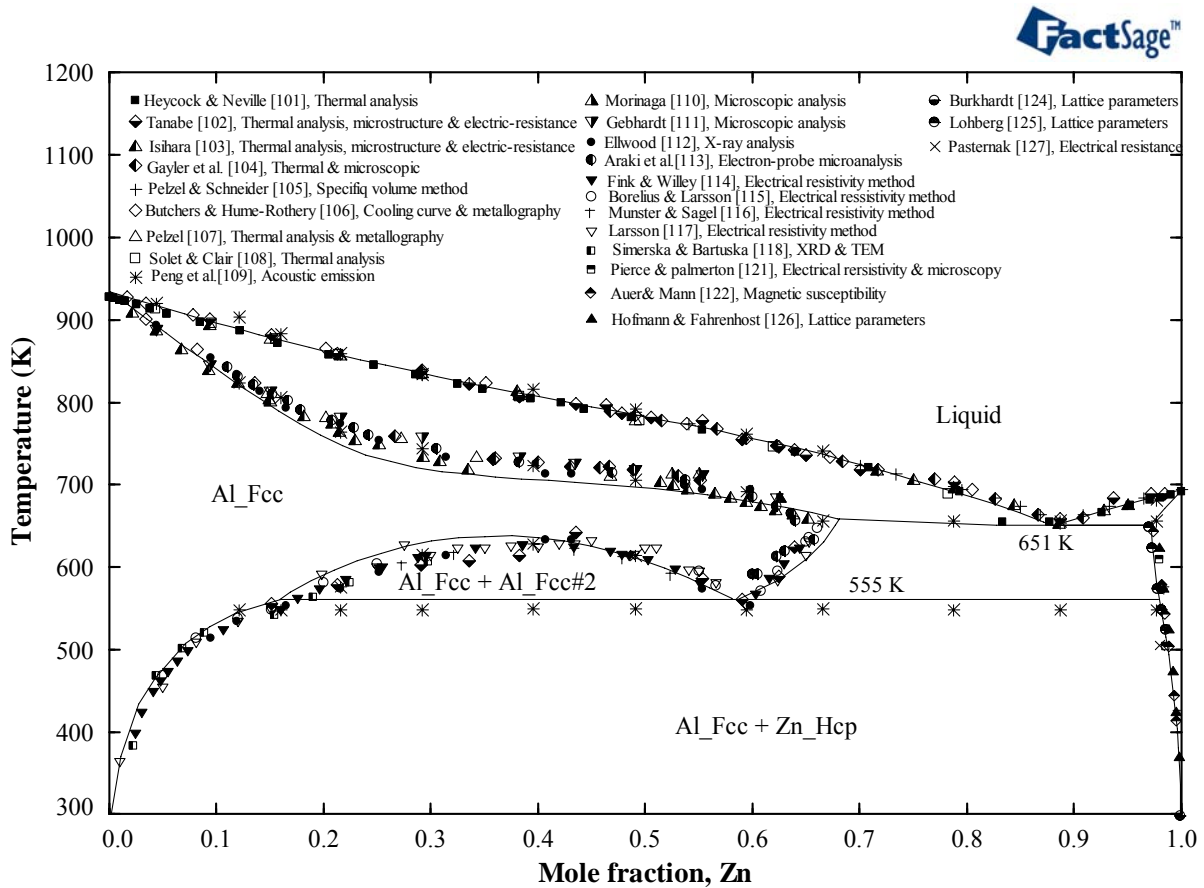
Figure 4.23: Calculated Mg-Zn phase diagram in comparison with the experimental results from the literature

The isobaric phase diagram shows a large Fcc solid solution with a miscibility

gap and Zn-rich hcp solid solution. Except few discrepancies for the miscibility gap in

the Fcc phase, the phase diagram shows reasonable agreement with all the experimental

points. As shown in Figure 4.23, the model calculated miscibility gap for the Al-rich portion is high in temperature however, there are appreciable disagreements between the experimental data obtained by different groups of investigators for the Fcc miscibility gap as well as for the Al_Fcc$_2$/(Al_Fcc+Zn_Hcp) phase boundary. The solubility of Zn in Al increases from 0.33 at.% Zn at room temperature to 16.0 at.% Zn at the eutectoid temperature which is 555 K. Above 555 K the solvus curve lies on the Zn rich side of the Fcc miscibility gap where the solubility increases from 58.4 at.% Zn at 555 K to 68.0 at.% Zn at the eutectic temperature of 651 K.

The maximum solubility of Al in Zn was found to be 2.8 at.% Al at the eutectic temperature which lies between 2.6 and 2.9 at.% Al reported by Auer and Mann [122] and Lohberg [125], respectfully. Table 4.12 lists all the invariant points calculated in the present work in comparison with the experimental results.

Table 4.12: *Comparison between calculated and experimental values of the invariant reactions in the Al-Zn system*

Reaction type	Reaction	Composition (at.% Zn)	Temperature (K)	Reference
Eutectic	$L \leftrightarrow Al\_Fcc + Zn\_Hcp$	88.2	651.0	This work
		89.0	653.5	[101]
		88.7	658.0	[102]
		88.7	653.0	[103]
		-	654.0	[104]
		88.7	653	[105]
		88.7	655	[109]
Eutectoid	$Al\_Fcc_2 \leftrightarrow Al\_Fcc + Zn\_Hcp$	58.3	555.0	This work
		59.8	553.0	[112]
		-	548.0	[114]
		-	550.0 ± 0.5	[115]
		59.4	553.0	[117]
		-	548.0	[119]
		-	549.0	[120]
Critical point	$Al\_Fcc \leftrightarrow Al\_Fcc + Al\_Fcc_2$	38.5	634.0	This work
		38.5	626.0	[114]
		39.16	624.0	[119]

4.5.2 Thermodynamic properties

The calculated enthalpy of mixing at 953 K over the liquid phase in the Al-Zn system is shown in Figure 4.24. Good agreement has been achieved between the calculated results and the calorimetric data of Wittig and Keil [133]. The endothermic trend of the enthalpy of mixing is obvious due to the flat nature of the liquidus curve in the phase equilibrium diagram. It also reflects the fact that formation of Al-Al and Zn-Zn pairs is more favorable than the formation of Al-Zn pairs in the liquid phase.
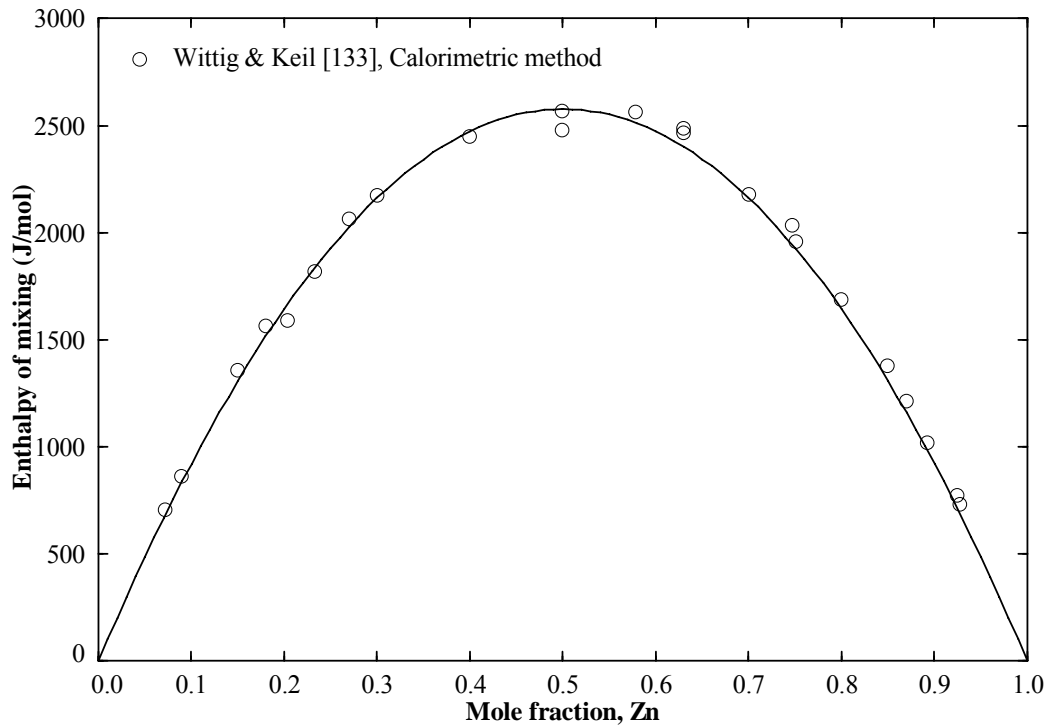
Figure 4.24: *Calculated enthalpies of mixing of Al and Zn in liquid Mg-Zn alloy at 953 K in comparison with the experimental results*

The calculated activity in the liquid Al-Zn alloys at 1000 K and 1073 K can be seen in Figure 4.25. As expected, both activities of Al and Zn show positive deviation from the ideal solution behavior. It can be seen from the same figure that the activity of Zn at different temperatures shows some deviation from the results of Lutz and Voigt

[141] and Yazawa and Lee [143] but agrees well with the values of Bolsaitis and Sullivan [142]. This is due to the less accurate vapor pressure method used by [141] and [143].
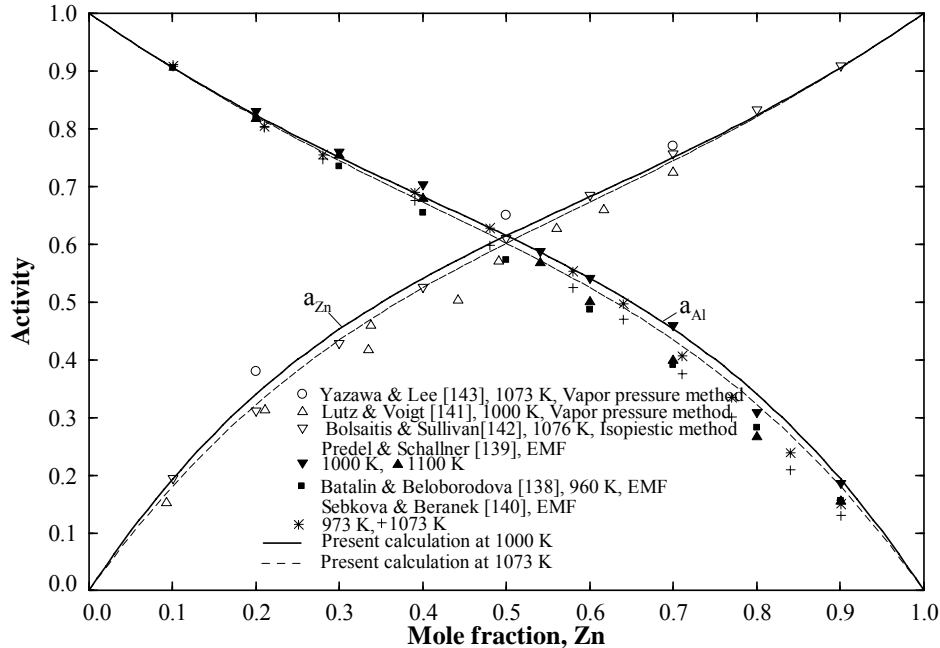
Figure 4.25: Calculated activity of Al and Zn in the liquid state at 1000 K and 1073K

Figure 4.26 illustrates the calculated enthalpy of mixing in the extended Al_Fcc solid solution at 653 K in comparison with the experimental results from the literature. Reasonable consistency has been achieved with the EMF results of Hilliard *et al.* [134] and Corsepius and Munster [135] but the current calculation differs markedly from the solution calorimetric results of Wittig and Schoffl [136] and Connell and Downie [137]. The results of Wittig and Schoffl [136] and Connell and Downie [137] show that in the composition region around 50.0 at.% Zn there is a fall in the enthalpy values which indicates an ordered phase formation in the solid solution though no confirmatory evidence of it could be found.The most reliable experimental works [104,110,112,114] on phase equilibrium diagram also could not found the evidence of any kind of phase

change and hence more emphasis has given to the results of [134] and [135] in the present assessment.
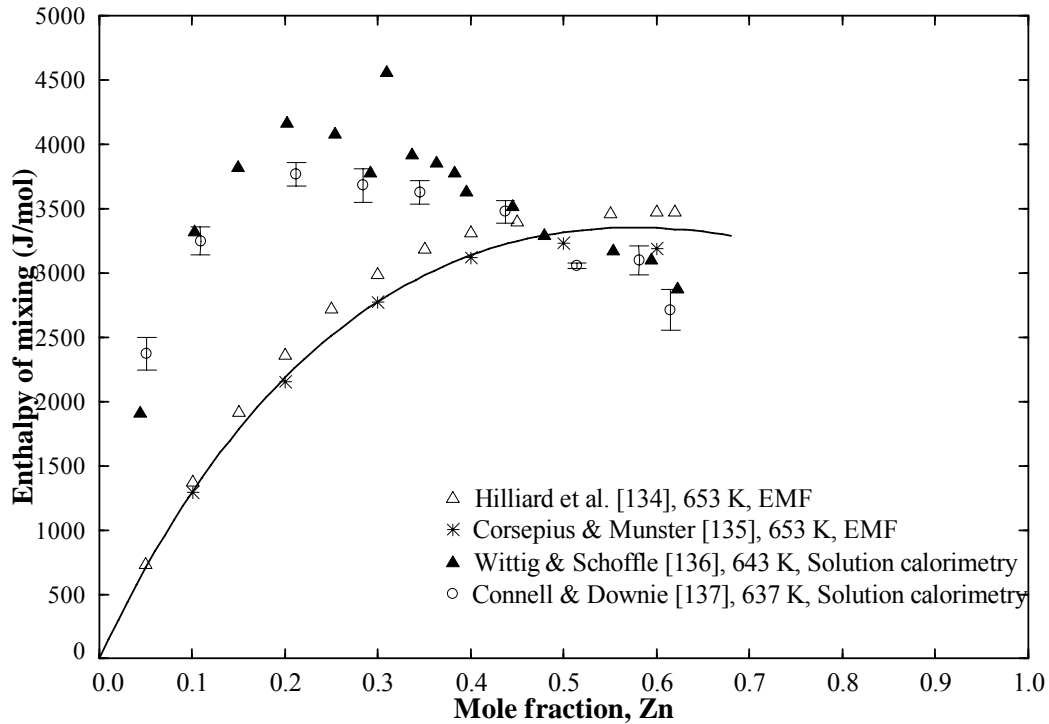
Figure 4.26: *Calculated enthalpies of mixing in the Al_fcc solid solution at 653 K in comparison with the experimental results*

The calculated activity of Al and Zn and the partial Gibbs energy of Al in the Fcc phase at 653 K is shown in Figures 4.27 and 4.28 respectively. The Al activity curve shows good consistency with the experimental points whereas the activity of Zn shows large deviation from the experimental points in Figure 4.27. The temperature of 653 K is only about 25 K higher than the critical temperature of the miscibility gap. Due to the close approximate of this temperature to the miscibility gap, the behavior of the thermodynamic properties can be expected to be similar to that of miscibility gap. Hence at 653 K, the Gibbs energy curve is expected to be flat enough similar to the miscibility gap in the composition range of 25.0 to 45.0 at.% Zn. This means the partial Gibbs energy will change slowly with increasing composition as shown in Figure 4.28.

However, the values obtained by Piacente *et al.* [147] and Takahashi and Asano [148] change rapidly with composition where both of them used the less accurate vapor pressure method. Nevertheless the current assessment is consistent with the experimental results for the Al activity, partial Gibbs energy and partial enthalpy of mixing as can be seen in Figures 4.27, 4.28 and 4.29.
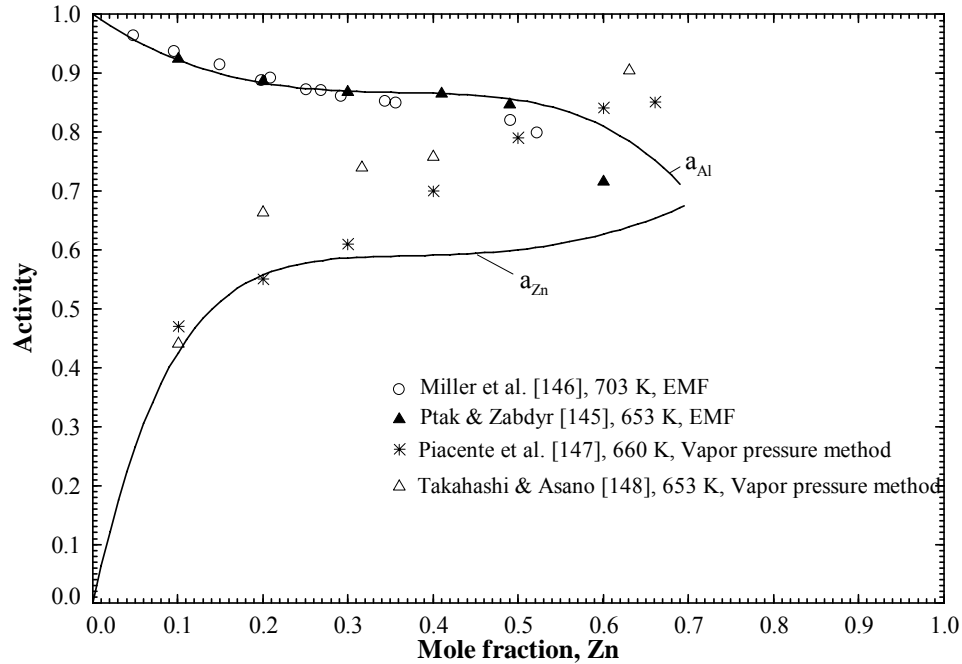
Figure 4.27: *Calculated activity of Al and Zn in the fcc phase at 653 K*

The calculated partial Gibbs energy of Al in the fcc phase can be seen in Figure 4.28 where reasonable agreement with the experimental data of Hilliard *et al.* [134] and Corsepius and Munster [135] was obtained except for some mismatch at higher than 50.0 at.% Zn.
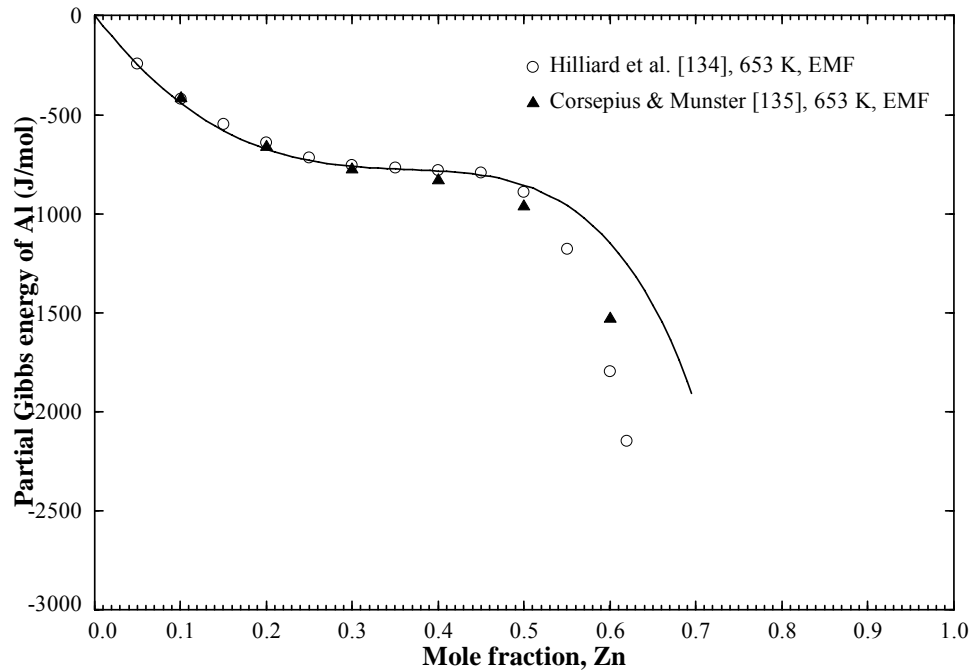
Figure 4.28: *Calculated partial Gibbs energy of Al in the fcc phase at 653 K*

Figure 4.29 shows the calculated partial enthalpy of mixing of Al at 653 K in comparison with the experimental points of Hilliard *et al.* [134] where good agreement is accomplished.
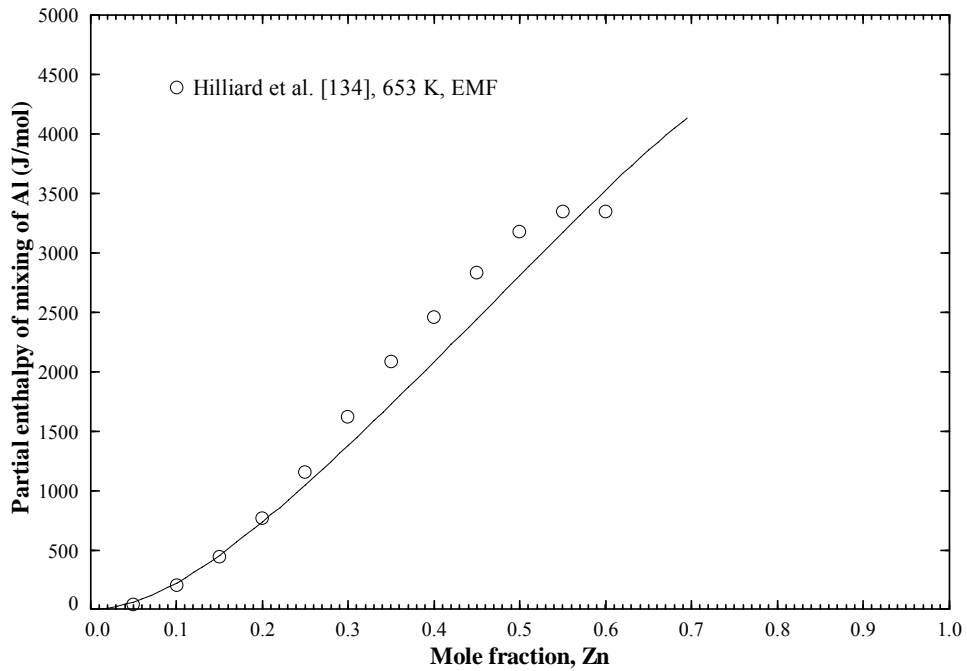
Figure 4.29: *Calculated partial enthalpy of mixing of Al in the fcc phase at 653 K*

4.6 Al-Ca Binary System

4.6.1 Equilibrium Phase Diagram

The most recent work on the Al-Ca binary system has done by Aljarrah and Medraj [151]. They critically evaluated all the available experimental data in the literature and used the modified quasichemical model to describe the liquid phase. In the present work, some modifications have made by adjusting the values of the composition dependent coordination numbers and the excess Gibbs energy parameters to increase the consistency with the experimental results. According to equation 3.17 the optimized Gibbs energy for the liquid phase can be written as:

$$\Delta^{ex} G_{AlCa}^{liq} = \text{-}30572.52 \ + \ 10.58 \ T + \ (1.32T) \ X_{AlAl} \ + \ (\text{-}4890.6\text{-}0.38T) \ X_{CaCa} \qquad \text{J/mol}$$

$$\text{……………. (4.8)}$$

The coordination number for the first nearest neighbors of Al and Ca atoms ($Z_{AlAl}^{Al}, Z_{CaCa}^{Ca}$) were set equal to 6. The tendency of maximum short range ordering near the composition of most stable intermediate phase (in this case Al$_2$Ca) was obtained by setting $Z_{AlCa}^{Al} = 3$ and $Z_{AlCa}^{Ca} = 6$. These were determined by iterative process to get the optimum result.

All the optimized parameters for different phases are shown in Table 4.13. The Gibbs energies of the pure Mg and Zn were taken from Dinsdale's compilation [160].

Table 4.13: *Optimized model parameters for different phases of the Al-Ca binary system*

Phase	Terms	a (J/mol-atom)	b (J/mol-atom.K)
Liquid	Δg^0_{AB}	-30572.52	10.58
	g^{i0}_{AB}	0.0	1.32
	g^{0j}_{AB}	-4890.6	-0.38
Al$_4$Ca	ΔG_f	-18506.59	-3.31
Al$_2$Ca	ΔG_f	-30225.80	-6.29
Al$_{14}$Ca$_{13}$	ΔG_f	-25111.14	-5.14
Al$_3$Ca$_8$	ΔG_f	-16254.45	-4.78

The re-optimized Al-Ca binary system is shown in Figure 4.30, which shows reasonable agreement with the experimental data from the literature. Neither Al nor Ca dissolves into one another and therefore no solid solution appear in the phase diagram. Table 4.14 lists all the invariant points in comparison with the experimental data as well as the calculation of Aljarrah and Medraj [151].
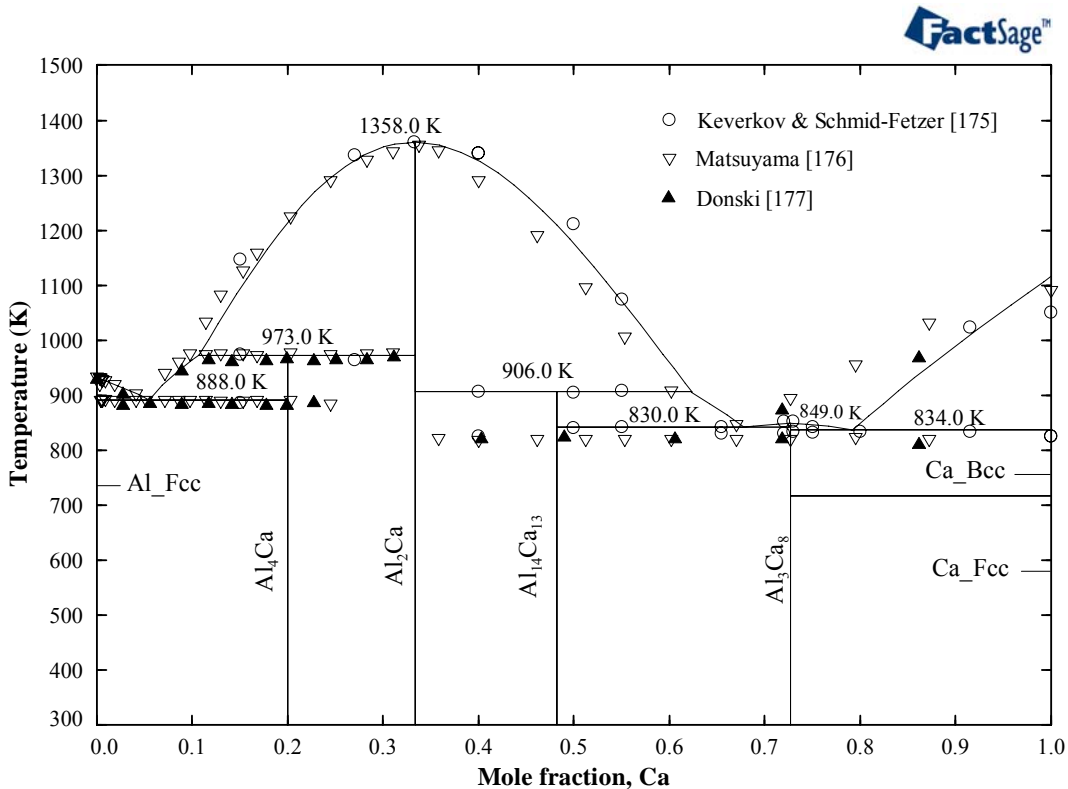
Figure 4.30: *Re-optimized Al-Ca phase diagram in comparison with the experimental results from the literature*

Table 4.14: *Comparison between the present calculation and the calculated and experimental values from the literature of the invariant reactions in the Al-Ca system*

Reaction type	Reaction	Composition (at.% Ca)	Temperature (K)	Reference
Eutectic	$L \leftrightarrow Al\_Fcc + Al_4Ca$	5.5	888.0	This work
		4.8	885.2	[151]
		5.1	886.2	[175]
		5.2	889.2	[176]
		5.5	883.2	[177]
	$L \leftrightarrow Al_{14}Ca_{13} + Al_3Ca_8$	67.8	830.0	This work
		66.5	830.2	[151]
		66.3	829.2	[175]
		64.5	818.2	[176]
		66.9	823.2	[177]
	$L \leftrightarrow Ca\_Bcc + Al_3Ca_8$	79.3	834.0	This work
		79.6	827.2	[151]
		80.0	833.2	[175]
Peritectic	$L + Al_2Ca \leftrightarrow Al_4Ca$	10.5	973.0	This work
		8.0	973.2	[151]
		-	973.2	[175]
		-	973.2	[176]
		-	963.2	[177]
	$L + Al_2Ca \leftrightarrow Al_{14}Ca_{13}$	62.2	906.0	This work
		61.0	904.2	[151]
		-	906.2	[175]
Congruent	$L \leftrightarrow Al_2Ca$	33.3	1358.0	This work
		33.3	1356.2	[151]
		33.3	1359.2	[175]
		33.3	1352.2	[176]
	$L \leftrightarrow Al_3Ca_8$	72.7	849.0	This work
		72.7	843.2	[151]
		72.7	852.2	[175]

4.6.2 Thermodynamic properties

The re-optimized excess Gibbs energy parameters have also been used to calculate the different thermodynamic properties in the liquid phase of the Al-Ca system. Figure 4.31 and 4.32 depict the calculated enthalpy of mixing and activity of Al and Ca in the liquid phase along the experimental values from the literature. Reasonable agreement with the experimental results can be seen from those figures except some discrepancy for

the activity of Al. Better agreement was not possible without deteriorating the liquidus curve.
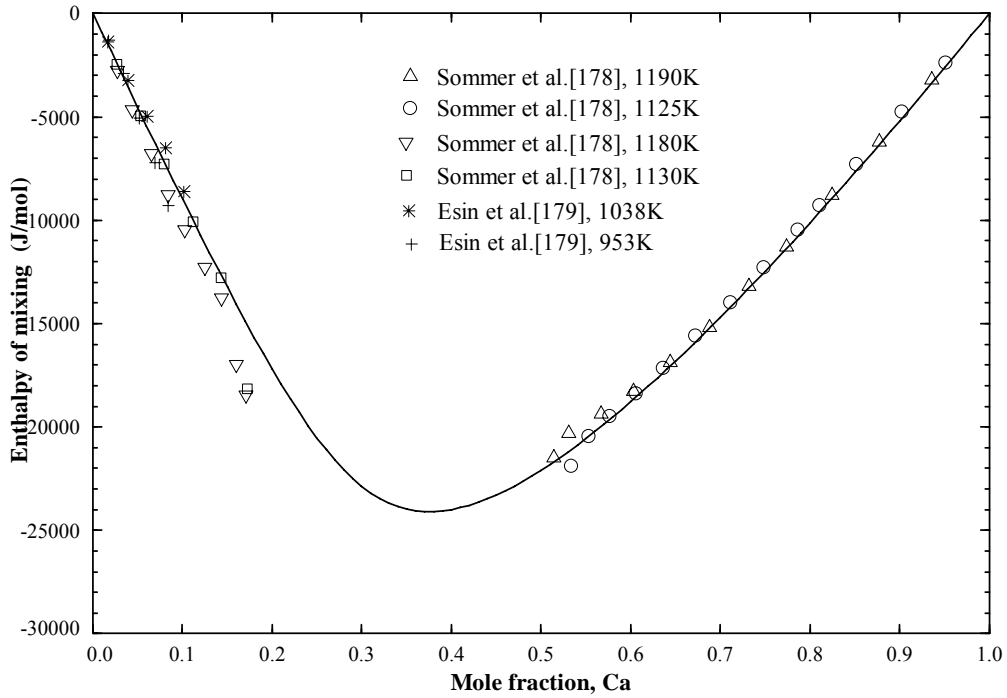
Figure 4.31: *Calculated enthalpies of mixing of Al and Ca in liquid Al-Ca alloy at 1100 K in comparison with the experimental results*
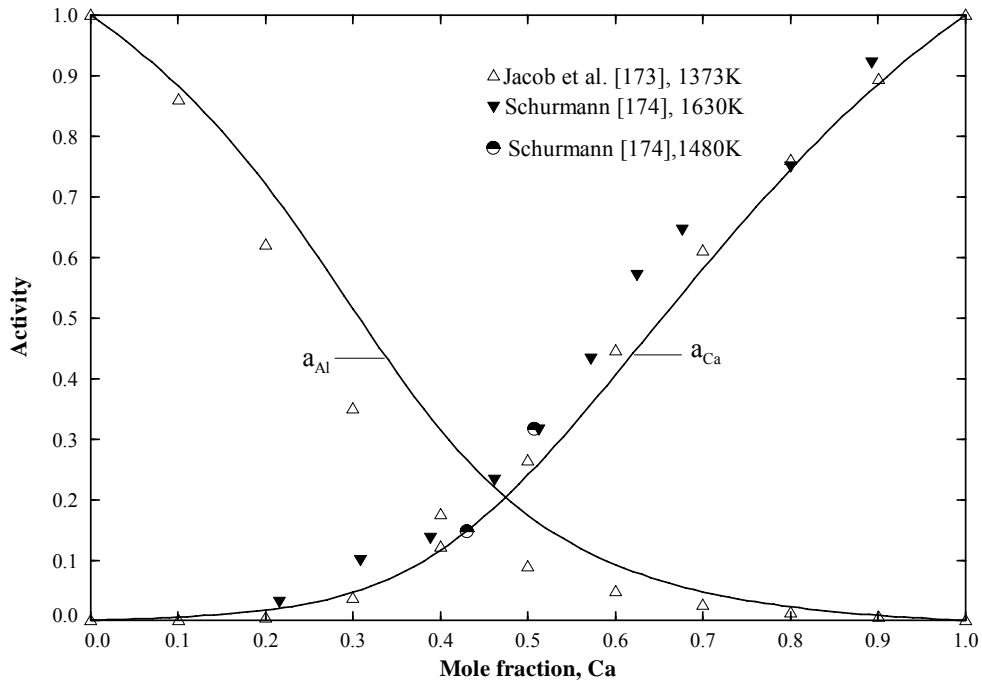
Figure 4.32: *Calculated activity of Al and Ca in the liquid state at 1373K*

4.7   Al-Ca-Zn Ternary System

A self-consistent thermodynamic database for the Al-Ca-Zn system has been created by extrapolating the three constituting binaries Al-Zn, Ca-Zn and Al-Ca. Ternary interaction parameters were used in order to achieve consistency with the available experimental data from the literature. The asymmetric Toop geometric model [165] was used for extrapolation since Al and Ca are chemically similar while Zn is chemically different. Hence Al and Ca were put in the same group while Zn was in a different group. Two ternary compounds: CaAlZn and $CaAl_2Zn_2$ reported by Ganiev *et al*. [155] and Gantsev *et al*. [156] in the literature were considered during the present optimization.

4.7.1 Ternary Phase Diagram

The main features of the Al-Ca-Zn ternary system will be discussed in this section by means of polythermal projections, isoplethal analysis and isothermal sections. The optimized ternary parameters both for the liquid phase and ternary compounds are presented in Table 4.15.

Table 4.15: *Optimized model parameters for different phases of the Al-Ca-Zn ternary system*

Phase	Terms	a (J/mol)	b (J/mol.K)
Liquid	$L_{AlCa(Zn)}$	-3854.0	0
	$L_{AlZn(Ca)}$	-4100.0	0
	$L_{CaZn(Al)}$	-35530.0	0
Phase	**Terms**	**a (J/mol-atom)**	**b (J/mol-atom.K)**
CaAlZn	ΔG_f	-33000.0	0.748
$CaAl_2Zn_2$	ΔG_f	-29700.0	0.449

4.7.1.1 Polythermal Projection. The liquidus projection of the Al-Ca-Zn system is shown in Figure 4.33 where the heavier solid lines represent the univariant valleys and the arrows on these lines indicate the directions of decreasing temperature. There are eight ternary eutectic (E_1 to E_8) points, ten quasi-peritectic (U_1 to U_{10}) points and nine maximum (m_1 to m_9) points present in this system. Details of all the ternary invariant points are summarized in Table 4.16.
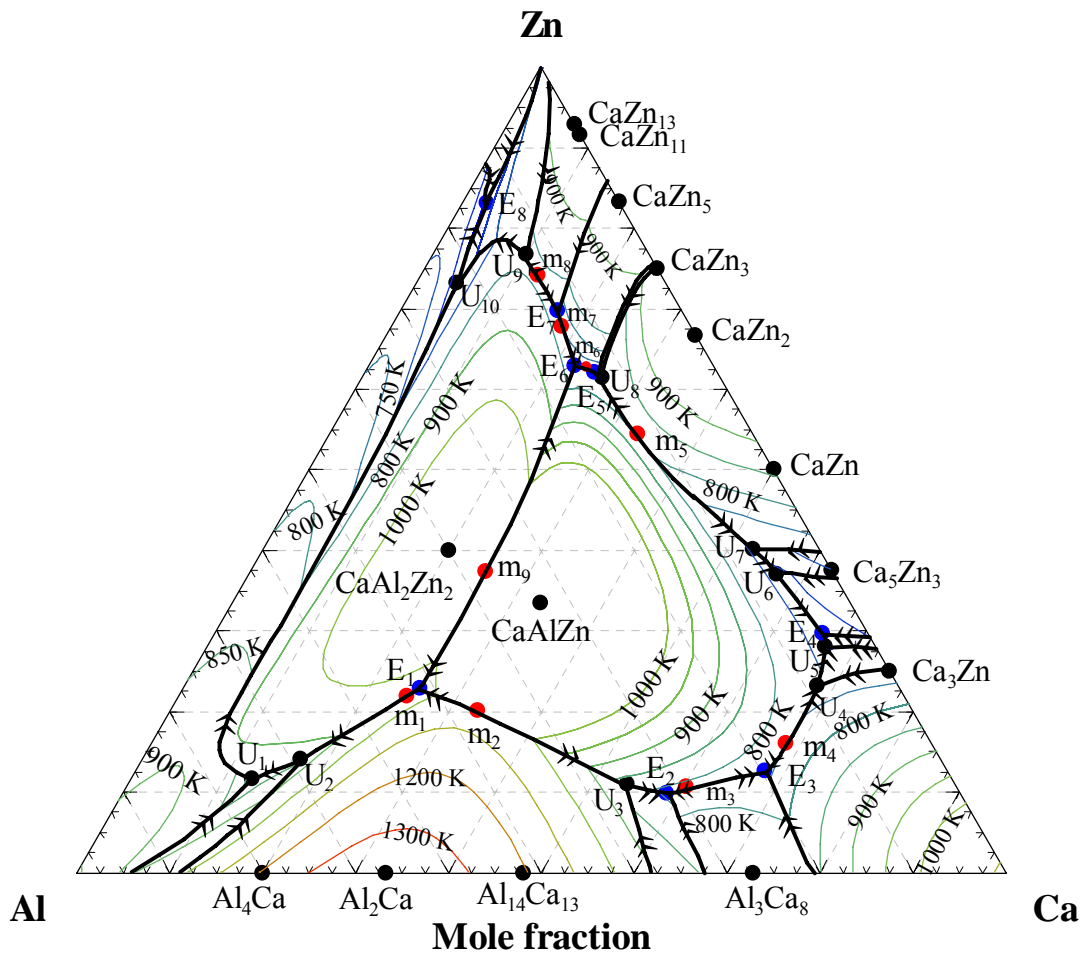
Figure 4.33: Calculated liquidus surface of the Al-Ca-Zn ternary system

Table 4.16: *Calculated invariant reactions and special points in the Al-Ca-Zn system*

Type	Reaction	Composition (at.%)			Temp (K)	Reference
		Al	**Zn**	**Ca**		
E_1	L $\leftrightarrow$ Al$_2$Ca+CaAlZn+CaAl$_2$Zn$_2$	51.8	22.7	25.8	952.0	This work
E_2	L $\leftrightarrow$ Al$_{14}$Ca$_{13}$+Al$_3$Ca$_8$+CaAlZn	31.5	9.6	58.9	777.2	This work
E_3	L $\leftrightarrow$ Ca_Bcc+Al$_3$Ca$_8$+CaAlZn	19.6	12.4	68.0	752.2	This work
E_4	L $\leftrightarrow$ AlCaZn+Ca$_3$Zn+Ca$_5$Zn$_3$	4.8	29.5	65.7	648.0	This work
E_5	L $\leftrightarrow$ CaZn$_5$+AlCaZn+CaZn$_3$	12.9	61.9	25.2	729.9	This work
E_6	L $\leftrightarrow$ AlCaZn+CaZn$_5$+CaAl$_2$Zn$_2$	14.8	62.9	22.3	729.5	This work
E_7	L $\leftrightarrow$ CaZn$_5$+CaZn$_{11}$+CaAl$_2$Zn$_2$	13.4	69.6	17.0	748.8	This work
E_8	L $\leftrightarrow$ Zn_Hcp+Al_Fcc+CaZn$_{13}$	13.6	84.0	2.4	636.4	This work
		11.18	88.46	0.46	653.0	[152]
U_1	L+Al$_4$Ca $\leftrightarrow$ Al_Fcc+CaAl$_2$Zn$_2$	75.3	11.6	13.1	818.0	This work
U_2	L+Al$_2$Ca $\leftrightarrow$ Al$_4$Ca+CaAl$_2$Zn$_2$	69.0	14.0	17.0	848.3	This work
U_3	L+Al$_2$Ca $\leftrightarrow$ Al$_{14}$Ca$_{13}$+CaAlZn	35.6	10.6	53.8	823.7	This work
U_4	L+Ca_Bcc $\leftrightarrow$ CaAlZn+Ca_Fcc	8.5	23.2	68.3	716.0	This work
U_5	L+Ca_Fcc $\leftrightarrow$ CaAlZn+Ca$_3$Zn	8.9	29.6	61.5	630.0	This work
U_6	L+CaZn $\leftrightarrow$ CaAlZn+Ca$_5$Zn$_3$	6.2	37.2	56.6	662.2	This work
U_7	L+CaZn$_2$ $\leftrightarrow$ CaZn+CaAlZn	7.0	40.2	52.8	678.0	This work
U_8	L+CaZn$_2$ $\leftrightarrow$ CaZn$_3$+CaAlZn	12.7	61.5	25.8	732.0	This work
U_9	L+CaZn$_{11}$ $\leftrightarrow$ CaAl$_2$Zn$_2$+CaZn$_{13}$	13.4	76.5	10.1	767.0	This work
U_{10}	L+CaAl$_2$Zn$_2$ $\leftrightarrow$ Al_Fcc+CaZn$_{13}$	21.6	73.5	4.9	620.0	This work
m_1	L $\leftrightarrow$ Al$_2$Ca+CaAl$_2$Zn$_2$	53.0	22.0	25.0	962.0	This work
		48.8	24.8	26.4	983.0	[156]
m_2	L $\leftrightarrow$ Al$_2$Ca+CaAlZn	18.0	50.0	32.0	1080.0	This work
		15.2	51.5	33.3	1123.0	[156]
m_3	L $\leftrightarrow$ Al$_3$Ca$_8$+CaAlZn	29.0	10.6	60.4	779.0	This work
m_4	L $\leftrightarrow$ CaAlZn+Ca_Bcc	15.7	16.0	68.3	760.3	This work
m_5	L $\leftrightarrow$ CaAlZn+CaZn$_2$	9.9	57.0	33.1	786.0	This work
		7.6	59.1	33.3	648.0	[156]
m_6	L $\leftrightarrow$ CaAlZn+CaZn$_5$	13.8	62.8	23.4	710.0	This work
		-	-	-	653.0	[156]
m_7	L $\leftrightarrow$ CaAl$_2$Zn$_2$+CaZn$_5$	13.8	67.9	18.3	748.5	This work
m_8	L $\leftrightarrow$ CaZn$_{11}$+CaAl$_2$Zn$_2$	13.3	74.1	12.5	775.5	This work
m_9	L $\leftrightarrow$ CaAlZn+CaAl$_2$Zn$_2$	37.0	37.0	26.0	1013.0	This work
		36.4	36.4	27.2	923.0	[156]

4.7.1.2 Isoplethal Analysis. Isoplethal analysis is another way to show different vertical sections and pseudo binary sections of a ternary phase diagram. Both Kono *et al.* [152] and Gantsev *et al.* [156] reported some pseudobinary sections and those will be compared with the present calculation. Figure 4.34 compares the current work with all the vertical sections reported by the different experimental works of [152] and [156].

(c)

Liquid

Gantsev et al.[156]

L+CaAl$_2$Zn$_2$

Liquid+CaAlZn

CaAlZn+CaAl$_2$Zn$_2$

Temperature (K)

Mole fraction, CaAl$_2$Zn$_2$

(d)

Gantsev et al.[156]

Liquid+CaAlZn

Liquid

Liquid+CaAl$_2$Zn$_2$

Liquid+CaZn$_{11}$

Liquid+CaAlZn+CaAl$_2$Zn$_2$

CaZn$_5$+CaAlZn+CaAl$_2$Zn$_2$

CaZn$_5$+CaZn$_{11}$
+CaAl$_2$Zn$_2$

Temperature (K)

Mole fraction, CaZn$_{11}$

(e)

Gantsev et al.[156]

Liquid

Liquid+Al$_2$Ca

Liquid+CaAl$_2$Zn$_2$

Al$_2$Ca+CaAl$_2$Zn$_2$

Temperature (K)

Mole fraction, CaAl$_2$Zn$_2$

111

Figure 4.34: Calculated isoplethal analysis of sections (a)Al-AlCaZn, (b) Al-CaZn$_{13}$, (c) CaAlZn-CaAl$_2$Zn$_2$, (d) CaAlZn-CaZn$_{11}$, (e) Al$_2$Ca-CaAl$_2$Zn$_2$, (f) Al$_2$Ca-CaAlZn, (g) CaAlZn-CaZn$_2$, (h) CaAlZn-CaZn$_5$

112

From Figure 4.34, it can be seen that most of the pseudo binary sections show reasonable agreement with the experimental results from the literature. It was impossible to make consistency with the two different sets of experiments when both works assumed different ternary compounds. Due to this fact, the sub-liquidus phases can be different sometime from the experimental result as can be seen in Figure 4.34 (b).

From Figure 4.34 (c) to Figure 4.34 (h) some discrepancy can be observed with the experimental points of Gantsev *et al.* [156] where they only reported the saddle point for each pseudo binary section. In the present work, it was not possible to achieve complete consistency with the work of [152] because they considered different number of intermetallic compounds: CaAlZn and CaAl$_3$Zn in this system. More experimental work on the liquidus curve will be more significant for adequate validation in this regard.

4.7.1.3 Isothermal section. The calculated isothermal sections at different temperatures of the Al-Ca-Zn system are demonstrated in Figures 4.35 to 4.37.
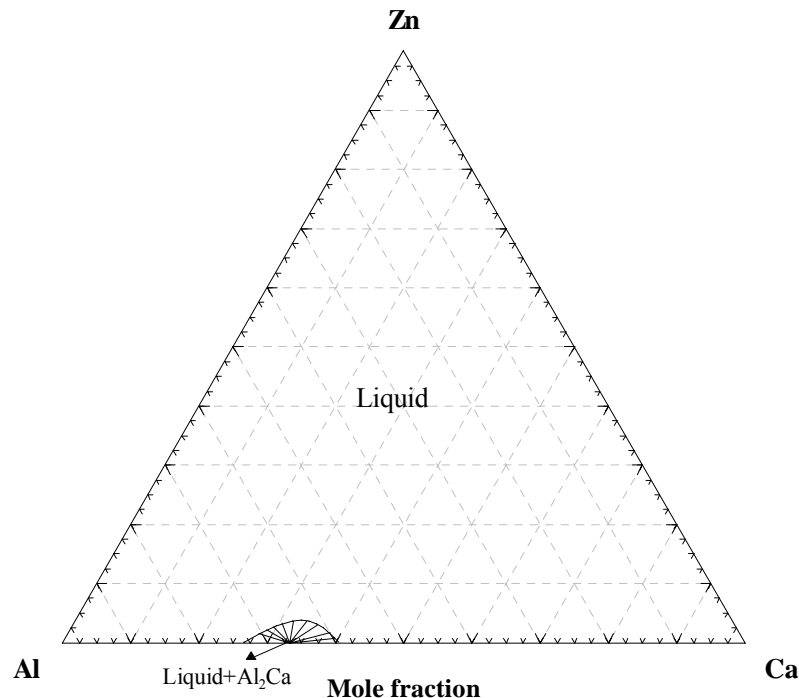
Figure 4.35: *Calculated isothermal section of the Al-Ca-Zn ternary system at 1320 K*

The solidification starts at around 1355 K. At a temperature higher than this one there is no phase boundary and only the homogenous liquid phase exists throughout the whole Gibbs triangle. Figure 4.35 shows the isothermal section of the Al-Ca-Zn system at 1320 K where only the crystallization of the Al_2Ca phase initiates and it exists in equilibrium with the liquid phase.

By cooling from 1320 K to 950 K solidification of some more phases appear in the ternary system which can be seen in Figure 4.36. But still the liquid phase dominates in the diagram. The new phases that appear at this temperature are: Al_4Ca, Al_2Ca, Ca_Bcc, $CaZn_5$, $CaZn_{11}$ and the two ternary phases: CaAlZn and $CaAl_2Zn_2$.
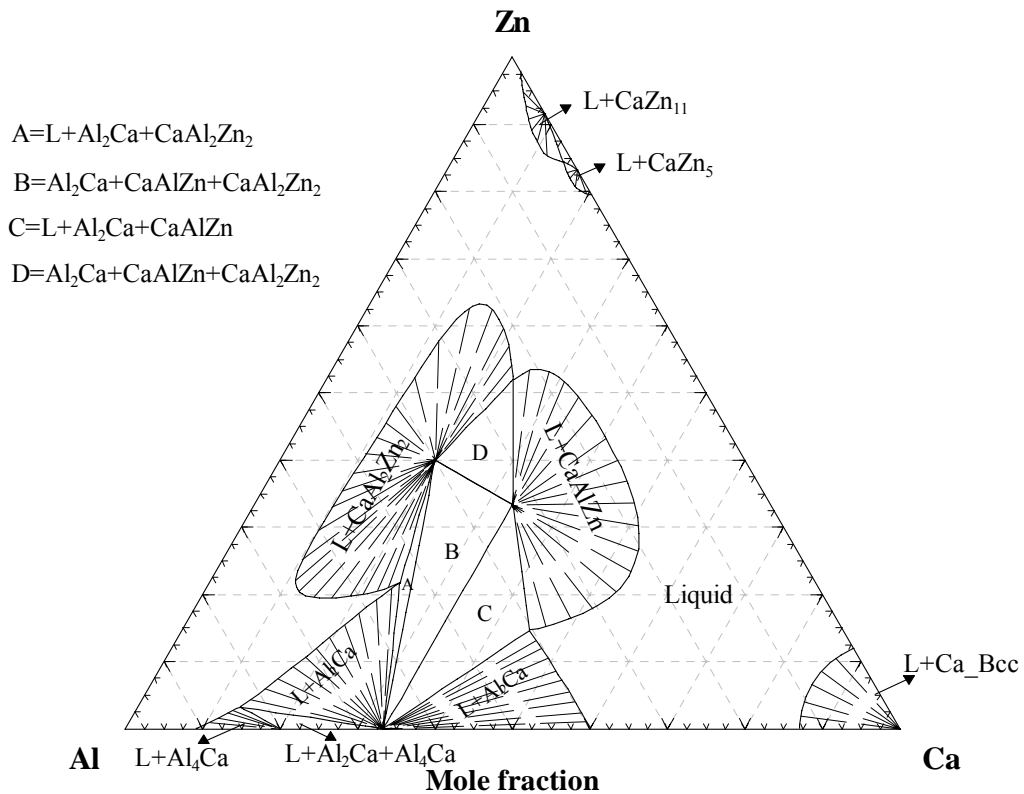
Figure 4.36: Calculated isothermal section of the Al-Ca-Zn ternary system at 950 K

Further crystallization takes place during cooling from 950 K to 650 K and Figure 4.37 shows the features of the ternary phase diagram at 650 K. It can be seen from the same figure that, almost all the phases including the two ternary compounds appear at this temperature.

Figure 4.37: *Calculated isothermal section of the Al-Ca-Zn system at 650 K with two ternary compounds where A denotes: CaAlZn and B denotes: CaAl₂Zn₂*

CHAPTER 5

Concluding Remarks, Contributions and Suggestions for Future Work

5.1 Concluding Remarks

An inclusive description of the Mg-Ca-Zn and Al-Ca-Zn ternary systems was carried out in the present work and the following summaries can be drawn:

- Thermodynamic modeling on the Mg-Ca-Zn and Al-Ca-Zn ternary systems was done based on the well established CALPHAD method.

- Critical assessment of all the available experimental data and optimization of the three binary systems: Mg-Zn, Ca-Zn and Al-Zn as well as of the two ternary systems: Mg-Ca-Zn and Al-Ca-Zn was carried out.

- The Modified Quasichemical Model was used for the liquid and Al_Fcc solid solution phases in order to account for the presence of short-range ordering.

- The Mg_2Ca Laves phase was remodeled by sublattice model to permit its incorporation with the $MgZn_2$ phase in the Mg-Ca-Zn ternary system.

- The Al-Ca binary system was re-optimized in order to increase the consistency of some of the invariant points from the most recent optimization work.

- The calculated phase equilibrium diagrams for all the binary systems and also their thermodynamic properties such as enthalpy of mixing, activity, partial

enthalpy of mixing and heat of formation showed reasonable agreement with the experimental data.

- Self-consistent databases for the Mg-Ca-Zn and Al-Ca-Zn ternary systems were created by combining the optimized model parameters of the corresponding binary systems and by introducing ternary interaction parameters and ternary compounds.

- Two ternary compounds reported by Clark resulted in the best consistency with the experimental results in terms of liquidus projection, isoplethal analysis and isothermal sections for the Mg-Ca-Zn ternary system.

- The calculated Al-Ca-Zn ternary system considering two ternary compounds which were accepted by most researchers, showed reasonable agreement with the experimental data.

5.2 Contributions

Despite the high potential of the Mg-Ca-Zn and Al-Ca-Zn alloy systems, few conclusive works in terms of thermodynamic modeling have been done so far. The significant contributions of the present research work include:

- As part of a broader research project to create a self-consistent database for the Mg alloys, thermodynamic descriptions of the Mg-Ca-Zn and Al-Ca-Zn ternary systems have been established in the present work.

- The presence of the short range ordering in the liquid phase was considered during optimization process which permits the composition of maximum short-range ordering in a binary system to be freely chosen.

- Two ternary compounds were considered in the Mg-Ca-Zn system for the first time which eventually gave better consistency with the experimental results.

- The Al-Ca-Zn ternary system was modeled for the first time considering two ternary compounds and verified with the limited experimental data available in the literature.

- The extended solid solution of the Al-Zn binary system was modeled using the modified quasichemical model for the first time which gave better representation of the thermodynamic properties.

5.3 Suggestions for Future Work

The recommendations for further studies on the Mg-Ca-Zn and Al-Ca-Zn systems to refine the thermodynamic modeling are summarized as follows:

- Additional experimental work is necessary to obtain more information about the ternary compounds in the Mg-Ca-Zn and Al-Ca-Zn ternary systems regarding their melting points, crystal structure, solubility limits and enthalpies of formation.

- In preparing the ternary compounds, samples have to be heat treated for long time (one month at least because of slow kinetics of formation of these compounds).

References

[1] U.R. Kattner, The Thermodynamic Modeling of Multicomponent Phase Equilibria, *Journal of Metals*, Vol. 49, No. 12, 1997, pp. 14-19.

[2] Y.A. Chang, S. Chen, F. Zhang, X. Yan, F. Xie, R. Schmid-Fetzer and W.A. Oates, Phase Diagram Calculation: Past, Present and Future, *Progress in Materials Science*, Vol.49, 2004, pp.313-345.

[3] Y.B. Kang, A.D. Pelton, P. Chartland, P. Spencer and C.D. Fuerst, Thermodynamic Database Development of the Mg-Ce-Mn-Y System for Mg Alloy Design, *Metallurgical and Materials Transactions A*, Vol. 38A, 2007, pp. 1231-1243.

[4] L. Kaufman and H. Bernstein, Computer Calculation of Phase Diagrams with Special Reference to Refractory Metals, Academic press, New York, 1970.

[5] P. Liang, T. Tarfa, J.A. Robinson, S. Wagner, P. Ochin, M.G. Harmelin, H.J. Seifert, H.L. Lukas and F. Aldinger, Experimental Investigation and Thermodynamic Calculation of the Al-Mg-Zn System, *Thermochemica Acta,* Vol. 314, 1998, pp. 87-110.

[6] Y.B. Kim, F. Sommer and B. Predel, Calorimetric Investigation of Liquid Aluminum-Magnesium-Zinc Alloys, *Journal of Alloys and Compounds*, Vol.247, 1997, pp.43-51.

[7] M. Ohno, D. Mirkovic and R. Schmid-Fetzer, Phase Equilibria and Solidification of Mg-rich Mg-Al-Zn Alloys, *Materials Science & Engineering, A: Structural Materials: Properties, Microstructure and Processing*, Vol. A421, No.1-2,2006, pp.328-337.

[8] P. Donnadieu, A. Quivy, T. Tarfa, P. Ochin, A. Dezellus, M.G. Harmelin, P. Liang, H.L. Lukas, H.J. Seifert, F. Aldinger and G. Effenberg, On the Crystal Structure and Solubility Range of the Ternary Phase in the Mg - Al - Zn System, *Zeitschrift fuer Metallkunde*,Vol.88, No.12,1997, pp.911-916.

[9] M. Aljarrah, Thermodynamic Modeling and Experimental Investigation of the Mg-Al-Ca-Sr System. PhD thesis, Concordia University, Montreal (Canada), 2008.

[10] J.F. Nie and B.C. Muddle, Precipitation Hardening of Mg-Ca (-Zn) Alloys, *Scripta Materialia*, Vol 37, No.34, 1997, pp. 1475-1481.

[11] B.-S. You,W.-W. Park, I.-S. Chung, The Effect of Calcium Additions on the Oxidation Behavior in Magnesium Alloys, *Scripta Materialia*, Vol. 42, No.11, 2000, pp.1089-1094.

[12] H. Watari, *Japanese Science and Technology Quarterly Report*, No.18, www.nistep.go.jp, as on 20 September 2008

[13] H. Somekawa, Y. Osawa, T. Mukai, Effect of Solid-solution Strengthening on Fracture Toughness in Extruded Mg-Zn Alloys, *Scripta Materialia*, Vol. 55 , Issue.7, 2006, pp. 593-596.

[14]AIST, http://www.aist.go.jp./aist_e/research_units/research_section/mrisus/mrisus_main.html, as on 20 September 2008

[15] H. Somekawa and T. Mukai, High Strength and Fracture Toughness Balance on the Extruded Mg-Ca-Zn Alloy, *Materials Science & Engineering, A: Structural Materials: Properties, Microstructure and Processing*, Vol. A459, Issue.1-2, 2007, pp.366-370.

[16] T.G. Nieh and J.Wadsworth, Superplasticity and Superplastic Forming of Aluminum Metal Matrix Composites, *Journal of Metals*, Vol. 44, No.11, 1992, pp. 46-50.

[17] V.A. Shvets, V.O. Lavrenko, V.M. Talash, Experience of Application of Protectors Made of Al-Zn-Ca Alloys. *Materials Science*, Vol. 42, No.4, 2006,pp.563-565.

[18] D.M. Moore and L.R. Morris, U.S. patent 4, 126, 448, November, 1978.

[19] O. Boudouard, Alloys of Zinc and Magnesium**,** *Comptes Rendus Hebdomadaires des Seances de l'Academie des Sciences*, Vol. 139 , 1904, pp.424-426.

[20] R. Agarwal, S.G. Fries, H.L. Likas, G. Petzow, F. Sommer, T.G. Chart and G. Effenberg, Assessment of the Mg-Zn System, *Zeitschrift fuer Metallkunde*, Vol.83, Issue.4, 1992, pp. 216-223.

[21] G. Grube, Alloys of Magnesium with Cadmium, Zinc, Bismuth and Antimony, *Zeitschrift Fuer Anorganische Chemie*, Vol. 49, 1906, pp. 72-92.

[22] G. Bruni, C. Sandonnini and E. Quercigh, The Ternary of Magnesium, Zinc and Cadmium, *Zeitschrift Fuer Anorganische Chemie*,Vol. 68, 1911, pp. 73-90.

[23] G. Bruni and C. Sandonnini, The Ternary of Magnesium, Zinc and Cadmium II, *Zeitschrift Fuer Anorganische Chemie*, Vol. 78, 1913, pp. 273-297.

[24] R.J. Chadwick, The Constitution of the Alloys of Magnesium and Zinc, *Journal of The Institute of Metals*,Vol 39, 1928, pp. 285-297.

[25] W. Hume-rothery and E.D. Rounswfell, The System Magnesium-Zinc, *Journal of The Institute of Metals*,Vol. 41,1929, pp. 119-138.

[26] S. Samson, The Crystal Structure of Mg_2Zn_{11}: Isomorphism between Mg_2Zn_{11} and $Mg_2Cu_6Al_5$, *Acta Chemica Scandinavica*, Vol. 3, No.8, 1949, pp. 835-843.

[27] M.I. Zaharov and A.B. Mladzeevskiy, Thermal Investigation of the Intermetallic Compounds in the System Zinc-Magnesium, *Izvest.Sebt.Fiz.-Khim.Anal.*, Vol. 9, 1936, pp.195-202.

[28] F. Laves, Constitution of Magnesium-Zinc Alloys, *Naturwissenschaften*, Vol. 27, 1929, pp.454-455.

[29] G.G. Urazov, N.A. Filin, A.V. Shashin, The Fusion Diagram of the System Aluminum-Magnesium-Zinc, *Metallurg*, 1940, Vol. 15, No. 6, pp.3-11.

[30] E. M. Savitskii and V.V. Baron, Constitution Diagram and Mechanical Properties of the Mg-Zn System, *Doklady Akademii Nauk SSSR*, 1949, Vol. 64,pp.693-696.

[31] K.P. Anderko, E.J. Klimek, D.W. Levonson and W. Rostocker, Constituent Studies on the System Magnesium-Zinc, *Transactions of The American Society for Metals*, Vol. 49, 1957, pp. 778-793.

[32] J.J. Park and L.L.Wyman, Phase Relationships in Magnesium Alloys, *WADC Tech. Rept. 57-504*, Astia Document No. AD142110, 1957, pp. 1-27.

[33] J.B. Clark and F.N. Rhines, Central Region of the Magnesium-Zinc Phase Diagram, *Journal of Metals*, Vol 9, 1957, pp. 425-430.

[34] T. Takei, The Equilibrium Diagram of the System Magnesium-Zinc, *Kinzoku-no Kenkyu, Japan Institute of Metals*, Vol 6, 1929, pp. 177-183.

[35] S. Ishida, The Magnesium-Zinc Phase Diagram, *Nippon Kogyo Kwai-Shi*, Vol.45, 1929, pp.256-268, 611-621, 786-790.

[36] W. Koster and F. Muller, Observations on the Phase Mg_7Zn_3 and Its Decomposition, *Zeitschrift fuer Metallkunde*, Vol.39, 1948, pp. 352-353.

[37] I. Higashi, N. Shotani, M. Uda, T. Mizoguchi and H.katoh, The Crystal Structure of $Mg_{51}Zn_{20}$, *Journal of Solid State Chemistry*, Vol. 36, 1981, pp. 225-233.

[38] M. Hansen,The Constitution of the Alloys of Magnesium and Zinc, *Journal of The Institute of Metals*,Vol 39, 1928, pp. 298-300.

[39] W. Schmidt and M. Hansen, Solidus and Solvus of the Magnesium Solid Solutioin of Magnesium-Zinc Alloys, *Zeitschrift fuer Metallkunde*, Vol. 19, 1927, pp. 452-455.

[40] G. Grube and A. Burkhardt, The Electrical Conductivity, Thermal Expansion and Hardness of Magnesium-Zinc, *Zeitschrift fuer Elektrochemie und Angewandte Physikalische Chemie,* Vol 35, 1929, pp. 315-331.

[41] E. Schmid and H. Seliger, Investigation of the Solid Solutions of Magnesium, *Metallwirtsch.*, Vol. 11, 1932, pp. 409-412.

[42] H. Adenstedt and J.R. Burns, The Determination of Solidus Temperature in Magnesium Alloys by Dilatometric Measurements, *Transactions of The American Society for Metals,* Vol. 43, 1951, pp.873-887.

[43] J.B. Friauf, The Crystal Structure of Magnesium Di-zincide, *Physical Review*, Vol. 29,1927, pp.34-40.

[44] Y. Komua and K. Tokunga, Structural Studies of Stacking Variants in Mg-base Friauf-Laves Phases, *Acta Crystallography*, Vol.B36, 1980, pp.1548-1554.

[45] J.L.C Damms, P. Villars and J.H.N. van Vucht (Ed.), *Atlas of Crystal Structure Types for Intermetallic Phases*, Vol.3, ASM Intrenational, Materials Park, OH, July 1991, pp. 4937-4939.

[46] J.B. Clark, L. Zabdyr and Z. Moser, Mg-Zn, *Phase Diagrams of Binary Magnesium Alloys,* ASM, Metals Park, OH, 1988, pp. 353-365.

[47] O. Redlich, and A.T Kister, Thermodynamics of Nonelectrolyte Solutions, X-Y-T Relations in a Binary System, *Journal of Industrial and Engineering Chemistry Washington D. C.*, Vol. 40, 1948, pp. 341-345.

[48] M. Hillert, The Compound Energy Formalism, *Journal of Alloys and Compounds*, Vol. 320, 2001, pp. 161-176.

[49] M. Kawakami, The Heat of Mixing in Molten Metals, *Science Reports of the Tohoku Imperial University, Series 1: Mathematics, Physics, Chemistry*,Vol.19, 1930, pp.521-49.

[50] R. Hultgren, P.D. Desai, D.T. Hawkins, M. Gleiser and K.K. Kelly, Selected Values of the Thermodynamic Properties of Binary Alloys, ASM, Metals Park, OH, 1973.

[51] H. Pyka, Untersuchungen zur Thermodynamik Glasbildender Ternärer Legierungen, PhD thesis, University Stuttgart, Stuttgart (Germany) 1984.

[52] R. Agarwal and F. Sommer, Calorimetric Investigations of Mg-Zn and Mg-Y Liquid Alloys, *Proceedings of 8th National Symposium Thermal Analysis*, Publisher: Indian Thermal Analysis Society, Bombay, India, 1991, pp. 249-254.

[53] J. Terpilowski, Thermodynamic Properties of Liquid Zinc-Magnesium Solutions, *Bull. Acad. Polon. Sci.*, Vol 10, 1962, pp. 221-225.

[54] S.P. Chiotti and E.R. Stevens, Thermodynamic Properties of Mg-Zn Alloys, *Transactions of the American Society for Metals,* Vol. 233, Issue.1,1965, pp.198-203.

[55] Z. Moser, Thermodynamic Properies of Dikute Solutions of Magnesium in Zinc, *Metallurgical Transactions*, Vol. 5, Issue.6,1974, pp.1445-1450.

[56] A.M. Pogodaev and E.E. Lukashenko, Thermodynamic Study of Molten Magnesium and Zinc Alloys, *Russian Journal of Physical Chemistry*, Vol. 46, Issue.2, 1972, pp. 334-339.

[57] Z. Kozuka, J. Moriyama and I. Kushima, Activity of the Component Metal in Fused Binary Alloys-Zn-Al and Zn-Mg Systems, *Journal of Electrochemical Society of Japan*, Vol. 28, Issue.10, 1960, pp. 523-526.

[58] A. Schneider, H. Klotz, J. Stendel and G. Strauss, Thermochemistry of Magnesium Alloys, *Pure and Applied Chemistry*, Vol. 2, 1961, pp. 13-16.

[59] R.C. King and O.J. Kleppa, A Thermochemical Study of Some Selected Laves Phases, *Acta Metalurgica*, Vol. 12, Issue.1, 1964, pp. 87-97.

[60] T.O. Pedokand, S.N. Shkol'Nikov and E.V. Tomazova, Thermodynamic Study of Magnesium-Zinc Alloys in a Solid State, *Tr. Lenigr. Politekhn. In-Ta,* Vol. 348, 1976, pp. 34-39.

[61] L. Donski, Alloys of Calcium with Zinc, Cadmium, Aluminum, Thallium, Lead, Tin, Bismuth, Antimony and Copper, *Zeitschrift Fuer Anorganische Chemie,* Vol.57, 1908, pp. 185-193.

[62] G. Bruzzone, E. Franceschi and F. Merlo, M_5X_3 Intermediate Phases Formed by Ca, Sr and Ba, *Journal of the Less-Common Metals*, Vol. 60, 1978, pp. 59-63.

[63] M.L. Fornasini and F. Merlo, $CaZn_3$: A Structure with Mixed $BaLi_4$ and $CeCu_2$-Like Ordering, *Acta Crystallography*, Vol. B36, 1980, pp. 1739-1744.

[64] G.E.R. Schulze and J. Wieting, The Structural Characteristics of The $CaZn_2$ Lattice, *Zeitschrift fuer Metallkunde*, Vol. 52, 1961, pp. 743-746.

[65]W. Haucke, The Crystal Structure of $CaZn_5$ and $CaCu_5$, *Zeitschrift fuer Anorganische und Allgemeine Chemie*, Vol. 244, 1940, pp.17-22.

[66] A. Iandelli and A. Palenzona, Zinc-rich Phases of the Rare-earth-zinc Alloys, *Journal of the Less-Common Metals*, Vol. 12, No.5,1967, pp.333-343.

[67] J.A.A. Ketelaar, The Crystal Structure of Alloys of Zinc with the Alkali and Alkaline Earth Metals and of Cadmium with Potassium, *Journal of Chemical Physics*, Vol. 5,1937, pp.668.

[68] R. Paris, Ternary Alloys, *Publications Scientifiques et Techniques du minist'ere de L'Air, Ministère de L'Air*, No.45, 1934, pp. 1-86.

[69] A.F. Messing, M.D. Adams and R.K. Steunenberg, Contribution to the Phase Diagram Calcium-Zinc, *Transactions of the ASM.*, Vol. 56, 1963, pp. 345-350.

[70] V.P. Itkin and C.B. Alcock, The Ca-Zn System, *Bulletin of Alloy Phase Diagrams*, Vol. 11, No 4, 1990, pp. 328-333.

[71] C.O. Brubaker and Z.-K. Liu, A Computational Thermodynamic Assessment of the Ca-Zn system, *CALPHAD*, Vol. 25, No. 3, 2001, pp. 381-390.

[72] P.J. Spencer, A.D. Pelton, Y-B. Kang, P. Chartrand, C.D. Fuerst, Thermodynamic Assessment of the Ca-Zn, Sr-Zn, Y-Zn and Ce-Zn system, *CALPHAD*, Vol. 32, No.2, 2008, pp. 423-431.

[73] P. Chiotti and R.J. Hecht, Thermodynamic Properties of the Calcium-Zinc System, *Transactions of the Metallurgical Society of AIME*, Vol. 239, 1967, pp. 536-542.

[74] J. Delcet and J.J. Egan, Thermodynamics of Liquid Ca-Zn Alloys, *Metalallurgical Transactions B*, Vol 9B, pp.728-729.

[75] T. Miyazaki, J. Kaneko and M. Sugamata, Structures and Properties of Rapidly Solidified Mg-Ca based Alloys, *Materials Science and Engineering*, Vol. A 181/182, 1994, pp.1410-1414.

[76] A.A. Nayeb-Hashemi and J.B. Clark, The Ca-Mg (Calcium-Magnesium) System," *Bulletin of Alloy Phase Diagrams*, Vol.8**,** 1987, pp.58-65.

[77] R. Agarwal, J. Lee, H. Lukas and F. Sommer, "Calorimetric Measurements and Thermodynamic Optimization of the Ca-Mg System," *Zeitschrift fur Metallkunde*, Vol.86, No.2, 1995, pp.103-108.

[78] M. Aljarrah and M. Medraj, Thermodynamic Modeling of the Mg-Ca, Mg-Sr, Ca-Sr and Mg-Ca-Sr Systems using the Modified Quasichemical Model, *CALPHAD (Computer Coupling of Phase Diagrams and Thermochemistry),*Vol.32, No.2, 2008, pp.240-251.

[79] A.D. Pelton, S.A. Degterov, G. Eriksson, C. Robelin and Y. Dessureault, The Modified Quasi-chemical Model I – Binary Solutions, *Metallurgical and Materials Transactions B*, Vol. 31B, 2000, pp. 651-659.

[80] A.D. Pelton, and P. Chartrand, The Modified Quasi-chemical Model: Part II. Multicomponent Soutions, *Metallurgical and Materials Transactions A*, Vol. 32A, 2001, pp. 1355-1360.

[81] P. Chartrand, and A.D. Pelton, The Modified Quasi-chemical Model: Part III. Two Sublattices, *Metallurgical and Materials Transactions A*, Vol. 32A, 2001, pp. 1397-1407.

[82] H. Vosskühler, The Phase Diagram of Magnesium-rich Mg–Ca Alloys, *Zeitschrift fuer Metallkunde*, Vol. 29, 1937, pp. 236–237.

[83] N. Baar, On The Alloys of Molybdenum with Nickel, Manganese with Thallium, and Calcium with Magneisum, Thallium, Lead, copper, and Silver, *Zeitschrift Fuer Anorganische Chemie*, Vol. 70,1911, pp. 362–366 (From British Library www.bl.uk, "Ca–Mg (Calcium–Magnesium)", Landolt-Bornstein Series IV/5c, pp. 22–25).

[84] J.L. Haughton, Alloys of Magnesium. Part 6—The Construction of The Magnesium-rich Alloys of Magnesium and Calcium, *Journal Institute of Metals*,Vol. 61, 1937, pp. 241–246.

[85] H. Nowotny, E. Wormnes and A. Mohrnheim, Investigation on the Al–Ca, Mg–Ca, and Mg–Zr Systems, *Zeitschrift fuer Metallkunde*, Vol. 32, 1940, pp. 39–42.

[86] W. Klemm and F. Dinkelacker, On the Behavior of Magnesium with Calcium, Strontium and Barium, *Zeitschrift Fuer Anorganische Chemie*, Vol. 255, 1947, pp. 2–12.

[87] E.C. Burke, Solid Solubility of Calcium in Magnesium, *Journal of Metals, Transaction AIME*, Vol. 203, 1955, pp. 285–286.

[88] W.Bulian and E. Fahrenhorst, Solubility of Calcium in Magnesium, *Metallforschung*, Vol.1, 1946, pp.70.

[89] F. Sommer, B. Predel and D. Assmann, "Thermodynamic Investigation of Liquid Alloys in the Systems Mg-Ca, Mg-Sr, and Mg-Ba," *Zeitschrift fur Metallkunde*, Vol. 68, No.5, 1977, pp.347-3491.

[90] V.P. Mashovets and L.V. Puchkov, "Vapour Pressure over Molten Alloys in the System Mg-Ca," *Zhurnal Prikladnoi Khimii*, Vo.38, No.5, 1965, pp.1009-1014.

[91] F. Sommer, "Thermodynamic Activities of Liquid Alloys in the System Ca-Mg Using a Modified Ruff Method," *Zeitschrift fur Metallkunde,* Vol.70, No.8, 1979, pp. 545-547.

[92] J.B. Clark, The Solid Constitution in the Mg-rich Region of the Mg-Ca-Zn Phase Diagram, *Trans. AIME*, Vol 221, 1961, pp. 644-645.

[93] J.B. Clark, *Joint Committee on powder Diffraction Standards (JCPDS) Card 12-266*, 1961.

[94] J.B. Clark, *Joint Committee on powder Diffraction Standards (JCPDS) Card 12-569*, 1961.

[95] J.F. Nie and B.C. Muddle, Precipitation Hardening of Mg-Ca (-Zn) Alloys, *Scripta Materialia*, Vol 37, No.34, 1997, pp. 1475-1481.

[96] T. Horie, H. Iwahori, Y. Seno and Y. Awano, Development of High Creep-resistant Magnesium Alloy Strengthened by Ca Addition, *Proceedings of the Magnesium Technology 2000*, eds.H.I. Kaplan, J. Hryn and B. Clow, The Minerals, Metals and Materials Society, 2000, pp.261-269.

[97] T.V. Larinova, W.W. Park and B.S.You, A Ternary Phase Observed in Rapid Solidified Mg-Ca-Zn alloys, *Scripta Materialia*, Vo. 45, 2001, pp.7-12.

[98] P.M. Jardim, G. Solorzano and J.B.V. Sande, Second Phase Formation in Melt-spun Mg-Ca-Zn Alloys, *Materials Science and Engineering A*, Vol.381, No.1-2, 2004, pp.196-205.

[99] P.M. Jardim, G. Solorzano and J.B.V. Sande, Precipitate Crystal Structure Determination in Melt Spun Mg-1.5wt%Ca-6wt%Zn Alloy, *Mircoscopy and Microanaysis*, Vol. 8, 2002, pp. 487-496.

[100] C.O. Brubaker and Zi-Kui Liu, A Computational Thermodynamic Model of the Ca-Mg-Zn System, *Journal of Alloys and Compounds*, Vol. 370, 2004, pp. 114-122.

[101] C.T. Heycock and F.H. Neville, The Freezing Points of Alloys Containing Zinc and Another Metal, *Journal of the Chemical Society Transactions*, Vo. 71,1897, pp.383-398.

[102] T. Tanabe, Studies in The Aluminium-Zinc System, *Journal of the Institute of Metals*, Vol.32, 1924,pp. 415-427.

[103] T. Isihara, On the Equilibrium Diagram of the Aluminum-Zinc System, *Science Reports of the Tohoku Imperial University*,Vol.13, 1924, pp.18-21.

[104] M.L.V. Gaylor, M. Haughton and E.G. Sutherland, The Constitution of Aluminum-Zinc Alloys of High Purity: the Nature of the Thermal Change of 443 °C, *Journal of the Institute of Metals*, Vol. 63, 1938, pp.123-147.

[105] E. Pelzel and H. Schneider, Contribution to the Understanding of Zn Alloys, *Zeitschrift fur Metallkunde*, Vol. 35, 1943, pp.124-127.

[106] E. Butchers and W.Hume-Rothery, On the Constitution of Aluminum-Magnesium-Manganese-Zinc Alloys: The Solidus, *Journal of the Institute of Metals*, Vol. 71, 1945, pp. 291-311.

[107] E. Pelzel, The Positions of the Liquidus and Solidus Curves in the Al-Zn System from 30 to 70 wt.% Al, *Zeitschrift fur Metallkunde*, Vol.40, 1949, pp.134-136.

[108] I.S. Solet and H.W.S. Clair, Liquidus Temperatures and Liquid Densities of Zinc-Aluminum Alloys, *Bureau of Mines Report of Investigations 4553*, 1949, pp.1-7.

[109] Q. F. Peng, F.S. Chen, B.S. Qi, Y.S. Wang, Measurement of Aluminum-zinc Phase Diagram by Acoustic Emission During Solidification, *Transactions of the American Foundrymen's Society*, Vol. 99 ,1991, pp.199-202.

[110] T. Morinaga, On the Equilibrium Diagram of The Aluminum-Zinc System, *Nippon Kinzoku Gakkaishi*, Vol.3, 1939, pp.216-221.

[111] E. Gebhardt, Equilibrium Experiments on the Systems Zinc-Aluminum and Zinc-Aluminum-Copper, *Zeitschrift fur Metallkunde*, Vol. 40, 1949, pp. 136-140.

[112] E.C. Ellwood, The Solid Solutions of Zinc in Aluminum, *Journal of the Institute of Metals*, Vol. 80, 1951, pp. 217-224.

[113] H. Araki, Y. Minamino, T. Yamane, K. Azuma,Y. S Kang,.; Y. Miyamoto, Partial Phase Diagrams of the Aluminum-rich Region of the Aluminum-Zinc System at 0.1 MPa and 2.1 GPa, *Journal of Materials Science Letters*, Vol. 11, No.3,1992, pp.181-183.

[114] W.L Fink and L.A. Willley, Equilibrium Relations in Aluminum-Zinc Alloys of High Purity, II, *Transactions of the Metallurgical Society of AIME*, Vol.12, 1936, pp. 244-260.

[115] G. Borelius and L.E. Larsson, Kinetics of Precipitation in Aluminum-Zinc Alloys. *Arkiv foer Matematik, Astronomi och Fysik*, Vol. 35A, No. 13,1948, pp.1-14.

[116] A.Munster and K. Sagel, Miscibilty Gap and Critical Point of the Aluminum-Zinc System, *Zeitschrift fuer Physikalische Chemie*, Vol. 7,1956, pp.267-295.

[117] L.E. Larsson, Pre-precipitation and Precipitation Phenomena in the Al-Zn System, *Acta Metallurgica*, Vol.15, 1967, pp.35-44.

[118] M. Simerska and P. Bartuska, The X-Ray Diffraction and Electron Microscopic Investigation of Stable and Metastable Equilibria in Al-rich Al-Zn Alloys, *Czech Journal of Physics*, Vol. B24, 1974, pp.553-559.

[119] H. Terauchi, N. Sakamoto, K. Osamura, Y. Murakami, Small Angle X-ray Critical Scattering in an Aluminum-Zinc Alloy with Critical Composition, *Transactions of the Japan Institute of Metals*, Vol.16, No.7,1975, pp.379-83.

[120] J.M. Holender and J. Soltys, The Studies of the Eutectoidal Decomposition of Al-59 at.% Zn at the Temperature Close to the Critical Temperature, *Diffusion and Defect Data--Solid State Data, Pt. A: Defect and Diffusion Forum*, Vols.66-69, 1989, pp. 1461-1466.

[121] W.M. Pierce and M.S. Palmerton, Studies on the Constituent of Binary Zinc-based Alloys, *Transactions of the Metallurgical Society of AIME*, Vol.68, 1923, pp. 767-795.

[122] H. Auer and K.E. Mann, Magnetic Investigation of the Aluminum-Zinc System, *Zeitschrift fur Metallkunde*, Vol. 28, 1936, pp.323-326.

[123] M.L. Fuller and R.L. Wilcox, Phase Changes During Aging of Zinc-Alloy Die Castings, II-Changes in the Solid Solution of Aluminum in Zinc and Their Relation to Dimensional Changes, *Transactions of the Metallurgical Society of AIME*, Vol.122, 1936, pp. 231-246.

[124] A. Burkhardt, Zinc Alloys as a Substitute Material, *Zeitschrift fur Metallkunde*, Vol.28, No.10, 1936, pp.299-308.

[125] K. Loehberg, X-Ray Determination of the Solubility of Aluminum and Copper in Zinc, *Zeitschrift fur Metallkunde*, Vol.32, 1940, pp. 86-90.

[126] W. Hoffman and G. Fahrenhost, Precipitation Rates in High Purity Zinc-Aluminum and Zinc-Copper Alloys, *Zeitschrift fur Metallkunde*, Vol.42, 1950, pp. 460-463.

[127] A. Pasternak, The Solid Solubility of Metals in Lead and Zinc, *Bulletin International de l'Academie Polonaise des Sciences et des Lettres, Classe des Sciences Mathematiques et Naturelles, Serie A: Sciences Mathematiques*,1951, pp.177-192.

[128] J.L. Murray, The Alumnum-Zinc System, *Bulletin of Alloy Phase Diagrams*, Vol. 4, No.1, 1983, pp.55-73.

[129] S.A. Mey and G. Effenberg, A Thermodynamic Evaluation of the Aluminum-Zinc System, *Zeitschrift fur Metallkunde*, Vol.77, No.7 1986, pp. 449-453.

[130] S.A. Mey, Re-evaluation of the Aluminum-Zinc System, *Zeitschrift fur Metallkunde*, Vol.84, No.7 1993, pp. 451-455.

[131] S.L. Chen and Y.A. Chang, A Thermodynamic Analysis of the Al-Zn System and Phase Diagram Calculation, *CALPHAD*, Vol.17, No.2, 1993, pp.113-124.

[132] M. Mathon, K. Jardet, E. Aragon, P. Satre and A. Sebaoun, Al-Ga-Zn System: Re-assessments of the Three Binary Systems and Discussion on Possible Estimations and on Optimisation of the Ternary System, *CALPHAD*, Vol.24, No.3, 2000, pp.253-284.

[133] F.E. Wittig and G. Keil, Heats of Mixing of Binary Liquid Aluminum-B-Metal Alloys (Zinc, Cadmium, Indium, Thallium, Tin, Lead and Bismuth), *Zeitschrift fur Metallkunde*, Vo.54, No.10, 1963, pp.576-590.

[134] J.E. Hilliard, B.L. Averbach and M. Cohen, Thermodynamic Properties of Solid Aluminum-Zinc Alloys, *Acta Metallurgica*, Vol. 2, 1954, pp.621-631.

[135] H. Corsepius and A. Muenster, On the Thermodynamic Properties of Solid Alumium-Zinc Alloys, *Zeitschrift fuer Physikalische Chemie*,Vol. 22,1959,pp.1-19.

[136] R.E. Wittig and L. Schoeffl, Heat of Formation in the Aluminum-Zinc System at 330, 370 and 430° C, *Zeitschrift fur Metallkunde*, Vo.51,1960, pp.700-707.

[137] R.A. Connell and D.B. Downie, The Enthalpies of Formation of α-Phase Al-Zn Alloys, M*etal Science Journal*, Vol.7,1973, pp.12-14.

[138] G. Batalin and E.A. Beloborodova, The Activity of Al in the Liquid, *Russian Metallurgy*, Vol.4, 1968, pp. 121-125.

[139] B. Predel and U. Schallner, On the Thermodynamic Properties of Binary Aluminum Alloys Containing Gallium and Zinc, *Zeitschrift fur Metallkunde*, Vo.60, No.11, 1969, pp.869-877.

[140] J. Sebkova, M. Beranek, Application of the EMF Method for Measurement of Aluminum Activities in Liquid Aluminum Alloys, *Sbornik Vysoke Skoly Chemicko-Technologicke v Praze, B: Anorganicka Chemie a Technologie*, Vol. B18, 1974, pp. 217-225.

[141] G.J. Lutz and A.F. Voigt, A Radioactive Tracer Dew Point Method for Measuring Vapor Pressures of Binary Alloys, the Zinc-Aluminum System, *Journal of Physical Chemistry*, Vol. 67, No.12, 1963, pp.2795-2799.

[142] P. Bolsaitis and P.M. Sullivan, The Activity of Zinc in Liquid Zn-Al Alloys from Isopietic Measuremnts, *Transactions of the Metallurgical Society of AIME*, Vol.245, 1969, pp. 1435-1438.

[143] A. Yazawa and Y.K. Lee, Thermodynamic Studies of the Liquid Aluminum Alloy Systems, *Transactions of the Japan Institute of Metals*, Vol.11, No.6,1970, pp.411-418.

[144]A.K. Nayak, Thermodynamic Analysis of Aluminum-Zinc Alloys from Calorimetric Measurements, *NML Technical Journal*, Vol. 23, No.1-2, 1981, pp.3-10.

[145] W. Ptak and L. Zabdyr, Determination of Thermodynamic Properties of Aluminum-Zinc Solid Solutions by EMF Measurements, *Archiwum Hutnictwa*, Vol. 16, No.3, 1971, pp. 253-267.

[146] R.E. Miller, J.L. Straalsund and D.B. Masson, The Effect of Electron Concentration on the Thermodynamic Properties of Two Alloy Phases in the Al-Zn-Ag System, *Metallurgical Transactions*, Vol.3, 1971, pp.545-550.

[147] V. Piacente, V.D. Paolo and G. D'Ascenzo, The Activity of Zinc in Solid Al-Zn Alloys, *Thermochimica Acta*, Vol.16, 1976, pp. 63-68.

[148] T. Takahashi and N. Asano, Thermodynamic Studies of Solid Aluminum-Zinc Alloys, *Niihama Kogyo Koto Senmon Gakko Kiyo, Rikogaku-hen*, Vol.18,1982, pp.78-84.

[149] D. Kevorkov and R. Schmid-Fetzer, The Al-Ca system, Part 1; Experimental Investigation of Phase Equilibria and Crystal Structures, *Zeitschrift fur Metallkunde*, Vol.92, 2001, pp.946-952.

[150] K. Ozturk, L.Q. Chen and Z.-K. Liu, Thermodynamic Assessment of the Al-Ca Binary System Using Random Solution and Associate Models, *Journal of Alloys and Compounds*, Vol. 340, No.1-2, 2002, pp.199-206.

[151] M. Aljarrah and M. Medraj, Thermodynamic Assessment of the Phase Equilibria in the Al-Ca-Sr System using the Modified Quasichemical Model, *Journal of Chemical Thermodynamics*, Vol. 40, No. 4, 2008, pp.724-734.

[152] N. Kono, Y. Tsuchida, S. Muromachi and H. Watanabe, Study of the Al-Ca-Zn Ternary Phase Diagram, *Light Metals*, Vol. 35, 1985, pp.574-580.

[153] G. Cordier, E. Czech and H. Schafer, $CaAl_2Zn_2$, The First Example of an "Inverse" $ThCr_2Si_2$ Structure, *Zeitschrift fuer Naturforschung, Teil B: Anorganische Chemie, Organische Chemie*, Vol. 39B, No.12,1984, pp.1629-1632.

[154] A. Prince, The Al-Ca-Zn System, *Bulletin of Alloy Phase Diagrams*, Vol.10, No.5, 1989, pp.540-545.

[155] I.N. Ganiev, M. S. Shukroev and K.M. Nazarov, Effect of Phase Composition on the Electrochemical Behavior of Aluminum-Zinc-Calcium Alloys, *Zhurnal Prikladnoi Khimii*, Vol. 68, No.10, 1995, pp.1646-1649.

[156] I. N. Gantsev, K.M. Nazarov, M.M. Khakdodov and N.I. Gantseva, Interaction of Binary Eutectics in Al-Zn-Ca (Sr, Ba) Systems, *Evtektika V, Mizhnarodna Konferentsiya, Dnepropetrovsk*, National Metallurgical Academy of Ukraine, Dnepropetrovsk, Ukraine, 2000, pp.56-58.

[157]Y.Zhong, Investigation in Mg-Al-Ca-Sr-Zn System by Computational Thermodynamics Approach Coupled with First-Principles Energetics and Experiments. PhD Thesis, The Pennsylvania State University, Pennsylvania (USA), 2005.

[158] K.C. Hari Kumar and P. Wollants, Some Guidelines for Thermodynamic Optimization of Phase Diagrams, *Journal of Alloys and Compounds*, Vol. 320, 2001, pp. 189-198.

[159] C. Bale, A.D. Pelton and W. Thompson, Factsage Thermochemical Software and Databases, http://www.crct.polymtl.ca, 2008.

[160] A.T. Dinsdale, Thermodynamic Data for the Elements, *CALPHAD*, Vol. 15, Issue. 4, 1991, pp. 317-425.

[161] A.D. Pelton, Y-B. Kang, Modeling Short-range Ordering in Solutions, *International Journal of materials Research*, Vol. 98, 2007, pp.1-10.

[162] F. Sommer, Association Model for the Description of Thermodynamic Functions of Liquid Alloys II. Numerical Treatment and results, *Zeitschrift fuer Metallkunde*, Vol. 73, No. 2, 1982, pp.77-86.

[163] F. Kohler, Estimation of the Thermodynamic Data for a Ternary System from the Corresponding Binary Systems, *Monatshefte fuer Chemie*, Vol. 91, No. 4, 1960, pp. 738-740.

[164] Y.M. Muggianu, M. Gambino and J.P. Bross, Enthalpies of Formation of Liquid Alloys Bismuth-Gallium-Tin at 723.deg.K. Choice of an Analytical Representation of Integral and Partial Excess Functions of Mixing, *Journal de Chimie Physique*, Vol. 72, No.1, 1975, pp. 83-88.

[165] G.W. Toop, Predicting Ternary Activities using Binary Data, *Transactions of The American Institute of Mining*, Vol. 233, No. 5, 1965, pp. 850-855.

[166] P. Chartrand and A.D. Pelton, On the Choice of Geometric Thermodynamic Models, *Journal of Phase Equilibria*, Vol. 21, No. 2, 2000, pp. 141-147.

[167] J. Hafner, S. S. Jaswal, M.Tegze, A. Pflugi, J. Krieg, P. Oelhafen and H. J. Guentherodt, The Atomic and Electronic Structure of Metallic Glasses: Search for a Structure-induced Minimum in the Density of States, *Journal of Physics F: Metal Physics*, Vol. 18, No.12, 1988, pp. 2583-2604.

[168] H. Tanaka, Relation Among Glass-forming Ability, Fragility and Short-range Bond Ordering of Liquids, *Journal of Non-Crystalline Solids*, Vol.351, 2005, pp.678-690.

[169] K.C. Kumar, I. Ansara and P. Wollants, Sublattice Modeling of the μ-Phase, *CALPHAD*, Vol.22, No.3, 1998, pp. 323-334.

[170] "Powder Cell for windows", Version 2.3, 1999, W.Kraus & G. Nolze, Federal Institute for Materials Research and Testing, Rudower Chausse 5, 12489 Berlin, Germany.

[171] C. Wagner and W. Schottky, Theory of Arranged Mixed Phases, *The Journal of Physical Chemistry B*, Vol. 11, 1930, pp. 163-210.

[172] H. Okamoto and T.B. Massalski, Thermodynamically Improbable Phase Diagrams, *Journal of Phase Equilibria,* Vol.12, No.2, 1991, pp.148-168.

[173] E.A. Smirnova, P.A. Korzhavyi, Yu.Kh.Vekilov, B. Johansson, and I.A. Abrikosov, Electronic Topological Transitions and Phase Stability in the Fcc Al-Zn Alloys. *The European physical Journal B*, Vol.30, 2002, pp.57-66.

[174] P.S. Rudman, B.L. Averbach:X-ray Measurements of Local Atomic Arrangements in Aluminum-Zinc and in Aluminum-Silver Solid Solutions, *Acta Metallurgica*, Vol.2, 1954, pp.576-582.

[175] D. Keverkov and R. Schmid-Fetzer, The Al-Ca System, Part 1; Experimental Investigation of Phase Equilibria and Crystal Structures, *Zeitschrift fur Metallkunde*, Vol. 92, 2001, pp.946-952.

[176] K. Matsuyama,On The Equilibrium Diagram of the Al-Ca System, *Science Reports of the Tohoku Imperial University*, Vol.17, 1928, pp.783-789.

[177] L. Donski, Alloys of Ca with Zn, Al, Ti, Pb, Sn, Bi, Sb and Cu, *Zeitschrift Anorganische und Allgemeine Chemie*, Vol. 57, 1908, pp.201-205.

[178] F. Sommer, J.J. Lee and B. Predel, Thermodynamic Investigation of Liquid Al- Ca, Al-Sr, Mg-Ni and Ca-Ni Alloys, *Zeitschrift fur Metallkunde*, Vol.74, 1983, pp.100-104.

[179] Y.O. Esin, V.V. Litovski, S.E. Demin and M.S. Petrushevski, Enthalpies of Formation of Aluminum-Strontium and Barium-Silicon Melts, *Russian Journal of Physics and Chemistry*, Vol.59, 1985, pp. 446.

[180] K.T. Jacob, S. Srikanth and Y. Waseda, Activities, Concentration Fluctuations and Complexing in Liquid Ca-Al Alloys, *Transactions of the Japan Institute of Metals,*Vol.29, 1988, pp.50-59.

[181] E. Schürmann, C.P. Fünders and H. Litterscheidt, Vapor Pressure of Ca above Ca-Si, Ca-Al and Ca-Al-Si Alloys, *Arch. Eisenhuttenews*, Vol.46, 1975,pp.473-476.